Norwegian University
of Life Sciences

Master's Thesis 2020 30 ECTS
Faculty of Science and Technology

Mapping the way to higher resolution

Assessing the feasibility of opportunistic precipitation networks for urban hydrology in Norway

Daniel Ambrosius Hofgaard Prince
Water and Environmental Technology

Acknowledgements

I would like to thank Vegard and Nils-Otto, my two supervisors, for providing great feedback and encouragement, Elin for providing encouragement, support, and much needed distractions, all of my housemates for showing consideration during these last few weeks, and Michael for a *very* timely proofreading. Further, i would like to thank all of my friends, classmates and lecturers at NMBU for making my time here fruitful, and very enjoyable. Finally, i would like to thank my family.

Ås, June, 2020

Daniel Ambrosius Hofgaard Prince

Summary

Continual urbanization in Norway and elsewhere combined with more intense precipitation forced by climate change requires better monitoring and understanding of precipitation in cities. This paper assesses the possibility of adopting two opportunistic networks, Commercial Microwave Links (CML) and Personal Weather Stations (PWS), to create high-resolution urban precipitation maps for use in flood modeling, calibrating sewage/runoff models and other urban hydrological applications.

The assessment was accomplished by identifying the supply-side stakeholders (owners/aggregators of the networks), assessing the networks with respect do density, clustering, extent, and topographical representativeness. Further, the error structures of both networks were attempted identified by geostatistical methods and identifying the effective quantization level for PWS and CML networks, respectively. Data from the PWS network was subsequently corrected using a simple quality control (QC) algorithm before five different interpolation methods (Nearest Neighbor (NN), Inverse Distance Weighting (IDW), and three geostatistical approaches) were applied to the PWS network and assessed by comparing the output to point measurements from the traditional gauge network to determine suitability. Finally, the possibility of using both opportunistic networks in combination with their traditional counterpart was assessed by implementing a weighted average approach called the Best Combined Spatial Predictor (BCSP).

This research finds that both networks have favorable characteristics in all respects except measurement error and availability. Further, a geostatistical model constrained by a climatological variogram is found to be the best performing with $R^2 = 0.848$ validated over 38 hours of precipitation spread over five days. The application of the model reveals that inadequate QC increases the model error term resulting in underestimation of locally intense precipitation.

This research concludes that both networks have considerable potential and identifies two distinct challenges going forward, namely improved QC and facilitating data access for PWS and CML networks, respectively.

Sammendrag

Stadig urbanisering kombinert med mer intens nedbør grunnet klimaendringer krever bedre forståelse og overvåking av nedbør i byer. Denne oppgaven utforsker muligheten av å benytte to opportunistiske nettverk bestående av kommersielle radiolinker (CML) og personlige værstasjoner (PWS) for bruk i høyoppløselige nedbørskart brukt til flom-modellering, kalibrering av avløp- og overvannsmodeller, samt andre urbanhydrologiske bruksområder.

Det er gjort en analyse av mulige interessenter (nettverkseiere) for å estimere potensiell nettverksstørrelse og identifisere utfordringer knyttet til datatilgang. De opportunistiske nettverkene ble videre sammenliknet med metrologisk institutts (MET) tradisjonelle nettverk med hensyn på tetthet, dekning, og topografisk representativitet. Usikkerhetsstrukturen i nettverkene er utforsket ved hjelp av geostatistiske metoder for PWS nettverket og indentifisering av effektivt kvantiseringsnivå for CML nettverket. Videre er PWS dataene forsøkt korrigert med en simpel kvalitetskontroll (QC) før anvendelse av fem forskjellige interpoleringsmetoder. Resultatet av disse er sammenliknet med punktdata fra tradisjonelle nedbørmålere i Osloområdet for å bestemme egnethet. Til slutt er muligheten av å aggregere data fra samtlige nettverk utforsket ved å implementere en kombinert modell (BCSP).

Resultatene i oppgaven viser at begge de opportunistiske nettverkene har gunstige kvaliteter sammenliknet med MET nettverket utenom måleusikkerhet og måletilgjengelighet. Videre vises det at geostatistisk interpolering på grunnlag av et klimatologisk semivariogram er mest nøyaktig med $R^2 = 0.848$ validert med 38 timer med nedbør over 5 dager. Modellen viser at utilstrekkelig kvalitetskontroll øker modellens usikkerhetsparameter som videre fører til underestimering av lokal ekstrem nedbør.

Oppgaven konkluderer med at begge nettverk har betydelig potensiale og identifiserer forbedret kvalitetskontroll og av tilrettelegging av datatilgjengelighet for henholdsvis PWS og CML nettverk som de viktigste utfordringene videre.

Table of Contents

List of Figures

List of Tables

List of Acronyms

API	Application Programming Interface
BCSP	Best Combined Spatial Predictor
CML	Commercial Microwave link
CRS	Coordinate Reference system
DSD	Drop size distribution
GPR	Gaussian Process Regression
IDW	Inverse Distance Weighting
IQR	Interquartile range
LID	Low impact Development
LOD	Lokal Overvannsdisponering
MET	"The Norwegian Metrological Insitute", also refers to their gauge network
NKOM	Norwegian Communications Authority
NN	Nearest Neighbor interpolation
OK	Ordinary Kriging
PWS	Personal Weather Station
QC	Quality Control
RK	Regression Kriging
RMSE	Root Mean Squared Error
WMO	World Meteorological Organization

1. Introduction

1.1 Motivation

Populations in Norway and internationally are continually becoming more urbanized. People are to a large extent living in dense metropolitan cities sprawling over large areas or in smaller urban settlements, as is the case in Norway where the population density is lower in general. Both planned and unplanned urban sprawl has adverse effects on the hydrologic system in which it occurs. Mainly, these effects manifest themselves as increased risk of flooding and higher pollution transport to the receiving water-body and are primarily due to four factors: *diversion or blockage of waterways and impermeable land cover* increase the risk of flooding (Jha et al., 2012) and *constructed drainage and the land use itself* increases the pollution transport.

Natural waterways are commonly diverted, either underground through culverting or displaced (i.e. outside of a natural depression) to free up the land for other uses. Culverting always reduces hydraulic capacity. By restricting the flow area to the size of the pipe or tunnel constructed, the culvert acts as a dam for runoff above design capacity. Below design capacity, a culvert might have the opposite effect, increasing the flowrate due to smother channels and a more efficient hydraulic cross-section (Niemczynowicz, 1999). As buildings and roads are constructed, they are usually covered by impermeable materials, i.e., roofs and pavement. Impermeable surfaces do not allow for infiltration. Therefore, the runoff volume is increased compared to natural surfaces such as woods and grasslands. Additionally, impermeable surfaces tend to have a lower roughness coefficient, increasing the velocity of overland flow, thereby lowering the hydraulic concentration-time of catchments and increasing the peak runoff discharge (Fletcher et al., 2013).

Constructed drainage systems such as combined- or separate sewers further decrease concentration-times (Fletcher et al., 2013). Additionally, they complicate the hydraulic system by introducing sub-surface pipe flow, which does not necessarily follow topographically imposed catchment boundaries.

Finally, the water quality in urban catchments differs drastically from their rural counterparts. Generally, pollutant loading is higher. The pollutant concentration and composition can, to some extent, be characterized by land use type and interaction with sanitary systems such as combined sewers.

A recently widely adopted method of local stormwater management called Low Impact Development (LID) , in Norwegian: LOD (Lokal Overvannsdisponering) , aims to restore the hydrologic response of an urbanized catchment to that of its pre-development state. Briefly, the method consists of fully retaining runoff from smaller showers at the source, attenuating runoff from larger showers in local, normally-dry basins, and mapping safe floodways to secure runoff from extreme precipitation events.

To design-, and determine the effectiveness of LID installations as well as provide efficient urban flood forecasting, extensive modeling is used. These models use information about the topography, land cover, soil type and associated infiltration capacity, sewage and runoff systems as well as information about precipitation. All of these except precipitation and infiltration capacity are continuous in time and well documented, i.e., non-changing and usually implemented accurately in models. Precipitation, however, is typically applied as uniform fields. Although this might give a general understanding of the hydraulic response, precipitation is never uniform, and to be able to model the response of a plausible precipitation event, one must take into account the spatial and temporal variation of precipitation. Infiltration capacity is hard to model as it is affected by a multitude of factors. One of them, the soil moisture content, is in turn affected by antecedent precipitation.

This variation must be captured by dense sensor networks combined with a mapping model. For urban catchments, the optimal resolution of precipitation maps, according to Fletcher et al. (2013), is between 1 and 10 minutes temporally and 100 to 500 meters spatially. Although traditional sensors such as rain gauges are very accurate and are cheap per-unit, the cost associated with dense network deployment such as installation and maintenance, makes them unfeasible as a single solution for mapping applications.

There exist other measurement systems that can aid in increasing the spatial and temporal resolution of measurements. These methods include radar and satellite which are both in wide-spread use. As these systems are deployed for a specific task, they have good measurement sensitivity and a geographical distribution which is optimized for coverage (Messer and Sendik, 2015). However, a central limitation for their deployment is cost in addition to other shortcomings explained further in section 2.2.1.

Conversely, opportunistic networks, networks that are already in place but not connected or in use for a different purpose (Uijlenhoet et al., 2018) (see also sections 2.2.2, 2.2.3),

enjoy the benefit of zero deployment cost and can have a very high spatial density. Two opportunistic networks are explored in this thesis, namely: Commercial microwave links (CML's) , a network of directional microwave antennae used for communications infrastructure such as cellphones, and Personal Weather Stations (PWS's) , a network of weather stations for personal use connected to the internet.

1.2 Aim and Research Questions

1.2.1 Aim

The aim of this thesis is to assess the viability of CML and PWS networks as a source for urban precipitation mapping in Norway for rain-event reconstruction as well as now-casting applications. By answering the research questions below, the thesis aims to determine whether these systems have an added benefit to existing systems and provide a foundation for larger-scale application. The study also hopes to identify or develop well-suited methods for signal processing, quality control, and map-reconstruction as to be able to determine their achievable (theoretical) accuracy. Finally, the study aims to obtain an indication of real-world accuracy by recreating a precipitation event and comparing the estimated precipitation to observed point value(s).

1.2.2 Research Questions

1: Who are the affected stakeholders? What companies and organizations own the data and who would be the potential customers for the data itself and the products on which it is based. What is the benefit to these stakeholders?

2: What is the current state of the art in urban precipitation mapping in Norway? What is the current resolution and accuracy of precipitation maps, and what data-sources are they based on?

3: What are the characteristics of CML and PWS networks in Norway, and how do they compare to those of the traditional gauge network?

4: What is the achievable accuracy using opportunistic networks in Norway? Are currently developed signal processing and mapping models for the opportunistic networks applicable to Norwegian conditions? What methods exist for the calibration of these models? What methods exist to aggregate data from the different networks?

2. Background

2.1 Spatio-Temporal Components of Precipitation

Precipitation is a phenomenon that is governed by very complex atmospheric interactions. The chief among these are moisture content and temperature, which together govern the condensation of water in the air. Additionally, solid particle concentration plays a role as the atmospheric water needs a nucleation site to condense to. These factors are again forced by wind and weather patterns occurring far away from where the precipitation falls. As these factors are near impossible to model in a deterministic manner, precipitation is best viewed as a stochastic process, a process that is partially or fully random.

However, precipitation is not completely random as it exhibits a strong correlation within short distances in both space and time. Within a geostatistical framework, this similarity is characterized by a semivariance function, also called a semivariogram or just variogram. The variogram is defined as half the variance of the difference (of the random function Z, e.g., precipitation intensity) between any two points separated by the vector $\vec{h}$ (Note: $\vec{h}$ can represent a difference between locations in space or time). The definition of the semivariance function is given in equation (2.1) where $\vec{u}$ is a point in space or time.

$$\gamma(\vec{h}) = \frac{1}{2}Var\{Z(\vec{u}+\vec{h}) - Z(\vec{u})\} = \frac{1}{2}E\{[Z(\vec{u}+\vec{h}) - Z(\vec{u})]^2\} \tag{2.1}$$

It builds on the assumptions that 1: The mean of $Z(\vec{u})$ is the same for all $\vec{u}$, i.e., there is no trend in the data. And 2: That the difference between two points $Z(\vec{u}+\vec{h}) - Z(\vec{u})$ for any distance must have zero mean and constant, finite variance over the study area. These assumptions are referred to as *the intrinsic assumption* or *hypothesis* (Legendre and Legendre, 1998, p. 718). The value of the semivariance function will then be independent on the position $\vec{u}$. One can further simplify the concept by assuming that the change in precipitation is independent of direction, that is, an *isotropic process*. The variogram will then be a function of the distance $|\vec{h}| = h$ only. Note that the latter

assumption is not always valid for precipitation; for instance, if there is strong wind during an event or a single prevailing wind direction over a longer time, the variation in that direction will generally be lower due to smoothing.

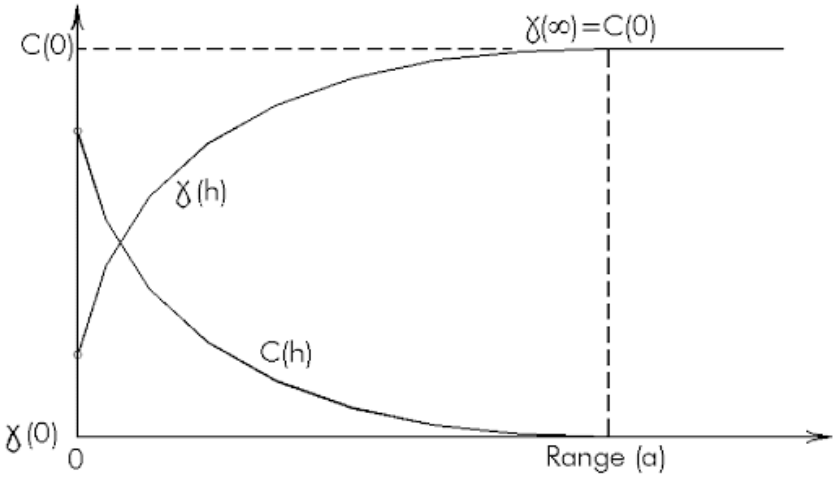

Figure 2.1: Variogram illustration

A variogram can be characterized by three main parameters: The *nugget* $\gamma(0) = b$, the *sill* $b+c$ and the *range* h_r where $\gamma(h_r) = b+c$. The *nugget* (non-zero intercept in fig. 2.1) is a measure of the local variation occurring at a single point or at scales finer than the resolution or sampling interval. The *sill* represents the variance of the entire field. The distance at which the variogram reaches the sill is the *range*, beyond which points are no longer considered spatially correlated (Legendre and Legendre, 1998, p. 729). Note that parameters b, and c are commonly referred to as C_0 and C_1 in the field of geostatistics though this is not done here to avoid confusion with the covariance function.

The nugget effect deserves a closer explanation as it can have two distinct interpretations: When characterizing a field it, corresponds to variation within zero distance illustrated by the following from which the term bears its name: Finding a gold nugget at a certain location, for example, does not guarantee that other nuggets are right next to it and the field itself of actual gold nuggets is discontinuous. Another interpretation that characterizes the *measurement* of a field is the variation occurring at finer scales than the measurement interval (distance between measurement stations) or the error of the measurements themselves. Precipitation, though locally varying, is a continuous process in time and space i.e., if it rains on one's left shoulder, it likely rains on the right one as well, so there is no variance at zero distance. The distinction between the field and its measurement is important, as accurate information about the field characteristics and sampling interval allows the measurement-nugget to be divided between its two causes: i.e., how much of the measured nugget is attributed to measurement error, and how much is due to the characteristics of the measurement network (measurement interval).

Another function used to describe spatial structure is the *covariance function* $C(h)$ (some times denoted $k(h)$ as a *kernel function*), which is more common in other fields such as machine learning, statistics and meteorology. Under the intrinsic assumption, it contains exactly the same information as the variogram and the two functions are related by (2.2) (Cressie, 1991, p. 67). Being mindful of this relationship is important as it enables researchers to leverage interdisciplinary knowledge and implement geostatistical prediction in production using highly optimized machine learning algorithms.

$$\gamma(h) = C(0) - C(h), C(0) = \sigma_Z^2 \tag{2.2}$$

The *true* variogram cannot be known, however it is commonly approximated by using a model function, called theoretical variogram, such as the exponential function (2.3), which in particular has an exact covariance analogue. Here, a and b correspond to the nugget and partial sill. As the model asymptotically reaches the sill, the practical range r where γ reaches 95% of the sill is approximately $r = 3^{1/\beta} l$ (Lloyd, 2006). δ_n in (2.4) is equal to 1 if $h = 0$ and zero otherwise (Rasmussen and Williams, 2006, p. 16).

$$\gamma(h) = b + c(1 - e^{-\frac{h}{l}^{\beta}}) \tag{2.3}$$

$$C(h) = b\delta_n + ce^{-\frac{h}{l}^{\beta}} \tag{2.4}$$

Fitting the variogram model is either done by computing the *empirical variogram* or by optimization algorithms. The experimental variogram (2.5) is computed by grouping pairs of observations by the distance between them in bins $B(h)$ centered on h where a bin contains N observations and computing their variance. Then the theoretical model is fit to the center of the bins, either by visual inspection or using regression.

$$\hat{\gamma}(h) = \frac{1}{2N(B)} \sum_{i,j \ in \ B(h)}^{N(B)} (Z(\mathbf{u})_i - Z(\mathbf{u})_j)^2 \tag{2.5}$$

The application of the variogram to describe the spatial structure depends on the assumption that there is no *external* trend in the data. However, precipitation is strongly affected by topographic features such as elevation and slope (Ly et al., 2011; Tobin et al., 2011), and other factors, including vegetative cover and solar radiation (Jin et al., 2016). These effects can be prominent even at smaller spatial scales; Mohr (2008) found that precipitation was expected to increase with 10% for every $100m$ increase in altitude below $1000masl$. Some geostatistical interpolation methods (described in section 2.1.1)

account for this by using linear regression against one or multiple background fields and treating the residuals as a random spatially correlated variable so that the assumption of a constant mean is still satisfied.

Precipitation measurements, as many other environmental variables, are almost always represented as temporally aggregated values. Most sensors present measurements as either an average $[mm/h]$ or accumulated $[mm]$ over a given time window e.g., one hour, and researchers further aggregate data to study daily, monthly or yearly averages for various purposes. By aggregating a stochastic function such as precipitation, one is by definition also reducing its variance and increasing the distance at which values are spatially correlated. Demonstrated by the variogram, aggregating will decrease the sill and increase the range. This behavior is a consequence of the central limit theorem in statistics and is quite intuitive as aggregating is an operation in which information (variance) is lost. Importantly, this fact implies that there is a relationship between the spatial resolution (aggregation time step) and the spatial structure of a precipitation map.

2.1.1 Models for Precipitation Mapping

A precipitation map is a continuous or near-continuous (i.e., gridded) field of precipitation intensity or accumulated precipitation over a given area. As precipitation is commonly measured at point locations, a precipitation map is generated through interpolation of likely values between the point observations. Multiple models exist for this purpose ranging from very simple deterministic models (Thiessen polygons, inverse distance weighting) to highly advanced geostatistical models (Kriging, Regression Kriging, Kriging with external drift) and further to black-box models (machine learning). For a comprehensive comparison of methods not included here, the reader is referred to Li and Heap (2014).

It should be noted that throughout this study, the terms *predictor* and *interpolator* are used interchangeably. Such is also the case for the terms *prediction* and *interpolation*, where they both consequently refer to predicting a point in space and not time. The term *prediction* is, in some sense, more applicable as some of the models used are not exact (at measurement points), and the underlying measurements have associated errors that are unknown.

The deterministic models can be collectively described by equation (2.6) where Z_i is the calculated precipitation at grid-point i, Z_j is the measured precipitation at point j, λ_j is the weight assigned to the measurement at j and n is the number of measurement stations. The models differ mostly in how the weight λ_j is calculated, and the number n of stations considered (Lyra et al., 2018).

$$\hat{Z}_i = \sum_{j=1}^{n} \lambda_{i,j} Z_j \tag{2.6}$$

The deterministic model commonly used in hydrology is called the Thiessen method (Thiessen, 1911), also called nearest neighbor (NN) interpolation. In this method the interpolation area is divided into n polygons $V_j, j = 1...n$. Each polygon includes all grid-points for which Z_j is the closest observation. The value of the closest observation is then assigned to all grid-points. The weights are then computed by the following rule:

$$\lambda_{i,j} = \begin{cases} 1, & if \hat{Z}_i \in V_j \\ 0, & otherwise \end{cases} \tag{2.7}$$

The benefit to this model is its simplicity and the fact that it will never interpolate or extrapolate (interpolation between an observation and the edge of the study area) an unlikely value i.e., $-1mm/h$. The chief disadvantage is that the method discounts neighboring measurements completely and is thereby very susceptible to measurement errors. Further, the method creates discontinuous regions between polygons (Ly et al., 2011).

Another geometric method is Triangulation with Linear Interpolation. This method is based on Delaunay triangulation, where each observation is connected by non-overlapping lines creating a mosaic of triangles. The value at each triangle corner is constrained to the observation at that point and the slope of the vertices is the spatial gradient $\left(\frac{mm/h}{m}\right)$ between corners. The triangles then span a plane in 3D space (precipitation being the third dimension) from which Z_i is taken (Lyra et al., 2018). This method has previously been used by the Norwegian meteorological institute for precipitation mapping purposes (Mohr, 2008; Tveito, 2016) but has since been superseded by a method called Optimal Interpolation which is similar to Kriging (Lussana et al., 2018).

The other deterministic models commonly used for precipitation mapping are Inverse Distance weighting (IDW) , which assigns a value based on the average of surrounding measurements weighted by the inverse of the distance to the point being interpolated. It relies on the assumption that that measurements close by an unknown point are more influential than those further away. The weights are computed by equation (2.8) where $\mathbf{d}_{a,b} = \mathbf{u}_a - \mathbf{u}_b$ and $\mathbf{u}$ are locations. The p parameter represents a *smoothing* effect where $p > 1$ will increase the weight of closer points and decrease weights further away, and $p < 1$ will do the inverse leading to a smoother field. Dirks et al. (1998) found that the optimal value of p was dependent on aggregation time and recommended $p = 2$ for daily and monthly precipitation and $p = 1$ for hourly. [Drawback is the tendency to produce

spots]

$$\lambda_{i,j} = \frac{\frac{1}{|\mathbf{d}_{i,j}|^p}}{\sum_{k=1}^{n} \frac{1}{|\mathbf{d}_{i,k}|^p}} \tag{2.8}$$

Kriging is a geostatistical method for interpolating points which incorporates the spatial structure described in section 2.1 into the weights for predicting Z_i. It does this under two constraints: Firstly, the prediction should be unbiased, which is accomplished by the weights summing to 1 and that the mean is stationary. Secondly, the prediction variance $\sigma_e^2 = Var(Z_0 - \hat{Z}_0)$ should be minimized. This is accomplished by solving the system of $n+1$ equations in (2.9) (Ly et al., 2011).

$$\begin{cases} \sum_{i=1}^{n} \lambda_i \gamma_{i,j} - \mu & for j = 1, ..., n \\ \sum_{i=1}^{n} \lambda_i = 1 \end{cases} \tag{2.9}$$

$$\begin{cases} \sum_{i=1}^{n} \lambda_i C_{i,j} + \mu & for j = 1, ..., n \\ \sum_{i=1}^{n} \lambda_i = 1 \end{cases} \tag{2.10}$$

Here, $\gamma_{i,j}$ is the semivariance between points $\mathbf{u}_i$ and $\mathbf{u}_j$ given by the distance between them. n represents the number of observation points and, μ is a Lagrange parameter included to constrain the solution to the un-biasedness criterion.

When applying the weights calculated from (2.9) directly to eq. (2.6) the process is called Ordinary Kriging (OK) . This is the most common kriging method, though there exist many other methods. One is Simple Kriging, which assumes the mean to be constant and known where OK assumes the mean to be constant, but unknown. In principle these methods are equivalent but by limiting $n = n(\mathbf{u})$ to stations in a local search window OK can account for a trend (changing mean) in the data (Goovaerts, 1997, p. 137). As the mean is assumed to be known, the un-biasedness criterion is no longer necessary, and the system is reduced to n equations without the Lagrange parameter.

In the case where the trend in the data is related to exhaustive secondary information such as elevation, methods such as Regression Kriging (RK) can be used. This method splits equation (2.6) into a sum of the trend and residual (see eq. 2.11) (Hengl et al., 2003). Here, the trend is estimated using (most commonly) generalized least squares regression between the background field, e.g. elevation and the target, e.g. precipitation and OK is performed on the regression residuals. The results are then added back

together.

$$\begin{aligned} \hat{Z}(\mathbf{u}) &= \hat{m}(\mathbf{u}) + \hat{\epsilon}(\mathbf{u}) \\ \hat{m} &= \beta_0 + \beta_1 q(\mathbf{u}) \\ \hat{\epsilon} &= \sum_{i=1}^{n} \lambda_i(\mathbf{u}) \epsilon(\mathbf{u}_i) \\ \epsilon(\mathbf{u}_i) &= Z(\mathbf{u}_i) - \hat{m}(\mathbf{u}_i) \end{aligned} \tag{2.11}$$

One of the key benefits of the Kriging method is that it is able to predict not only target values, but also the corresponding error variance at any point. A key aspect of the predicted variance is that it is dependent only on the semivariance (or covariance) function and the spatial configuration of measurements, i.e., independent of the observed values (Goovaerts, 1997, p. 179). In this way, it is possible to create a map of the prediction confidence and evaluate regions in need of more sensors. Further, this enables drawing points from a normal distribution with mean and variance equal to the kriging prediction and kriging variance, then adding them as an "observation". Doing this iteratively creates a *realization*, or possible reality of the field, rather than the most likely value at every point. This method is called *Stochastic simulation*.

Importantly, when using the kriging method for interpolation of precipitation, one must take into account that the spatial precipitation will change over time. Different precipitation types (convective, frontal, orographic) might differ vastly in their corresponding variograms. Further, if the temporal scale is fine enough e.g., less than the duration of a precipitation event, the spatial structure might vary throughout the storm and consequently be unique for each measured time-step. This complicates the application of kriging for nowcasting, as the variogram needs to be re-fitted at each time-step, making the model prone to erroneous measurement. This problem can be overcome by either fitting the variogram to an average of prior empirical variograms creating a *climatological variogram*, or one could pre-process the observations to filter out erroneous measurements before applying the model.

The general kriging methodology is also referred to as "Gaussian Process Regression" (GPR) (for simple kriging specifically) or best linear unbiased estimator (BLUE). These methods are more general as they are commonly used for non-spatial applications, and usually rely on the covariance function rather than the variogram. Further, there exist other methods of the black box type used for regression in machine learning applications. These can also be considered for spatial interpolation, though they do not have the same physical basis in the spatial structure and rely primarily on cross-validation techniques

to optimize against some form of prediction error.

It should be noted that precipitation, in addition to being non-continuous in time and space, is also skewly distributed with an absolute lower boundary of zero, i.e., negative precipitation does not exist. For smaller time-steps, this is especially relevant and implies that the intrinsic assumption is not exactly valid (Tveito, 2016). This fact somewhat diminishes the advantage of a statistical basis for the geostatistic interpolation methods over the deterministic and black box ones.

The above interpolation techniques have been compared for precipitation interpolation for various spatial and temporal scales, see (Wang et al., 2014; Hofstra et al., 2008; Haberlandt, 2007; Lyra et al., 2018; Ly et al., 2011), a review of which indicates that no single method is superior, though likely candidates are the Ordinary Kriging, Regression Kriging, and Inverse Distance Weighting methods. Reviews of interpolation methods for climate data (Li and Heap, 2014; Tveito, 2008; Sluiter, 2009) all recommend testing multiple methods for the same application.

2.2 Sensor Network Theory

In this section, the distinction between traditional precipitation networks and opportunistic networks is defined. Traditional networks are networks of ordinary rain gauges. The gauges can either be manual or reporting (see 2.2.1). Opportunistic networks are defined as networks already deployed by a third party but not currently in use for precipitation monitoring, the two included in this study are commercial microwave link (CML) networks (see 2.2.2), whose primary use is relaying information, and Personal Weather Station (PWS) networks which are personal weather stations. The inclusion of the latter in the definition might not seem obvious as they are quite similar to traditional networks. However, there are some important differences between them as discussed further in 2.2.3. Other forms of opportunistic networks might include the use of mobile phones to measure solar radiation or pressure (de Vos et al., 2020) or the windshield wiper frequency of cars to measure precipitation (Haberlandt and Sester, 2010). Opportunistic networks have three things in common: The sensors are already deployed, the sensor distribution is usually denser than its traditional counterpart, and importantly, the opportunistic user of the network has little to no control of its configuration or quality.

For precipitation, there are many objectives a sensor network needs to fulfill. First and foremost, it should give its users (usually the public or research organizations) a picture of precipitation that is clear enough for its application. This application can range from tracking climate data such as the mean annual precipitation over a country

to hydrologic monitoring of flooding and pollution discharge or short term precipitation prediction. These applications impose different criteria on the network in terms of representativeness, coverage, clustering, and resolution. In this section will pay specific attention to the requirements for urban hydrological applications for flooding.

The coverage of a network is herein defined as the network's spatial extent i.e., the border around the network outside which there are no sensors. For all applications, it is important that the network extends to or beyond the extents of the studied area so as eliminate the need for extrapolation in mapping applications. Networks for precipitation monitoring are usually country-wide, though they do not extend to bodies of water such as the sea, making the coastline an effective border. For urban hydrological applications, however, this is of little importance as precipitation falling in the ocean has no effect in cities. However, the presence of large upstream catchments should be considered if there is a risk of fluvial (river-borne) flooding.

Representativeness is a measure of how un-biased the network is with respect to factors that are explanatory for the measured variable, chiefly elevation. This is a real challenge for precipitation networks as they tend to be denser in populated areas, which are commonly low-lying and less dense in mountainous regions where there is more precipitation. This fact can lead to underestimation in many applications. For urban hydrology, this is of less importance where the primary cause of flooding is pluvial, from precipitation occurring close to the flooded area which is topographically homogeneous, as opposed to fluvial, where the source of floods are rivers with large upstream catchments where the topography is much more varied. A related measure is clustering, which describes how the network density varies throughout the network. A network of 10 stations would have a low degree of clustering if the stations were equally distributed, and clustering would be high if 8 of the stations were squashed together in a corner. With a fixed number of stations, a low degree of clustering is preferred, and the network should approximate a grid. However, if geostatistical methods are to be used, data of short scale variation needs to be gathered, so some degree of clustering is needed.

Density is the most important factor for urban applications. It describes how close the sensors are to each other on average and dictates how much of the spatial structure can be captured. The density required for hydrological applications is, in large part, dictated by the spatial structure of the storm event and the catchment response time, the latter of which is mostly dependent on slope and catchment area. Berne et al. (2004) found a relationship between catchment size (S [ha]), the required temporal (Δt [min]) and spatial (Δr [km]) resolutions by analyzing the spatiotemporal structure of precipitation in a Mediterranean climate:

$$\begin{aligned} \Delta t &= 0.7S^{0.3} \\ \Delta r &= 1.5\sqrt{\Delta t} \end{aligned} \tag{2.12}$$

The equations rely on the assumption that the temporal resolution should be equal to the catchment response time, the time between peak rainfall and peak discharge, usually approximated by the time it takes water to traverse the whole catchment. According to the authors, the equations are valid for catchments between 10 and 10000 ha, with slopes between 1 and 10% and with imperviousness between 10 and 60%. It should be noted that rain event spatial structure is dependent on climate, so the relationships presented might not be applicable to the Norwegian climate.

The final aspects of sensor networks are homogeneity and data quality. Homogeneity is a measure of how the network itself changes. Complete homogeneity is achieved when measurement variations are completely the consequence of variation in the climate. Any change to the network like changing the position or type of sensors, construction of buildings at the sensor site that affects the measurement, or the addition or relocation of sensors will all create breaks of homogeneity in the network (Tveito, 2016).

Data quality refers to the accuracy and quality of the sensors and can result in erroneous, missing, or biased measurements. These can be corrected by applying quality (QC) control procedures before any interpolation is done. Many QC methods exist for traditional networks as values can be checked against what is likely based on climatological data for the same station and season (temporal consistency tests) and data from other sensor types (humidity, wind, temperature) at the same location (Internal consistency checks) (Vejen et al., 2002; Plummer et al., 2003). For opportunistic networks, the selection of QC methods is more limited as the stations have no climatological data. Some bias-correction is possible (de Vos et al., 2019) and stations can be flagged for erroneous values through spatial consistency checks where neighbouring observations are compared (Nipen et al., 2020; de Vos et al., 2019). However, there exists little basis for correcting erroneous and missing values.

The homogeneity and data quality of a network is consequential for what methods can be used for later interpolation, prediction, or analysis. If the homogeneity is high, one can use rigorous, finely tuned models that expect each sensor to be "present". For these models to work, the data quality needs to be high so that there are few missing and erroneous values, and those that occur can be "fixed" by QC before further processing. This is especially important if aggregate analysis is to be done. Imagine that a sensor is offline for a single day and monthly precipitation is analyzed. The missing day will

invalidate the whole month unless fixed.

2.2.1 Traditional Sensors

Traditional sensors are defined in this paper as sensors and sensor systems that are commonly used in precipitation measurement. These include point sensors such as pluviometers and disdrometers as well as weather radar.

Pluviometers measure the mass of rain falling into a funnel of known area. For automatic reporting, a weighing system or tipping-bucket arrangement is used. The weighing system periodically records the weight of a collection bucket, and the tipping-bucket arrangement reports every emptying of a small bucket (typically corresponding to $0.1mm$ of precipitation). For unattended stations, the tipping-bucket is used as it does not require periodic emptying. Pluviometers are highly accurate if installed with proper wind shields, though they are still prone to wind-induced collection deficiency when the precipitation occurs as snow (Wolff et al., 2013). The world meteorological organization (WMO) has guidelines for the production, installment, calibration, and maintenance of pluviometers and other meteorological observation methods (WMO, 2014). If a measurement station adheres to these guidelines, it is deemed WMO compliant.

For the tipping-bucket arrangement, the temporal resolution is governed by the size of the bucket and logging frequency and effectively increases with precipitation intensity. This is because the rain rate is recorded as the number of tips per time interval multiplied by the bucket volume, which leads to inconsistent data when the rain-rate is lower than the bucket volume, i.e., less than one tip per time interval. This inconsistency can be corrected by recording the time of each tip and re-sampling to fixed time intervals later using fixed timeline processing (see fig. 3.1). Conversely, the same system will experience collection deficits if the precipitation intensity is large enough to overburden the tipping-mechanism e.g., if water over-tops the bucket before tipping. The tipping mechanism also has a risk of clogging due to debris or solid precipitation. An oft-overlooked aspect of traditional pluviometers is their spatial representativeness. The actual area in which the pluviometer measures is the area of its collection funnel which is so small as to be considered a point sample, the representative area of which (S_r) can be formulated as $S_r = \pi \left[\frac{\Delta r}{2}\right]^2$ using Δr from (2.12). Traditional gauge networks are designed taking the above factors into account and are, as a consequence, built out to maximize spatial representativeness of the network with regard to distance between sensors and other important factors such as elevation.

Disdrometers are optical or pressure-sensitive sensors that measure the hydrometeors (raindrops, snowflakes, etc.) more directly by recording their size and velocity and then binning them into a drop size distribution (DSD) . These parameters can be transformed

to precipitation intensity directly, but are also valuable for determining precipitation type and for error correction in surrogate measurement techniques such as weather radar where the reflectivity is highly dependent on the DSD. (Islam et al., 2012). Disdrometers are not as prone to wind-induced loss as pluviometers with no risk of clogging, but are costly instruments and normally not used in networks.

Weather radar has seen widespread use in recent years, mainly due to its ability to measure over a very large area, a disk centered at the radar installation with a typical radius between 150 and 300 km. The system works by scanning the atmosphere around the radar at different angles (from the horizontal) and measuring the power of the reflected signal for each radial segment along the beam. The data is then processed by extensive error correction algorithms to eliminate reflections from non-meteorological objects such as birds, ground- and sea clutter, as well as effects due to anomalous propagation (radar beam bending due to unusual gradients in temperature and humidity) (Elo, 2012). The end product is in the form of a cartesian grid of reflectivity values with a resolution on the order of $1x1km^2$ at $5min$ intervals (Berne and Krajewski, 2013) and is typical for C-band radar. Using modern X-band radar such as the IDRA used by Ochoa-Rodriguez et al. (2015), resolutions of $100x100m^2$ and $1min$ are possible, though at the expense of range which decreases to approximately $15km$. The system is very useful for classifying the precipitation type and intensity (low, moderate, extreme), but less so for estimating the actual precipitation intensity. This is because the relation between water content and reflectivity is highly dependent on the DSD, which is largely unknown at the sampling location.

2.2.2 Commercial Microwave Links

This section contains a small summary of CML's for use in precipitation measurement and mapping. For further information, the reader is referred to a critical survey (Messer and Sendik, 2015) and two excellent reviews (Uijlenhoet et al., 2018; Chwala and Kunstmann, 2019) on the topic.

Commercial microwave links (CML) are directional antennas used for point-to-point communications applications. They are primarily deployed by cellular network operators as part of their backhaul networks interconnecting base-stations and servers. They operate with frequencies between 5 and 40 GHz with future installations to facilitate 5G extending to 80 GHz. The fact that precipitation causes considerable attenuation of the signal at these frequency ranges has been known since 1946 (Robertson and King, 1946). Further, Atlas and Ulbrich (1977) found that the relationship between attenuation A and precipitation R is essentially independent of DSD at the same wavelengths. They also found that the relationship can be described with equation (2.13) where k is the

specific attenuation in dB/km and R is in mm/hr. (ITU-R, 2005). Note that the values k and R are at a specific point in time and position along the link.

$$k = aR^b \tag{2.13}$$

a and b in equation (2.13) are constants mainly dependent on the polarization and frequency of the radio waves, the temperature (Chwala and Kunstmann, 2019), and to a much lesser extent, the DSD which Jameson (1991) affected the attenuation only when b deviated from 1. Curve fitting to empirical data for different DSD performed by Chwala and Kunstmann (2019) found a b between 1.193 for 10 GHz to 0.858 for 50 GHz, where the scatter was smallest when $b = 1.020$ at $30\,\mathrm{G}Hz$. The linearity ($b \approx 1$) of equation (2.13) is important as it allows the approximation $\int f(x)^d dx \approx [\int f(x)dx]^d$ which is important for determining the path-averaged precipitation intensity ($\bar{R}$) as a function of the total attenuation (A)

$$A = \int_0^L aR(l)^b dl \overset{b\approx 1}{=} a(\bar{R})^b L, \tag{2.14}$$

where L is the total length of the link, $A[\,\mathrm{dB}] = TSL - RSL$ is the total attenuation over the link where TSL and RSL are Transmitted and Received Signal Level respectively. Inverting this relation, and omitting the bars (R and k both denote average values hereafter), the following relation to determine precipitation intensity is obtained:

$$\begin{aligned} R &= \left[\frac{k}{a}\right]^{1/b} \\ k &= \frac{A}{L} \end{aligned} \tag{2.15}$$

Two characteristics, *bias* and *sensitivity* are important in this relation. The constant a can be viewed as a proxy for sensitivity, and b as a proxy for bias. For a given frequency, stronger precipitation corresponds to a higher attenuation. For a given rain rate, the corresponding attenuation increases with frequency. Additionally, higher frequencies have a higher bandwidth, i.e., they are able to transmit more information. As a consequence of the latter two points, CML network architects employ higher frequency links for shorter paths and lower frequency for longer paths. As a result, sensitivity is relatively equally distributed among different links and lies between 0.25 and 1.8 dB/[mm/hr]. Bias is a measure of how much the attenuation is affected by the distribution of precipitation along the link. It increases as the frequency diverges from 30 GHz. For shorter paths

with high frequencies, this isn't a problem except for the wet antenna attenuation effect discussed later, as the spatial structure is more likely to be homogeneous over shorter distances. For longer distances with lower frequencies, bias is somewhat mitigated by the averaging that occurs along the path.

The relationship in (2.15) is nothing new, and it has been applied in earlier studies (Atlas and Ulbrich, 1977; Jameson, 1991) to determine precipitation. Since then, the build-out of communications infrastructure has been tremendous. There are, as of 2017, an estimated 4 million CMLs worldwide (Ericsson, 2017) that can potentially act as precipitation measurement stations. When compared to the number of traditional gauges, which Kidd et al. (2017) estimated between 0.15 and 0.25 million, the added value is obvious with regard to the spatial resolution. Messer (2006) and Leijnse et al. (2007) were the first to explore this application, and it has been an ongoing field of research since.

The fact that measurements represent path-averages increases the spatial representativeness with increasing length i.e., the chance of not detecting a localized e.g., convective storm event is decreased. This comes at the expense of losing fine-scale variation, which is important for interpolating on a grid finer than the path lengths. A few studies have tried to account for this using tomographic techniques (Nebuloni et al., 2017; Giuli et al., 1991) and dynamic models (Roy et al., 2016). The majority of studies in this field have assumed the path-average to be representative of a point on the path center, then using geostatistical techniques with point support for interpolation. In principle, these techniques can be used with line support (Uijlenhoet et al., 2018), but the uncertainties associated with the point simplification have been found to be smaller than the physical errors associated with single-link precipitation retrieval (Rios Gaona et al., 2017).

The application of CML data for precipitation mapping faces many challenges. Most, if not all of them, are due to the opportunistic nature of the network, and many are not fully solved or require a unique solution for each application. The first challenge is network access. CML operators are not accustomed to sharing their signal loss data as they use it only for internal network monitoring purposes, and the open knowledge of it might prove a competitive disadvantage. More importantly, communications infrastructure is in many areas considered to be of critical importance, leading CML operators to more closely guard data access. Further, a system for data transfer needs to be created. For research purposes, historical data can be transferred via email. For use in real-time operational products however, data must be transferred in real-time. This has been accomplished in Gothenburg, Sweeden (Bao et al., 2017) and Germany (Chwala et al., 2016) using purpose-built software which has to be installed on the operator's internal network.

The quality of the signal-loss data is also highly variable from network to network. The data can be reported as an instantaneous value or as the minimum and maximum attenuation since the last sampling. For internal network monitoring, a sampling rate of 15 min with a power resolution 1 dB is considered adequate, and storage of the data can be non-existent or at resolutions as course as daily (Chwala et al., 2016). Considering the spatiotemporal characteristics of precipitation, a higher polling frequency and a power resolution of 0.1 dB(Uijlenhoet et al., 2018) is desired for use in precipitation mapping.

Another opportunistic trait of CML networks is their heterogeneity. Links are upgraded continually, often changing location and/or frequency in the process. Additionally, links may be unreachable at moments due to outages in other parts of the network. This limits the available post-processing techniques, as discussed in the beginning of this section.

Similarly to radar, not only precipitation causes attenuation of the electromagnetic signal. Other causes can be atmospheric ducting (when layering of humidity or temperature causes the beam to bend), increased humidity, dew accumulation on the antennae, or physical objects blocking the beam-path. These effects are important for determining the reference level attenuation and event detection. The former refers to the signal-loss corresponding to dry weather, which might fluctuate throughout the day and/or year. Event detection is the classification of a rain event. If a spike occurs in the signal loss, is it due to precipitation or not? One way to account for this is by using spatial consistency checks. However, this method only works in areas where the network is denser than the decorrelation-distance or range of precipitation. If not, the temporal structure of the signal can be used. Chwala et al. (2012) used a gliding windowed fast Fourier transform on data that was reported as 1 min averages, and Schleiss and Berne (2010) used the standard deviation of a 25 min gliding window on 30 s instantaneous data. If the link uses dual (both vertical and horizontal) polarization, event detection is more trivial as the differential attenuation $A_{horizontal} - A_{vertical}$ is affected only by the precipitation rate (Ruf et al., 1996). However, dual-polarization links are relatively rare. Alternatively, secondary information, such as nearby traditional gauges, satellite imagery, or radar, can be used if available.

Another source of attenuation that is caused by precipitation, but not directly related to its intensity, is the coating of the antenna surface by a film of water when it rains. This results in an overestimation bias predominantly affecting shorter links as the relative contribution of the water film to attenuation is higher. In literature, this is referred to as the *wet antenna attenuation effect*, the correction of which remains a challenge. In networks with little variation in link lengths and frequencies, it has been found that subtracting a constant from the attenuation solves this problem (Overeem et al.,

2016). However, in a more varied network, more advanced techniques that consider the links individually with regard to length, frequency, and temporal structure of the signal might need to be applied. Additionally, the duration and magnitude of the wet antenna attenuation is affected by the material of the antenna cover and other meteorological variables like temperature, wind, humidity, and solar radiation which affect drying. Due to these factors, the development of a WAA model not reliant on extensive secondary information is still an open challenge, though many methods have been presented (Uijlenhoet et al., 2018).

2.2.3 Personal Weather Stations

Personal Weather Stations (PWS), also called citizen weather stations, are small scale versions of meteorological sensors installed by amateurs and hobbyists on their own property (house, garden) to be able to monitor the weather when not at home. They are often sold as small units with integrated sensors for various climatological factors in a plug-and-play fashion. If they wish, users may connect these stations to public networks to aid in weather monitoring, prediction, and research, so-called Citizen Science. PWS systems have been available since the early 2000s and have seen extraordinary growth in recent years coinciding with the adoption of IoT (Internet of Things) technologies. This growth is exemplified by the number of PWS stations connected to the leading PWS network, Weather Underground, which has grown from 7000 to 0.25 million stations in less than ten years (Chen et al., 2018).

The main advantage of PWS is their density when aggregated in networks. The aggregation is either done through 3rd party services such as Weather Underground, which station owners have to *explicitly* connect to, or by the supplier/manufacturer of the station such as Netatmo. The latter option likely yields a higher degree of connectivity as data sharing is enabled by default upon installation. The density of PWS closely follows the density of the population. As a consequence, station densities are likely to be high in metropolitan areas, making them very applicable for urban flood modeling and forecasting. PWS are currently in use for operational temperature forecasting in Norway, where the number of PWS stations from only the Netatmo network outnumbered Norway's own network of WMO-compliant stations by a factor of 50 (Nipen et al., 2020). A recent study of PWS for precipitation monitoring in the Netherlands found that PWS had a density ten times higher than the manual gauge network and 100 times higher than the automatic one measured in $[\mathrm{N}_{\mathrm{stations}}/\mathrm{km}^2]$ (de Vos et al., 2019).

The largest challenge when using PWS networks is data quality i.e., inaccurate or no observations. de Vos et al. (2019) classifies three main causes of lacking data quality as *Instrumental errors*, *compromised setup* and *data processing issues*. The sensors are

produced with the aim of being affordable, so accuracy is expected to suffer. For precipitation sensors, this is illustrated by lack of wind shielding and small collection orifices, which can be viewed as instrumental errors. The most prevalent error source in PWS however, is a compromised setup. As stations are installed by hobbyists without the knowledge of proper placement, they may be installed in shielded locations, i.e., under a roof or a tree causing under-collection. Furthermore, the sensor tipping mechanism might be hindered if it is installed at an angle or clogged by debris, which will also cause over-estimation. Conversely, the station might report precipitation when it doesn't rain if the tipping mechanism is disturbed, which could happen when cleaning the station. Finally, errors can arise from data processing issues relating to the logging of measurements from the station and subsequent transfer through an aggregation network. Due to outages in wifi- and internet connection, sensors might often be unavailable and report no data or report measurements at a delay.

When analyzing PWS in the Netatmo network, de Vos et al. (2017) found that the time-stamp associated with measurements were from the time of (data) collection and not of the measurement itself. They also found that the last measurement was collected repeatedly in the event of a sensor outage.

In summary, any PWS network is highly heterogeneous, prone to errors, and exhibits systematic bias (under-collection) in the case of precipitation. Many of these challenges can be solved by innovative quality control methods, which due to the large network density can be stricter than their traditional counterparts: When using PWS for temperature monitoring, Nipen et al. (2020) used a QC method consisting of three separate filters exclusively based on spatial checks which are completely independent of past performance of the stations. This approach allowed even poorly placed stations to contribute when their placement did not affect the measurement. An approach more centered on station reputation has been proposed by Chen et al. (2018), where stations are assigned a trust score based on past performance compared with neighboring stations. A more traditional approach is proposed by de Vos et al. (2019) that takes both temporal and spatial characteristics into account. This QC method works by applying three separate filters for faulty zeroes, unrealistically high values, and outliers and is able to do bias correction. As PWS stations that measure precipitation usually also measure temperature and humidity, there exists the possibility of applying internal consistency checks. This has not yet been attempted but is an interesting research avenue.

2.3 Stakeholder Classification

In a supply chain where the principal commodity being exchanged is information in various forms, such as the case for precipitation maps and meteorological services in

general, it is common to classify stakeholders in the flow chain as *data suppliers, data processors, data users* and *end users*. Stakeholders are classified according to the way in which they benefit from being part of the supply chain. It is likely that individual organizations fulfill multiple roles within this classification. When identifying organizations for inclusion in CML or PWS precipitation mapping, this study will primarily focus on *data suppliers* and *data processors*, discounting the latter two except for a brief description.

The first group, *data suppliers*, consists of all companies and organizations operating point-to-point microwave links in the relevant frequency range ($> 5GHz$) for the CML networks. For the PWS networks, two distinct entities are included in this group: Private individuals who own the stations as well as the service or company that aggregates data from them. The primary role of this group is to log the raw data they possess and provide it together with relevant metadata. The role of the private individual is to maintain their station and allow for collection of its data. The value proposition for this group is an added revenue stream generated by selling the data to stakeholders in the second group: *data processing*. It is assumed that the achievable revenue is sufficient to recoup the costs of temporary data storage.

The stakeholders within *data processing* are providers of climatological- and meteorological data, more specifically providers or potential providers of precipitation maps. Their role would be twofold: Firstly, as customers and aggregators of the raw data, they would combine and homogenize data from multiple suppliers. Secondly, they would act as processors of the data. The data would be transformed into precipitation maps, likely through aggregation with other data sources such as traditional rain gauges and/or weather radar. The value proposition for the second group consists of adding value to the data by transforming it into spatial precipitation information for which there is a larger market. Conversely, the CML and PWS data can add precision, and thereby value, to existing products. It should be mentioned that the majority of stakeholders in this group are governmental institutions that are not dependent on direct revenue from sales but are funded through the state.

In the specific case of urban water management, the *data users* chiefly employ the precipitation maps directly through runoff modeling, real-time sewage control, calibration of sewage/runoff models, early flood warning systems, rain-event reconstruction, and short term precipitation forecasting. This group consists of consulting agencies, environmental agencies, city planners ,and researchers within hydrology, climate- and environmental science, sanitation, and runoff infrastructure.

The *end users* are classified as stakeholders extracting value through decision support for various applications such as sewage system improvement, planning, pollution moni-

toring, or simply whether to go outside or wait until a rain shower has passed.

3. Methods

To answer the research questions, a two-part study was conducted. The first part focuses on determining the first two questions, 1: to identify stakeholders and determine value propositions, and 2: to find the current capabilities of urban precipitation mapping. The supply-side stakeholders, *data users* and *end users*, were assumed to align well with those discussed in section 2.3. Further, only the most likely *data processing* stakeholder, namely The Norwegian Meteorological Institute (MET) , was considered. Consequently, the study focused on identifying *data suppliers* for the opportunistic networks. Finally, it was not attempted to quantify the value proposition to these stakeholders other than to assess whether the end products provided added benefit to current products. Current capabilities were assessed by reviewing the current products offered by MET, and the methodology for stakeholder identification is discussed in section 3.1.

The second part of the study focuses on the latter questions: 3: Determining the characteristics of the opportunistic networks in comparison to the traditional ones, and 4: determining the achievable accuracy the opportunistic methods provide. To answer these questions, the PWS and CML networks were analyzed with regard to their network characteristics (metadata) and compared to the traditional network with regard to requirements for urban hydrological applications. Further, to determine an applicable mapping method, five different interpolation techniques were tested in conjunction with a QC algorithm for the PWS network which were validated against the traditional sensor network. The best performing method was then used to create maps of prediction quality for the three networks at different aggregation times. Finally, the networks were aggregated to assess the potential quality over the traditional network alone.

For the metadata-analysis, it was decided to look at three study areas— mainland Norway as a whole, a rural area, and an urban area. The rural area was chosen as a rectangle surrounding the municipalities of Lillehammer, Hamar, and Gjøvik with an area just above 9000 km^2. The rural bounding box can be seen as a white overlay in fig. 4.3. The urban research area, hereafter called the Oslo area, intersects the municipalities Oslo, Bærum, Asker, Nesodden, and Kolbotn with an area a lot smaller, approximately 710 km^2, see fig 4.2. For interpolation and time-series analysis, only the Oslo study area

was used.

3.1 Stakeholder Identification and Data Acquisition

CML data suppliers were identified by first finding out how radio communications are managed in Norway in the hope of finding a registry of operators. It was found that they are managed through the National Communications Authority of Norway (NKOM) , which enforces the relevant regulations and manages auctions of the electromagnetic frequency spectrum for various uses.

Consulting their web page https://www.nkom.no/english, it was found that the operation of CML's can be done in one of three ways. Either through free use, simplified licensing, or through per-frequency licensing. Free use and simplified licensing are governed by the *free use of frequencies regulation* (Fribruksforskriften, 2012) articles 12 and 5 respectively. Free use includes two frequency bands in the 5 GHz range and one in the 60 GHz range and can be used with relatively low power systems, whereas simplified licensing includes frequencies in the 70 to 80 GHz range and allows the use of higher power systems. Free use and does not mandate registration, so no registry of operators exists. Use through simplified licensing mandates per-link registration; however, as of 11.02.2020, only five links were registered in this manner. The simplified license registry can be found at https://www.nkom.no/forenkletlisensiering/#/main. Per-frequency licensing gives the licensee the right to use a frequency band either nationwide or in a limited area for a specified use. A registry of licensees does exist, and it was decided to use this as a basis for identifying data suppliers.

The license registry (frekvensportalen: https://frekvens.nkom.no/#/main) was filtered to include only fixed use and frequencies above 5GHz. The resulting licensees were then contacted trying, where possible, to reach the departments/persons in charge of communications infrastructure directly. In cases where the licensee did not operate CML's directly but instead rented out the frequencies to third parties, an attempt was made to get information about their costumers and contact them in turn. 9 Likely companies were identified and contacted (see table 4.1). None of them would send updated metadata, so a data-set from the Telia network collected by Hoås (2018) was used. Repeated requests for signal-loss data were also made, but not responded to. The CML stations are listed in the **CML** row of table 4.3

PWS network operators were identified by a quick internet search as well as consulting literature on the subject (Butler, 2019; Nipen et al., 2020; de Vos et al., 2020). As these companies chiefly operate internationally, identifying them was comparatively easy. The PWS networks identified are listed in table 4.2. As the Netatmo network had the

broadest coverage (in Norway) as well as (free) access to individual stations through their API https://dev.netatmo.com/apidocumentation/weather#getpublicdata (Application Programming Interface) , it was chosen for this study.

An advantage of the Netatmo network is that all stations are of the same model and have equal error characteristics. From the manufacturer specifications, the Netatmo precipitation gauge has a measurement range between 0.2 and 150 mm/h, with a stated accuracy of 1 mmm/h and a tipping bucket volume (or resolution) of $0.1mm$ (Netatmo, 2020). These metrics were assumed unknown while producing the results. This was done as the actual error is likely far larger due to incorrect operation as discussed in section 2.2.3. Further, PWS networks, in general, can include multiple station models from differing manufacturers, and the model information might not be included in network metadata.

Metadata for the network was requested using bounding boxes for the national, rural and urban study areas. For the Oslo study area, it was found that the API returned stations outside the bounding box, so a negative buffer was introduced. This technique was necessary as the API only allows a fixed number of stations to be returned.

As Netatmo does not provide access to historical records, a logger was set up between the dates 2020-03-26 and 2020-05-11. The logger was written in python with the pandas (Reback et al., 2020) library using an AWS EC2 instance for hosting. The logger requested the last 60-minute accumulated precipitation from the stations in the Oslo study area using the same bounding box as for the metadata collection. After it was found that more stations were included in the time-series than the original metadata-set, the bounding box was divided into nine sub-areas, and metadata was re-requested for each subarea every 15 minutes over three days. The result of these requests are listed in the Oslo column of table 4.3, whereas the number of stations in the rural column is based on a single request.

Metadata for the traditional gauge network, as well as historical records for the study period, hereafter referred to as the MET data-set, were gathered using the FROST API https://frost.met.no/index.html, which allows access to all of the Norwegian meteorological institute's stations as well as partner stations owned and operated by municipalities and organizations. The number of stations is listed in table 4.3, where they are divided by owner and whether or not they are WMO certified.

3.2 Data Pre-Processing

Metadata from all sources were read into separate GeoDataFrames (Jordahl et al., 2020), a python object for geo-referenced tabular data. The CML data was added with line

geometries and the other networks as points. The CML data did not include elevation, and it was added to the data-set by overlaying a DTM raster of 50*50 meters (see appendix A) using QGIS software (QGIS Development Team, 2019). The elevation assigned did not include any assumptions of tower height and was calculated as the average between the base of the two towers creating the link. The MET metadata did not include information about the minimum temporal resolution of the stations, though the requests could be filtered by available temporal resolution. The available temporal resolution was gathered by repeated requests, specifying different temporal resolutions iteratively from *monthly* to *1-minute*. The responses were then merged together in the same order, where each station received the resolution of the finest resolution response it was included in.

After processing, the data-sets were then converted to the same coordinate reference system (CRS) EPSG:32632 or UTM32N. The column names and units were also homogenized into the same measurement units. The metadata was merged into a single table and stored as a GeoJSON file.

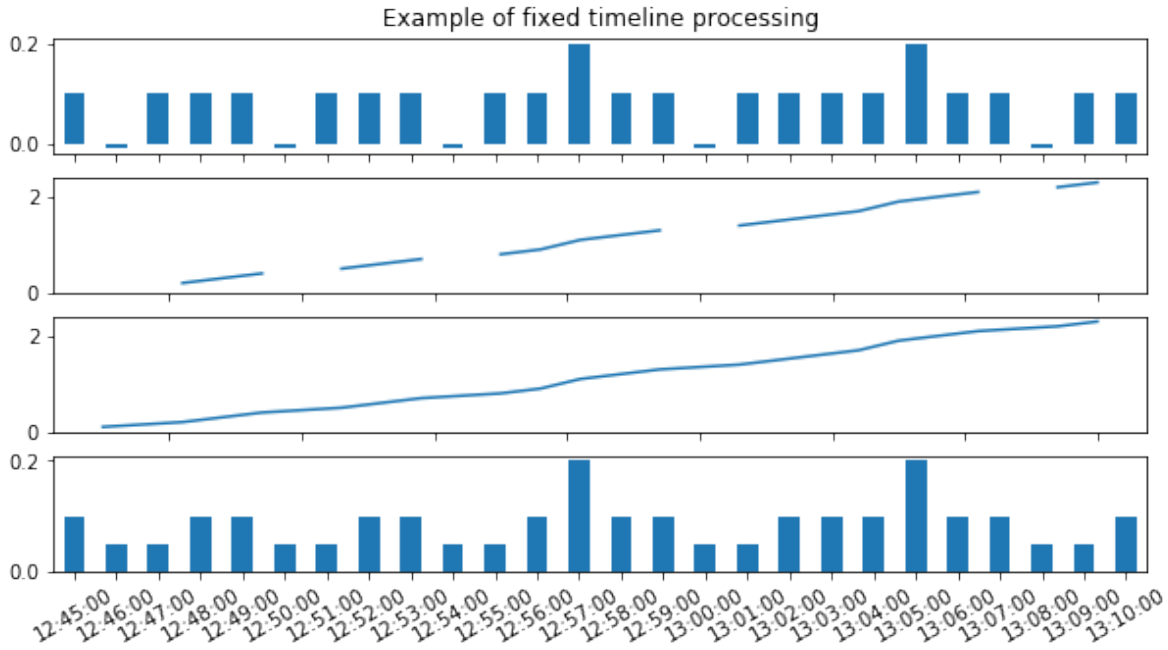

Figure 3.1: Fixed timeline processing example as applied to 1 min MET time-series. A cumulative sum is performed, missing values are interpolated, and the cumulative difference is taken. All values are in [mm] (cumulative mm for the second and third plot).

The 1 min MET time-series were returned only for minutes with > 0.1 mm of precipitation, i.e., the typical resolution of a tipping bucket pluviometer, creating holes in the time-series. The data were re-sampled using fixed timeline processing, exemplified in figure 3.1. The algorithm works by creating a cumulative sum of the time-series and linearly interpolating the missing values, and then the cumulative difference is taken.

The algorithm relies on two fundamental assumptions: 1: that the missing values in the data are a result only of precipitation being less than the tipping bucket volume, and not due to errors in measurement or data collection. And 2: That the rain rate is constant between tips up to a set duration, in this case, 15 minutes. If the duration of missing values is greater than the duration of assumed constant rain rate, the missing values are interpolated using a forward-fill method. The algorithm used is attached in appendix C.

3.3 Metadata Analysis

The stations from the different sources were first plotted together over a background map for the study areas to get an overview of coverage and network and clustering. Density plots were then generated nationally and for the two study areas using a rolling window approach: The area of interest was first gridded with a set resolution. Then, for each grid-cell, a circle was spanned of a given radius, and the number of stations within that circle was counted. The grid cell was then assigned a density [n/km^2 for each station type dividing the station counts by the area of the circle. The resulting densities were compared to optimal densities given typical catchment sizes using the methodologies presented in Berne et al. (2004) and Ochoa-Rodriguez et al. (2015).

Network representativeness was analyzed by creating cumulative elevation distributions, also called hypsometric curves (Zävoianu, 1985) for each network and the underlying topography. The curves were created nationally and for each study area. The topographic hypsometric curve was created based on the DTM raster given in appendix A using the rasterio python package (Gillies et al., 2013).

To determine expected accuracy of the CML network, the theoretical precipitation was calculated for all links in the network for two different attenuations: $A = 0.1\,\mathrm{dB}$ and $A = 1\,\mathrm{dB}$. The selected attenuations serve as lower and upper bounds for the quantization intervals that can be expected from CML network operators. As the relationship between precipitation and attenuation is nearly linear, these values are used as proxies for per link expected error (α) in [mm/h]. The calculation was done in with equation (2.15). Parameters a and b were calculated in with equations from ITU-R (2005). The specific method is listed as *calculate_alpha* in appendix C. The errors calculated were visualized as histograms and plotted together with the dependents: link length, frequency, and polarization.

3.4 Event Selection and Quality Control of Stations

After the Netatmo time-series was collected from the logger, it was analyzed with special attention to station availability and measurement age to determine the degree of network homogeneity and temporal accuracy. The median precipitation (fig. 3.2) was used to determine the study period. The interval between the dates 2020.04.27 and 2020.05.05 contained most of the precipitation and was selected. Time-series data from the MET network was then downloaded and plotted against the Netatmo network to gauge the consistency between the networks.

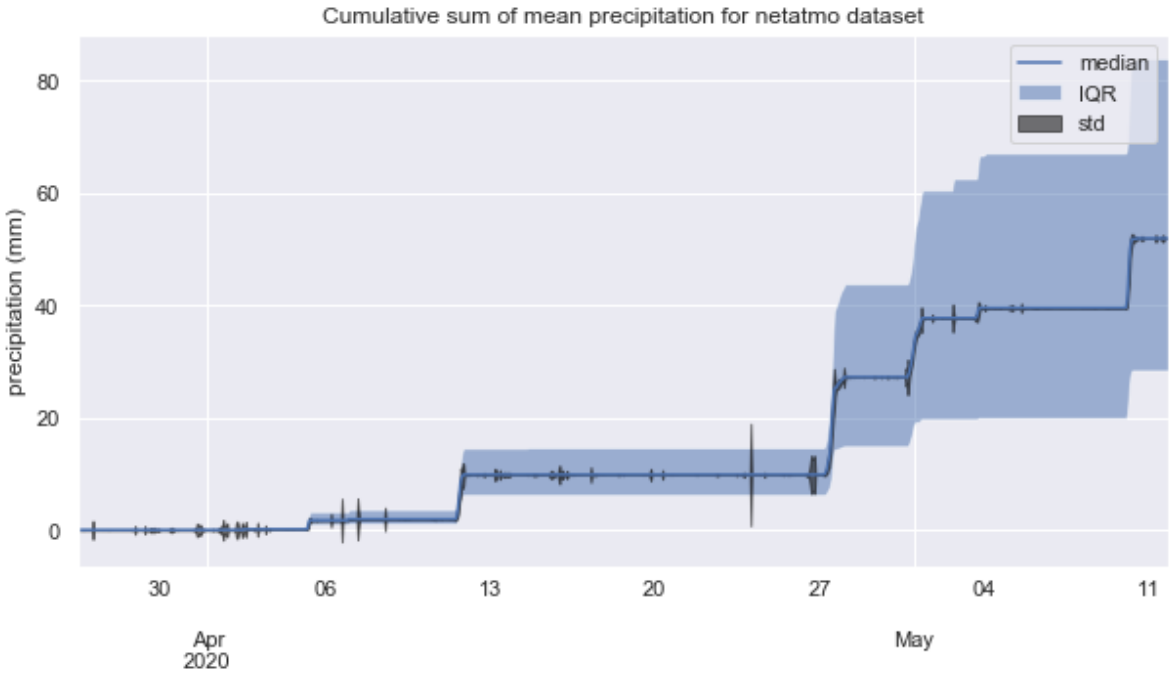

Figure 3.2: Cumulative median precipitation in the Netatmo network during entire collection period with associated interquartile range. The black line resembles ± the standard deviation of precipitation at each hour.

The quality control algorithm implemented was created based on methods employed by Nipen et al. (2020) and de Vos et al. (2019). Given that the network morphology is highly dynamic with a low station availability, it was decided to implement checks that only considered current measurements and spatial relationships and do not rely on any time-series information. This strategy enables the automatic inclusion of new stations in the network and could potentially allow stations that aren't accurate under certain conditions, e.g., wind shielding from a certain direction, to contribute to the network when the conditions are favorable.

The algorithm consists of three checks, an isolation check, a faulty zero check, and a buddy check. The isolation check is based on the assumption that nothing is known about the quality (placement, accuracy, etc.) of the stations beforehand, and can only be

determined by comparing neighboring measurements. The check essentially determines whether the number of neighboring measurements is sufficient and works by flagging stations that have fewer than $n_{isolation}$ neighbors within a radius of $r_{isolation}$ meters.

The faulty zero check aims to find malfunctioning stations that fail to report precipitation and can be viewed as a test of agreement between the station in question and the neighborhood consensus. The check finds the median precipitation of neighboring stations within a radius of r_{fz} meters. If the median is above zero and the station in question reports zero, the station is flagged.

The buddy check aims to remove stations that report unlikely values, thereby removing unrealistic short scale variation from the network. It works by finding the mean and standard deviation of the neighboring stations within a radius r_{buddy}. If the station under consideration reports a value that is more than two times the standard deviation away from the neighbor mean it is flagged.

In principle, the parameters can be adjusted individually; however, it was found that the following combination yielded acceptable results:

$$\left.\begin{aligned} n_{isolation} &= 5 \\ r_{isolation} \\ r_{fz} \\ r_{buddy} \end{aligned}\right\} = 3000\,\mathrm{m}$$

The QC algorithm is part of a pipeline algorithm that takes the network metadata, the network time-series, and a timestamp as arguments. It constructs a table consisting of the station metadata and precipitation and removes stations with missing precipitation measurements. The pipeline then applies the QC algorithm and drops stations with any of the above flags present. Alternatively, the pipeline can be configured not to drop stations, or drop stations with specific flags only.

For this study, it was assumed that the stations in the MET network were quality controlled and appropriately corrected before they were gathered through the API. Subsequently, no QC was applied to this network other than a cursory visual inspection of reported precipitation (see fig. 4.15). This inspection revealed that two stations, SN19670 and SN18815, were malfunctioning by reporting no precipitation for the whole, or part of the study period. The presence of these stations indicates that the quality of the data might, in reality, be lower than assumed.

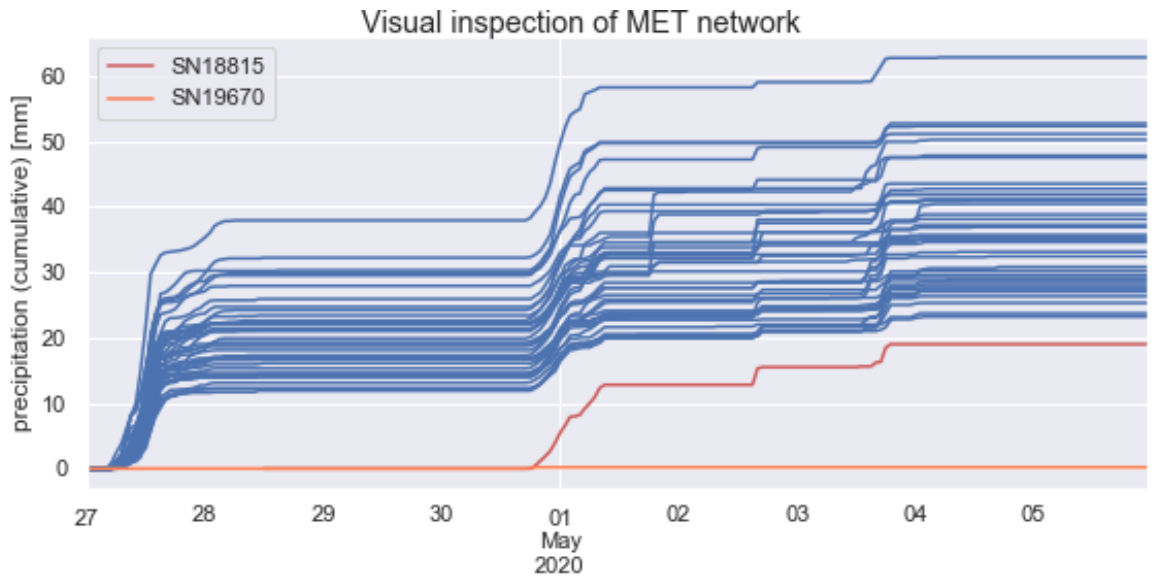

Figure 3.3: Visual inspection of MET time-series. Each line represents the cumulative sum of precipitation for a single station over the study period. The malfunctioning stations are marked in red.

As no precipitation data for the CML network was gathered, no quality control for this network type was implemented as part of this study.

3.5 Spatial Structure Analysis and Creation of Uncertainty Maps

To assess the spatial structure of precipitation in the Oslo study area, climatological variograms from the MET network were created. A climatological variogram can be viewed as the averaged variogram over multiple precipitation instances (time steps). It is created by producing an empirical variogram with equal binning, see (2.5), for each time step with precipitation over a given threshold. The empirical variograms are then standardized, dividing all the bins by the highest occurring variance. Finally, for each bin, the average over all the time steps is calculated and assigned to that bin in the climatological variogram. This is exemplified by equation (3.1) where $\hat{\gamma}(d)$ corresponds to the variogram value at bin d and N_t is the number of time steps included. After $\hat{\gamma}(d)_{climatological}$ is computed for all bins, a theoretical variogram model is fitted.

$$\hat{\gamma}(d)_{climatological} = \frac{1}{N_t} \sum_{i=1}^{N_t} \hat{\gamma}(d)_{i,standardized} \tag{3.1}$$

The variograms were created for 1-, 10-, 60-minute, and 1-day aggregation times from the MET network. Climatological variograms were also created for the Netatmo net-

work with and without applying QC to assess QC efficiency. The calculation, fitting, and plotting was accomplished using a slightly modified version of the skgstat package (Mälicke and Schneider, 2019). The empirical variograms were computed using a uniform binning structure so that an approximately equal amount of observation points were within each bin. Due to the large difference in network size, it was decided to use 10 bins for the MET network and 15 bins for the Netatmo network. The *gaussian* variogram model, eq. (2.3) with $\beta = 2$, was chosen as the theoretical model to fit as it most closely approximated the shape of the empirical variogram.

The computed variograms were used together with the best performing interpolator identified during validation to create maps with expected (standardized) error for the three networks considered in the Oslo area. The maps were first computed for a 60-minute aggregation time using the corresponding variograms for the Netatmo and MET networks. For the CML network, the expected error map was estimated using the MET variogram modified to include a zero nugget. The nugget values were added back in on a per-station basis using the expected error (α) at a 0.1 dB quantization interval. During the mapping procedure, the CML links were approximated by points at the link center. To construct the 10 and 5 minute error maps, the range of the variograms were modified to resemble the spatial structure corresponding to the aggregation time recommended by Berne et al. (2004) for intense precipitation.

3.6 Comparison of Interpolation Methods

Five separate interpolation algorithms were considered for precipitation mapping based on the Netatmo PWS network: Nearest Neighbor (NN), Inverse distance weighting (IDW), Universal Kriging with regional-linear drift (UK), and Gaussian Process Regression (GPR). The UK model differs from the Ordinary Kriging model discussed in section 2.1.1 in that it additionally fits a linear trend model over the surface (Goovaerts, 1997, p. 139). The constrained GPR model can be viewed as a statistical-black box hybrid model as it very closely resembles Simple Kriging, but tunes its parameters without using a variogram.

It should be noted that other explanatory variables, such as elevation, were not implemented for any of the models. The correlation was examined briefly by visual inspection and regression fitting (fig. 3.4), and the resulting correlation was found to be weak for both networks.

The NN and IDW models were made by modifying the KNeighborsResgressor from Pedregosa et al. (2011). The NN model was created by forcing $N_{neighbors}$ to 1, and the IDW model by setting $N_{neighbors}$ to the number of observations in the data-set at the current

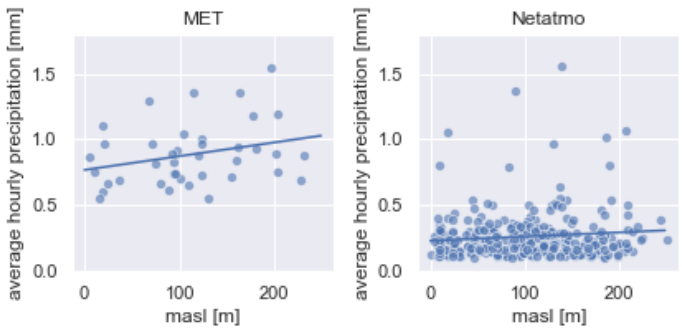

Figure 3.4: Mean precipitation for each station in the two networks plotted against station elevation. Stations were filtered to exclude ones where mean precipitation was less than 0.1 mm.

time, and implementing (2.8) as a custom weight function. Both the GPR models were created by implementing a aussian covariance function in the GaussianProcessRegressor from Pedregosa et al. (2011). For the manual model, the optimization was turned off, and the covariance function parameters were set to those of the calculated empirical variogram. The specific implementation of the models are listed in table 3.1 and the code in appendix D.

Interpolator	Parameters
NN	-
IDW	$p = 1$
UK	model: gaussian, variogram bins: 10, drift: regional linear, automatic fitting
GPR	
Constrained	model: gaussian, $nugget \in (0, 1)$, $sill \in (0.02, 1)$, $range \in (10, 10^5)$ m, automatic fitting
Manual	model: gaussian, $nugget = 0.42$, $sill = 0.55$, $range = 20902.1$ m

Table 3.1: Interpolator parameters. Parameters of manual GPR correspond to those determined by the climatological variogram in fig. 4.14(b).

It was decided to validate the interpolation methods against the MET dataset for all hours in the study period where the median precipitation was greater than or equal to 0.1 mm, which resulted in 38 observation sets (see fig.3.5). The stations were validated for both the entire MET network as well as for the two WMO compliant stations alone. The value for each (MET) station was predicted for each method for every observation set and stored in an array $\mathbf{y}_{predicted}$. Another array was created with the measured (true) values at the points: $\mathbf{y}_{true}$. The values were stored in the same order so that $y_{predicted,i}$ is at the same time and location as $y_{true,i}$ for all i.

To evaluate the performance, the following metrics were used: bias, relative bias, root mean squared error (RMSE) , and the coefficient of determination (R^2). The equations

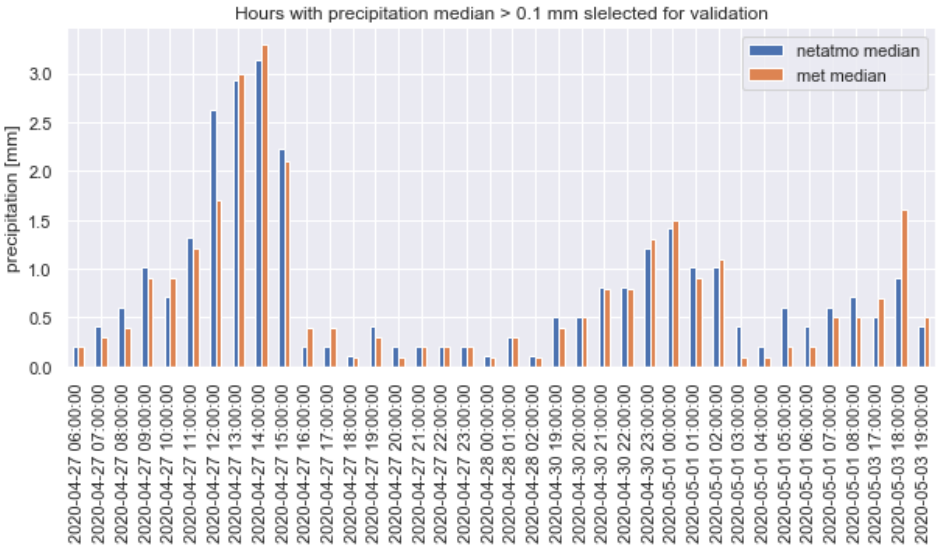

Figure 3.5: Median precipitation from netatmo and MET dataset for all hours included in validation.

for these metrics are given in (3.2). The bias and relative bias are used to assess whether the interpolated values are higher or lower than the measured values on average, the latter being relative to the mean of $\mathbf{y}_{true}$. RMSE is a measure of the error of the interpolation in [mm] (lower is better), and R^2 is a measure of how good the prediction of the interpolated value is, a perfect fit would yield $R^2 = 1$.

$$\begin{aligned} bias &= mean(\mathbf{y}_{predicted} - \mathbf{y}_{true}) \\ relative\ bias &= \frac{bias}{\bar{\mathbf{y}}_{true}} \\ RMSE &= \sqrt{\frac{\sum_i^n (y_{predicted,\,i} - y_{true,\,i})^2}{n}} \\ R^2 &= 1 - \frac{\sum (y_{true,\,i} - y_{predicted,\,i})^2}{\sum (y_{true,\,i} - \bar{\mathbf{y}}_{true})^2} \end{aligned} \tag{3.2}$$

Lastly, the possibility of combining the networks was assessed by implementing the Best Combined Spatial Predictor (PCSP) (Hengl, 2009, p. 35) algorithm to create a single precipitation map from the three networks. The algorithm combines predictions from different interpolation models (spatial predictors) weighing the predicted values $\hat{z}(\mathbf{u})$ by the inverse of their associated uncertainty (error) $\hat{\sigma}(\mathbf{u})$ at every point $\mathbf{u}$:

$$\hat{z}_{BCSP} = \frac{\sum_{i=1}^{n} \left(\hat{z}_{SP_i}(\mathbf{u}) \frac{1}{\hat{\sigma}_{SP_i}}(\mathbf{u}) \right)}{\sum_{i=1}^{n} \frac{1}{\hat{\sigma}_{SP_i}}(\mathbf{u})} \tag{3.3}$$

where there are $SP_i, i = 1, .., n$ spatial predictors. The algorithm can be applied to any set of predictors capable of producing error estimates where it is important that their errors are scaled equally. The resulting error, $\hat{\sigma}_{BCSP}(\mathbf{u})$, can be assessed by $\hat{\sigma}_{BCSP}(\mathbf{u}) \approx \min[\hat{\sigma}_{SP_1}(\mathbf{u}), ..., \hat{\sigma}_{SP_n}(\mathbf{u})]$. The resulting error is valuable to identify problematic areas with low coverage or high uncertainty, it has no statistical basis, and therefore shouldn't be used as an accurate error estimate.

The BCSP was applied to all three networks at 13:00, 2020-04-27. The models used were three versions of the manual GPR, the same that were used to compute uncertainty maps for a 10 minute aggregation time. Precipitation data for the CML network was synthesized by drawing samples from the predictor associated with the MET network. The sampling equates to drawing a number from a distribution centered on the predicted value with a standard deviation equal to the predicted error. If the sampling returned negative values, they were set to zero.

4. Results

The results are presented in approximately the same order as the methodology described to achieve them. Section 4.1 chiefly deals with research questions 1 and 2, concerning stakeholders and current capabilities, whereas the remaining sections detail the results concerning network characteristics, accuracy, and applicability.

4.1 Stakeholder Analysis and Current Capabilities

The results of the stakeholder identification are summarized in tables 4.1 and 4.2 for the CML and PWS networks respectively. For the CML case, most of the identified organizations either didn't respond to requests or would not disclose any information regarding network size metadata indicating that disclosing the information would constitute a risk to critical communications infrastructure. The respondents were also asked under what circumstances sharing the data would be permissible. In summary, the answers were that one or multiple of the following criteria had to be met: A non-disclosure agreement had to be signed, all work done with the data had to be done on internal servers, or the people working with the data had to have security clearances issued by The Norwegian National Security Authority (NSM).

Company	type	network size (number of links)
GlobalConnect	ISP	N.A.
Telenor	ISP/mobile	4300
Bane Nor	Infrastructure	secret
Statnet	Infrastructure	N.A
DSB	Emergency network	N.A
Telia	ISP/mobile	1400
Norwegian armed forces	military	secret
Avinor	Infrastructure	secret
Tampnet	ISP (offshore)	N.A.

Table 4.1: Overview of identified CML operators in Norway. Network size refers to number of links with a frequency above 5 GHz. "N.A." denotes stakeholders that likely operate CMLs but did not respond to requests, "secret" denotes stakeholders who confirmed operating CMLs, but would not specify network size.

Given the data in table 4.1, any estimate of total network size if all stakeholders decided to participate would be inaccurate. However, a minimum combined network size would be 6000 links. This corresponds to an average link density three times higher than for the network included in this study.

The information presented in table 4.2 was gathered by investigating what products the PWS network services provide to consumers through APIs and web services. The services can loosely be classified into station manufacturers, for-profit networks, and not-for-profit networks. The not-for-profit networks are CWOA (Citizen weather observer program), WOW UK, and WOW NL. The latter two are essentially the same network as they are made as a collaboration between the British and Dutch meteorological offices. Both of the WOW networks offer station access through APIs, and the CWOP provides access through a web page. The station manufacturers: (Netatmo, AmbientWeather, WeatherLink, and AcuRite) generally don't offer public access with the notable exception of Netatmo. The for-profit networks (Weather Underground, PWS weather, and Open Weather) generally do not provide individual station access, as their business model involves delivering end-products; forecasting, and current conditions etc., directly. However, it should be noted that partnerships such as the one between Netatmo and MET that serves as part of operational temperature forecasting (Nipen et al., 2020), where data is transferred directly, could possibly be entered in to with any of the services identified.

Name	coverage (Norway)	public access	individual station access
Weather underground	medium	paid	no
CWOA	low	free	yes
PWS weather	low	paid	yes
OpenWeather	unknown	paid	no
AcuRite	unknown	none	no
WeatherLink	unknown	none	no
AmbientWeather	low	none	no
Netatmo	high	free (limited)	yes
WOW UK	low	free	yes
WOW NL	low	free	yes

Table 4.2: Overview of PWS network services

To identify current capabilities, it was decided to look into two domains, historical precipitation maps, and nowcasting. The best available historical precipitation map is the seNorge2 precipitation data-set, available at senorge.no or in higher detail at thredds.met.no: `https://thredds.met.no/thredds/catalog/senorge/catalog.html`, METs archive. Its temporal resolution is 1 day going back to the year 1957 and its spatial resolution is 1 by 1 km. It is based on METs rain-gauges and an Optimal Interpolation procedure. Further details about its production can be found in its associated publication: (Lussana et al., 2018). However, a newer, non-operational dataset, seNorge_2018, with the same characteristics but better performance in mountainous areas is soon expected to supersede it (Lussana et al., 2019).

Current operational nowcasting is based on radar data from 11 C-band radars located along the Norwegian coast. The nowcast is updated every 7.5 minutes with a lead time of 90 minutes. Its spatial resolution is 1 by 1 km, and its availability extends to most of the Norwegian mainland, with the exception of areas far inland and at higher elevations. As it is a radar-based product, precipitation nowcasts are given categorically (low, moderate, heavy) (Yr.no, 2020).

4.2 Metadata Analysis

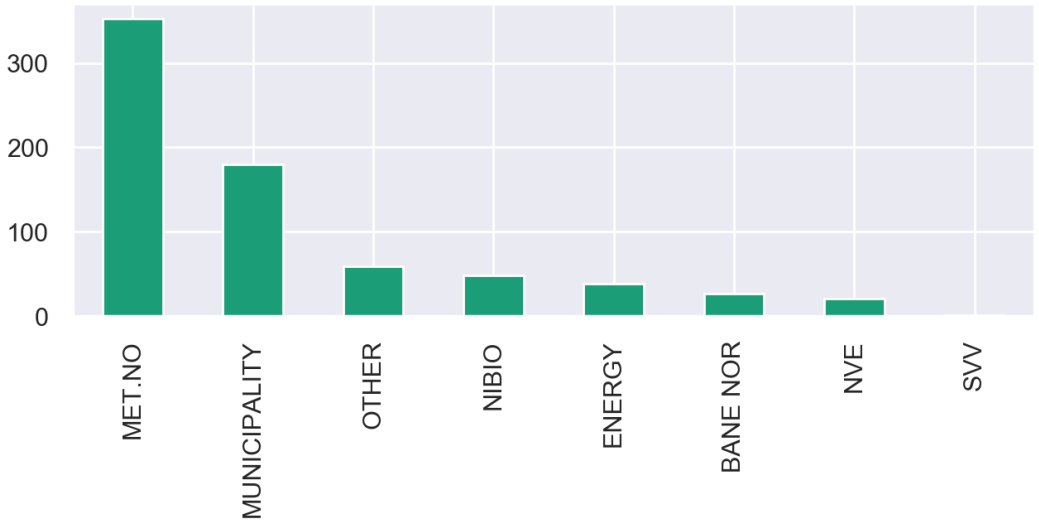

Figure 4.1: Distribution of station owners in the MET network

An overview of the number of stations is presented in table 4.3, where stations are classified by study area and source. In the MET network, approximately 50% of the stations are owned and operated by MET, and the remainder are operated by partners (fig. 4.1), most of them being municipalities. Nationally the CML network is about twice the size of the traditional network, including all partner stations. The same relationship is apparent in the rural study-area, though not in the Oslo area. This is explained by the large number of partner stations in Oslo owned and operated by the Oslo municipality. Regrettably, the number of stations from the Netatmo PWS network was not gathered due to limitations in the API it was gathered through. In the Oslo study area, the Netatmo network is almost 15 times larger than the MET network. However, as discussed later, the average number of stations available at any single moment is closer to 280 stations, making it six times larger than the MET network. In the rural study area, in which stations were gathered with a single request, the average density is about eight times higher than the MET network. It is highly likely that this relationship extends to the National level to some degree.

The stations from the networks within the Oslo study area are plotted by color together with the bounds of the study area in figure 4.2. From the figure, the difference in density is well illustrated. Looking at how the stations are distributed, extent and clustering can be assessed. The MET and Netatmo network are both clustered in populated areas with approximately the same spatial extent. The CML network has a slightly different structure: there is a cluster of short and medium-length links in the north-eastern quadrant of the study area, with fewer, and longer links in the remaining quadrants.

	stations in Norway	Stations in Oslo area	Stations in rural area
Netatmo	N.A.	676	146*
CML	1465	58	43
MET	727	46	18
WMO	205	2	7
non WMO	199	3	4
partners	323	41	7

Table 4.3: Number of stations from the three networks: Netatmo, MET through frost, and the CML network. (*): The netatmo stations in the rural area are based on a single request to their API and might be lower than the true value. **WMO** denotes WMO compliant stations in the MET network, **non WMO** denotes non WMO compliant stations owned and operated by MET, and **partners** denote stations from the MET data-set owned and operated by municipalities and other organizations.

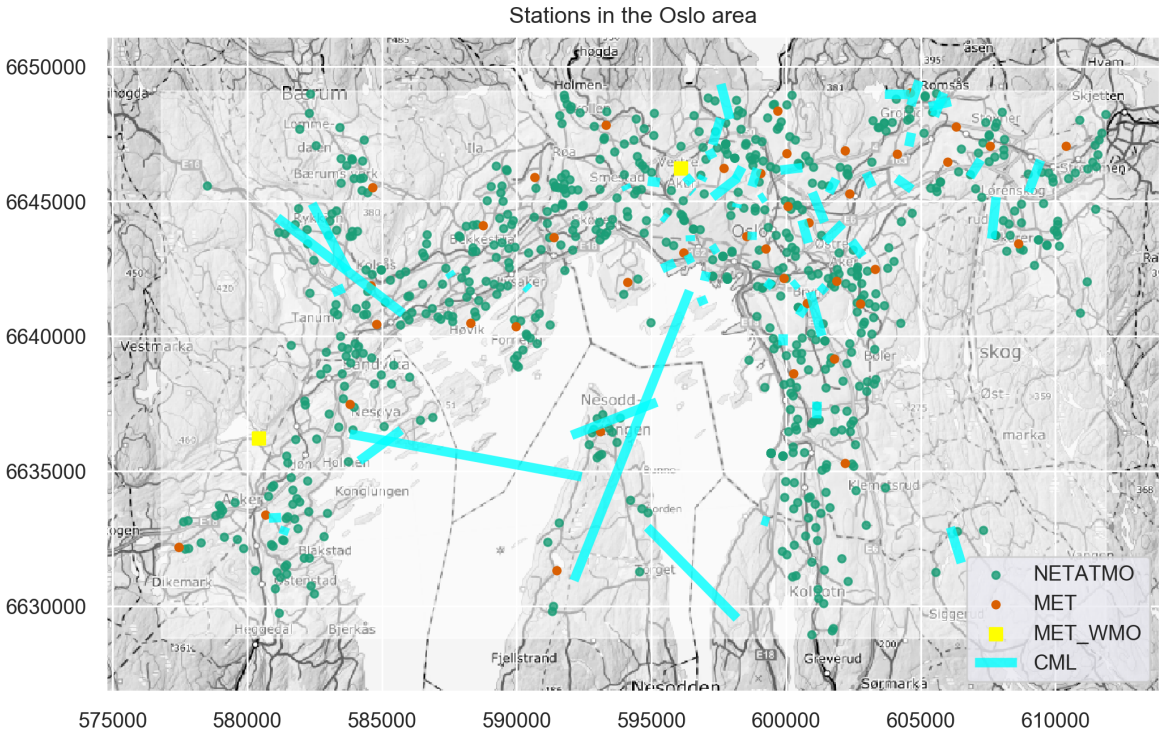

Figure 4.2: All stations within the oslo study area. The boundary of the study area is given by the white overlay. The CML stations have been fuzzed so that their locations are not exact.

The network characteristics differ significantly in the rural area (figure 4.6), where all networks are more evenly distributed. The Netatmo network still shows clustering in the population centers Gjøvik and Hamar but has the largest spatial extent with considerable coverage throughout the area. In the rural area, the CML network contains a higher degree of longer links than in Oslo, and the majority of them are across the Mjøsa river. This is a natural consequence of the geography and population distribution as large

distances of undeveloped land and rivers present barriers to buried communications infrastructure such as fiber-optic, or copper, cables.

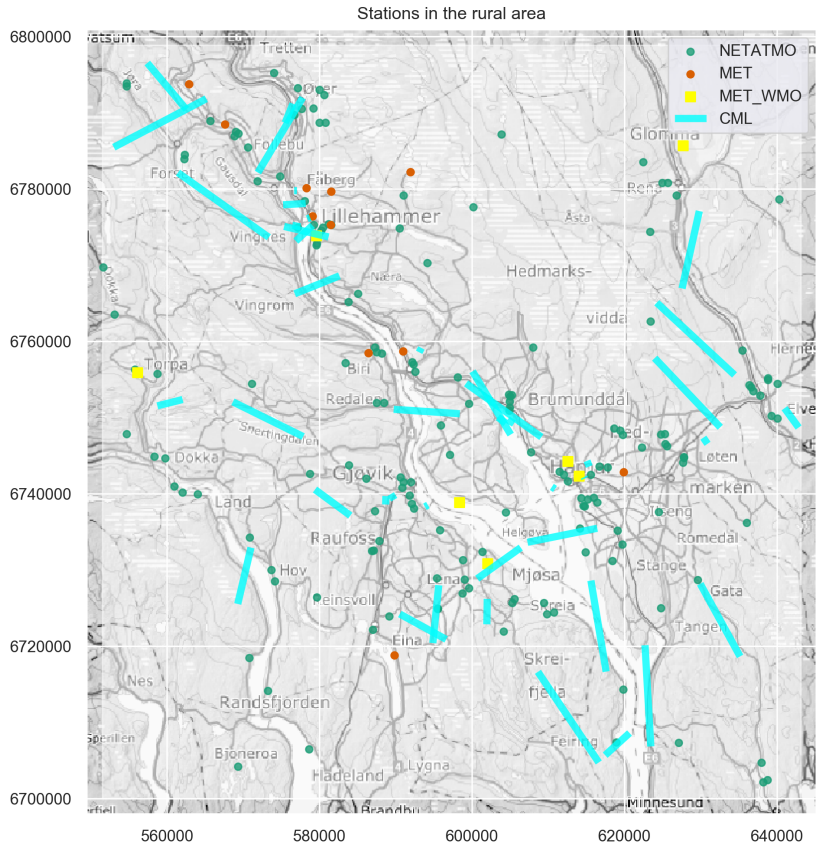

Figure 4.3: All stations within the rural area. The boundary of the study area is given by the white overlay. The CML stations have been fuzzed so that their locations are not exact.

4.2.1 Station Density and Coverage

Recommended network resolutions for urban hydrological applications are listed for select catchment sizes in table 4.4. The recommendations assume Δt is equal to the response time of the catchment and coverage of 87% of all variability. According to Fleig and Wilson (2013), more than half of the flood estimations performed at The Norwegian Water Resources and Energy Directorate (NVE) between 2007 and 2011 were requested for catchments under 20 km^2, and about 25% for catchments smaller than 5 km^2. Conversely, the municipality of Oslo considers response times of 10 minutes to be significant for localized flooding and 2 to 6 hours for city-wide flooding (Kvitsjøen, personal communication, May 5th, 2020). Consequently, the range of temporal resolutions up to 10 minutes are relevant for urban precipitation mapping.

$S[\,\mathrm{km}^2]$	$\Delta t\,[\mathrm{min}]$	$\Delta r\,[\mathrm{km}]$	$S_r[\,\mathrm{km}^2]$	$D_{target}\,[\mathrm{n/km}^2]$	$r_{range}\,[\mathrm{km}]$
5	4.52	3.19	7.98	0.125	9.56
10	5.56	3.54	9.83	0.102	10.61
25	7.32	4.06	12.93	0.077	12.17
50	9.01	4.50	15.92	0.063	13.51
100	11.09	5.00	19.61	0.051	14.99
1000	22.14	7.06	39.12	0.026	18.54
10000	44.17	9.97	78.05	0.013	22.80

Table 4.4: Recommended network resolution for intense precipitation reconstruction from Berne et al. (2004) in time (Δt) and space (Δr) for given urban catchment sizes calculated using (2.12). Also listed are the representative area (S_r) for a given rain gauge, and the associated network density ($D_{target} = 1/S_r$) as well as the range or decorrelation distance (r_{range}) for precipitation at the temporal resolution.

Figure 4.4 gives an overview of the station distribution and density of the CML and MET network nationally. Both networks have a high density in the area around Oslo. In the rest of the country, the CML coverage is far higher along the coast, specifically in population centers, whereas the MET network is more evenly distributed. Comparing the density to the target density associated with a 10 minute response time from table 4.4, we see that the MET network has low coverage throughout most of the country.

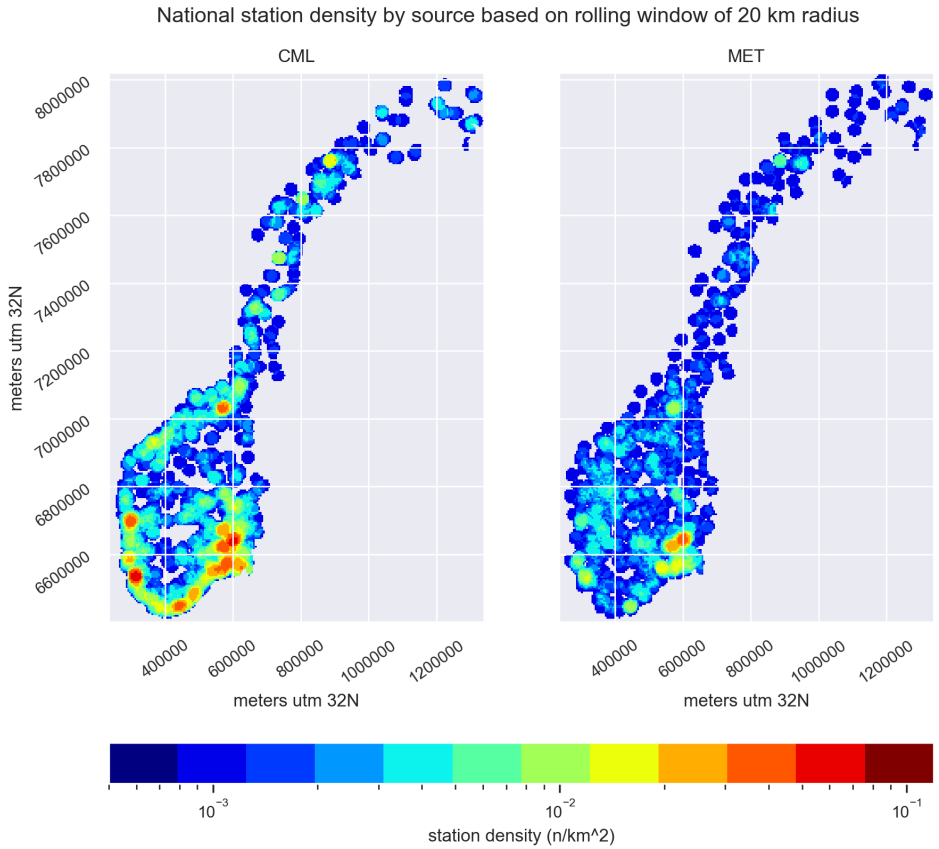

Figure 4.4: Station density of MET and CML stations netionally.

Figure 4.5 shows the same overview for the Oslo study area. Here, the MET network has a density surpassing the target density for 10 min concentration-times ($0.05\,\mathrm{n/km2^2}$) throughout most of the populated area. The same is true for a concentration-time of 5 minutes (corresponding to $0.1\,\mathrm{n/km^2}$) for most of the urban center. When looking at the CML network, the effect of clustering becomes apparent. Here, only part of the populated areas has sufficient density corresponding to 10 minute concentration-times. The density advantage of the Netatmo network is clear from figure 4.5, where the target density is sufficient for response times down to 5 minutes throughout the whole study area, with a density between 5 and 6 times greater than required in the Urban center.

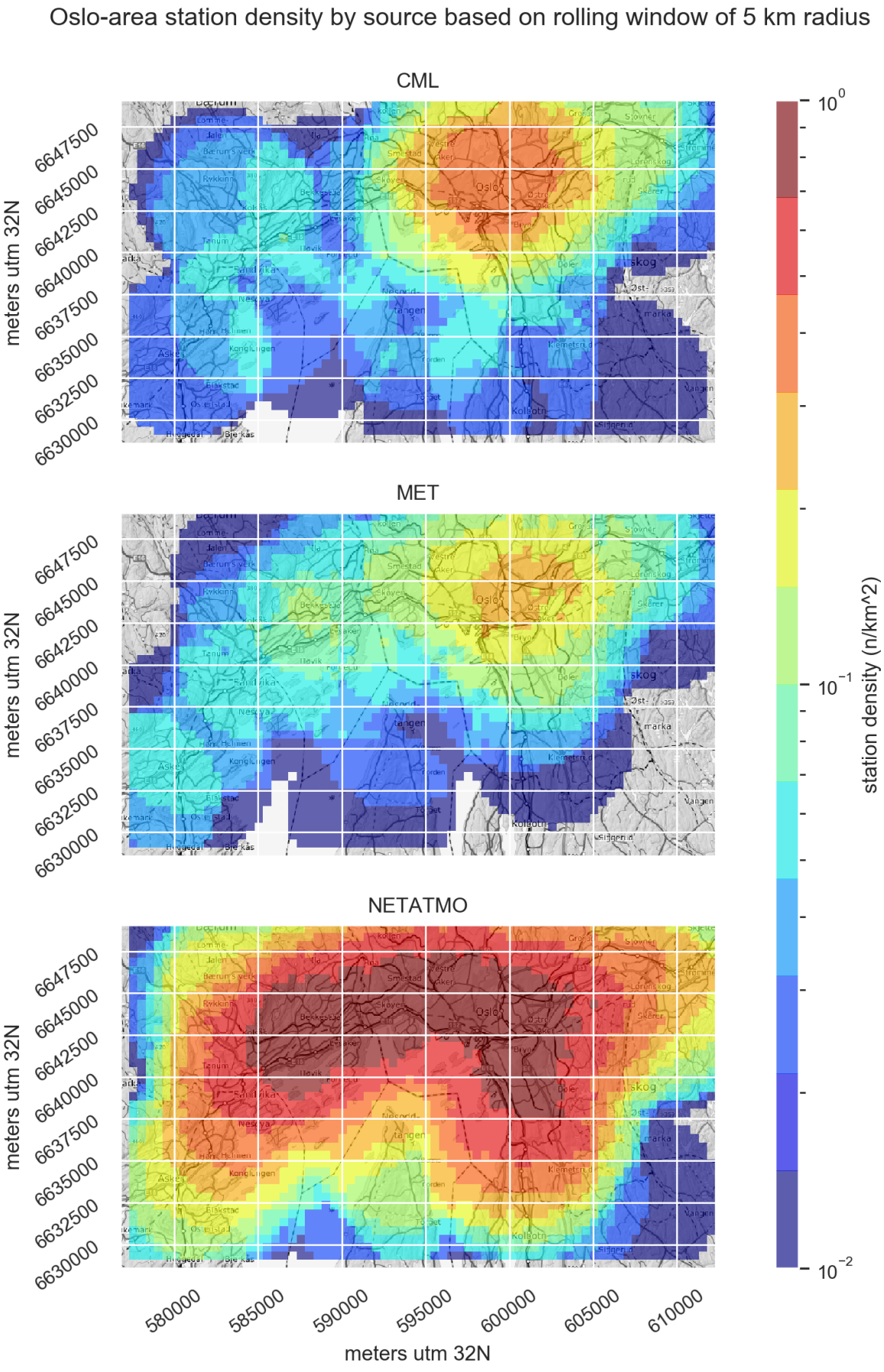

Figure 4.5: Station densities in the Oslo study area.

A corresponding map for the rural study area is presented in figure 4.6. In this area, all the networks have lower densities, and it is more relevant to look at the target densities for one- to three-hour concentration-times, namely $9 * 10^{-3}$ to $3 * 10^{-3}$ n/km^2. The Netatmo network exceeds both of these requirements, whereas the MET network meets only the lower criteria (3-hour concentration-time) in parts of the study area. The CML network exceeds the target resolution of $3 * 10^{-3}$ n/km^2 throughout most of the area, and meets the $9 * 10^{-3}$ n/km^2 where it is the most dense.

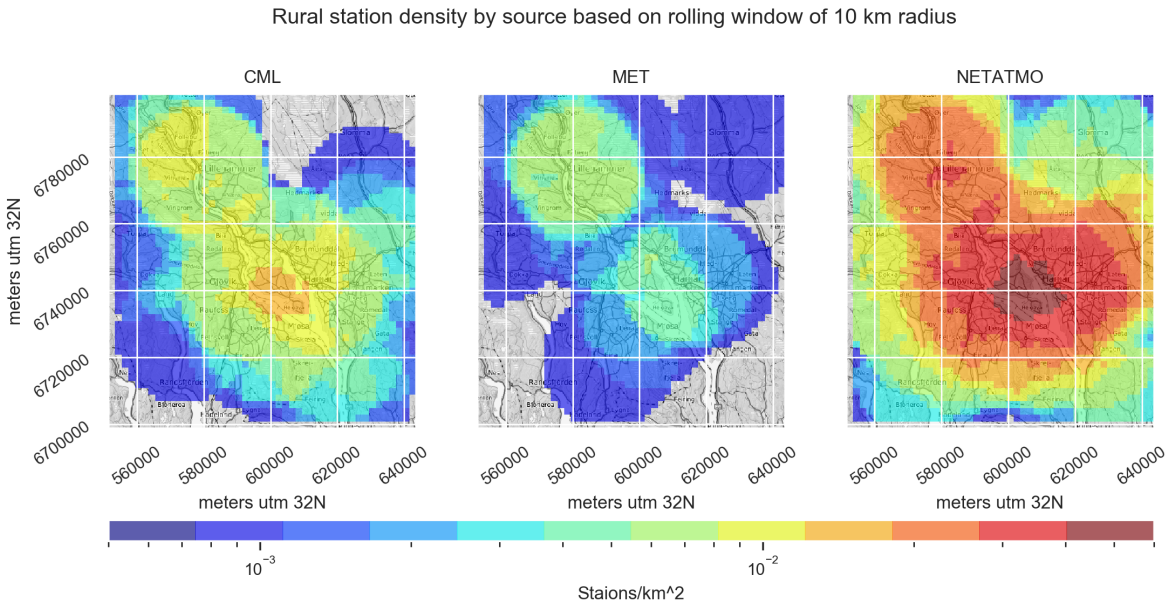

Figure 4.6: Station densities in the rural area.

From the hypsometric curves (figure 4.7), the networks' topographic representativeness can be assessed by inspecting how close the network distributions are to the topographic distribution (DEM). Both nationally and in the two study areas, all networks are biased towards lower elevations. For the national analysis (fig.4.7 a), all three networks follow a similar distribution. The extent of the MET network in terms of elevation exceeds the CML network by almost 500 meters. This is to be expected as MET, being a traditional network, stations are placed with topographic representativeness in mind. The distribution of Netatmo stations nationally is not a valid result as it is based on a sub-sample of approximately 140 stations.

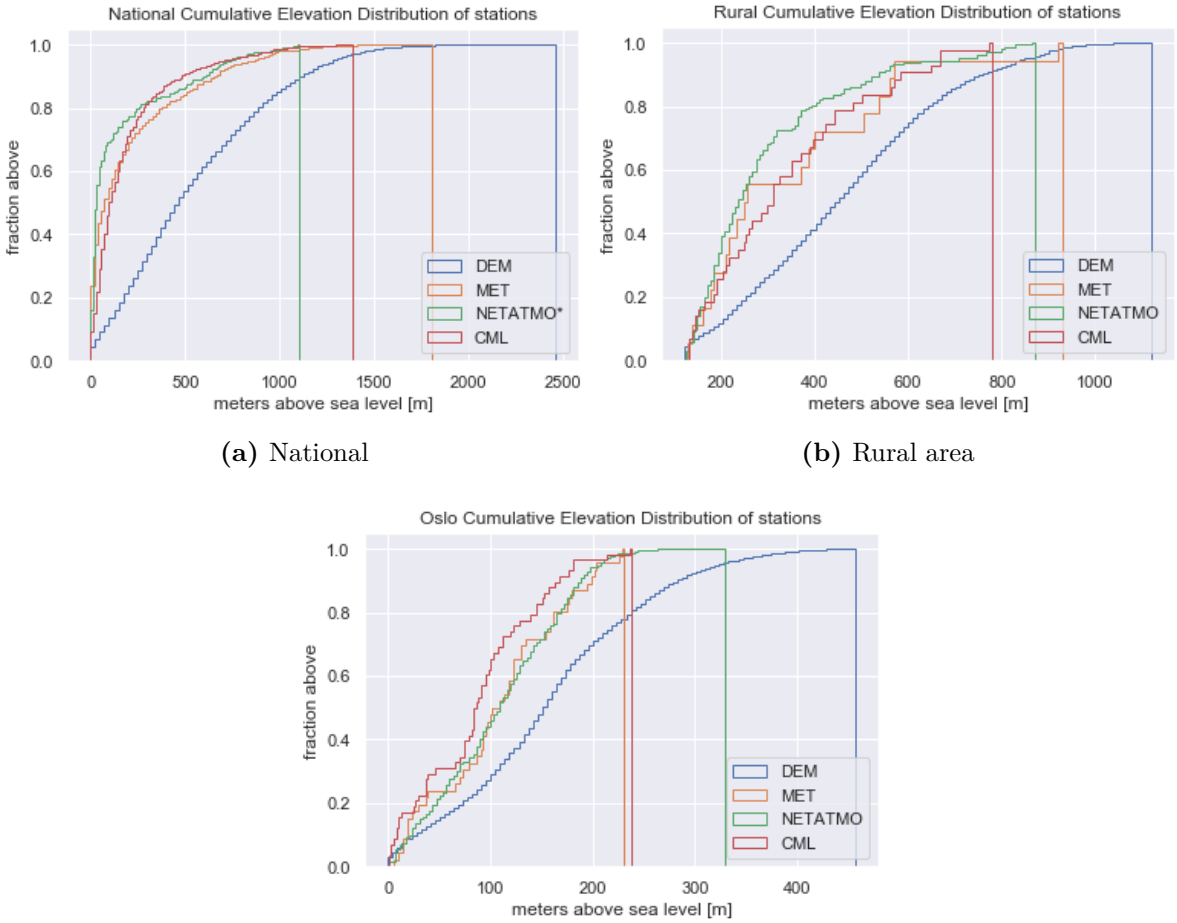

(a) National

(b) Rural area

(c) Oslo area

Figure 4.7: Hypsometric curves of three precipitation networks compared with topography. The vertical lines resemble the highest station elevation in each network. Note that the Netatmo curve for the national level is based on a small subsample of actual stations.

In the Oslo study area (4.7 c), the MET and Netatmo networks have a similar distribution with the CML network being slightly biased towards lower elevations. The Netatmo network has the largest extent at 230 meters, where the MET and CML networks extend to around 220 meters. Whether these relationships extend to other urban areas is uncertain in part due to the MET network being markedly denser around Oslo then elsewhere (fig. 4.4). In the rural area (4.7 b), the Netatmo network shows the largest bias, and the MET network has the largest extent.

4.2.2 CML Expected Error

The expected accuracy of the links constituting the CML network was assessed using two quantization levels (the resolution of attenuation in dB) lieu of actual measurement data as none was available. This assessment discounts all the other error sources discussed

in section 2.2.2, so the error estimates are likely conservative. Nevertheless, they give an accurate overview of some key aspects. In figure 4.8, the expected error is plotted together with its dependents: link length, frequency ,and polarization. Firstly, there is no appreciable correlation between error and polarization. There is a strong negative correlation between frequency and error, which is due to higher frequencies being more strongly attenuated. Secondly, the error increases with decreasing link length due to the total attenuation being lower as there is less rain between antennas for a given precipitation intensity. These relationships extend across quantization levels, though the spread in expected error is larger for a higher quantization.

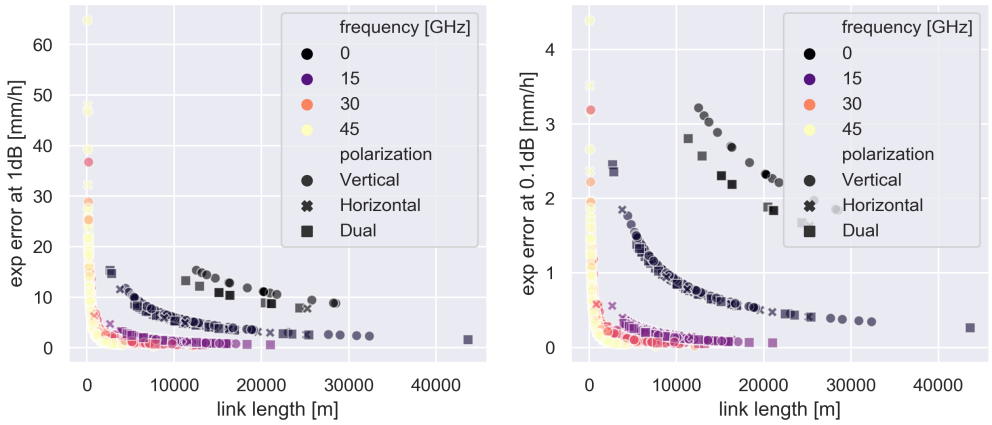

Figure 4.8: Expected error of CML stations plotted against length and frequency for two quantization values using equation (2.15), a and b coefficients determined recommendations fromITU-R (2005). The color in the legend corresponds to the lower frequency bound i.e. black refers to $f \in [0, 15)$ GHz.

The distribution of expected error (figure 4.9) reveals that the error nationally would be small for a quantization of 0.1 dB. However, for the case of a 1 dB quantization, the error shows a larger spread and is predominantly above 1 mm/h making it less suitable for accurate mapping. The expected error in the Oslo area is a lot higher than nationally, which is due to short links in the city center accounting for the majority of CMLs.

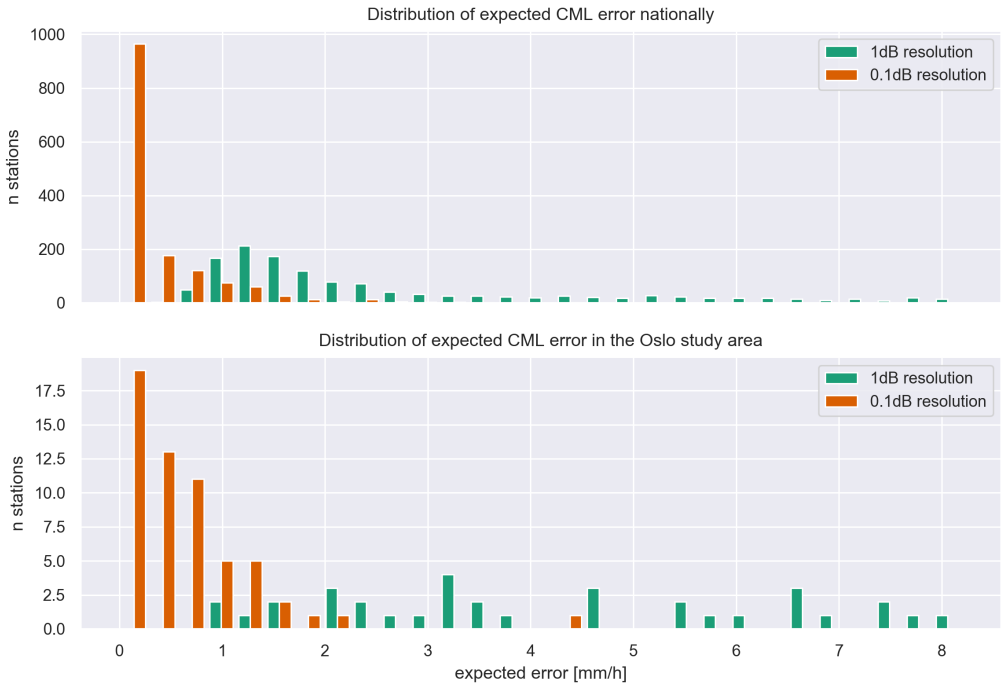

Figure 4.9: Distribution of expected error as mm/h both nationally and in the Oslo area from 0.1 dB and 1dB quantization of total attenuation. Calculated from frequency, polarization and length using equations from ITU-R (2005). Note that the 1 dB error extends beyond the graph.

4.3 Time-series Analysis

Accumulated precipitation throughout the study period is plotted for the MET and Netatmo networks in figure 4.10 together with the two WMO certified stations as reference. Both networks correspond well with the reference station SN18700 which is located centrally in Oslo. However, the other reference station located in Asker (lower left quadrant of figure 4.2) reports accumulated precipitation consistently higher than the 75th percentile of either the Netatmo or MET networks. The station in Asker is located in a region with varying topography outside of the density centers of either network, which could explain why it is so far from either network median. Further, both the average and median precipitation is higher in the Netatmo network than in the MET network. This is an unexpected result as PWS stations, and Netatmo stations specifically are believed to underestimate rainfall. de Vos et al. (2019) found a negative bias of 11% when comparing Netatmo stations to gauge adjusted radar. The peaks in the standard deviation where there is no change in the median indicate localized precipitation events when both the networks are in agreement. When the peaks are only visible in the Netatmo network, this could also be due to faulty measurements.

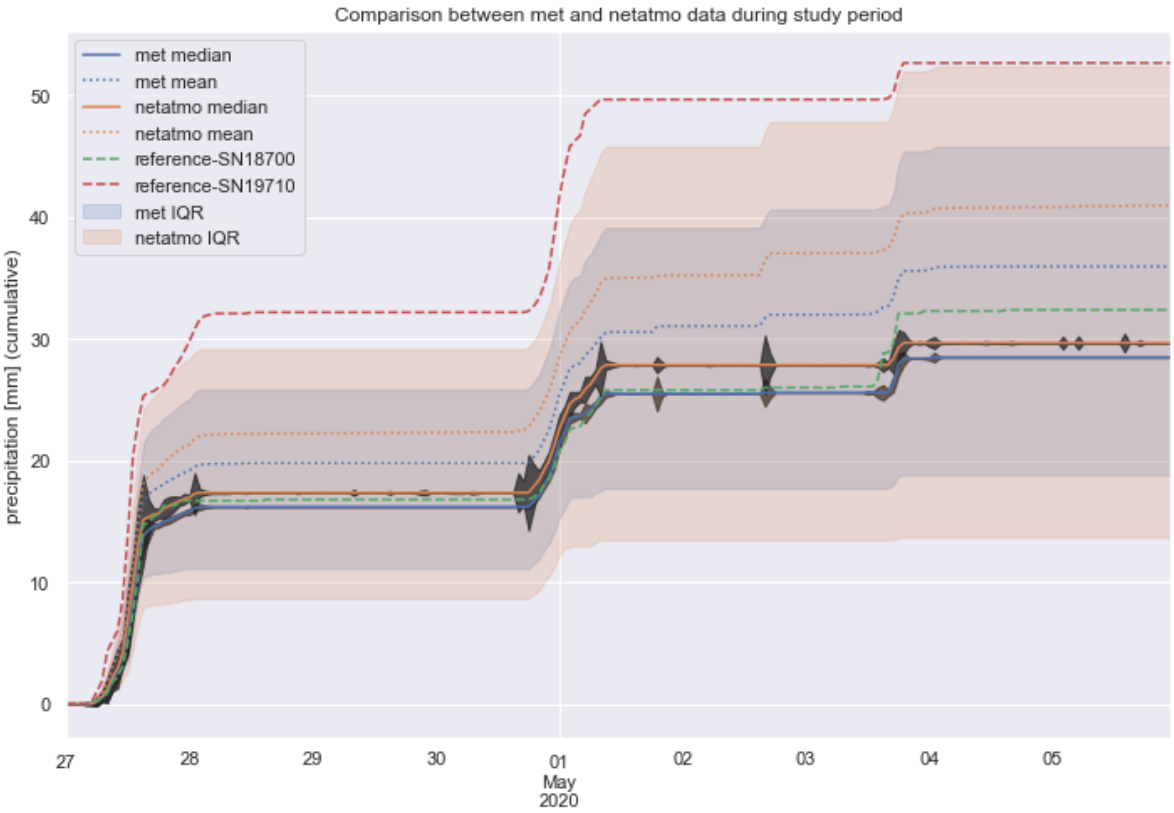

Figure 4.10: Cumulative precipitation over the study period. The interquartile range (IQR) is the area between the 25th and 75th percentile. The black shadow resembles median precipitation ± the standard deviation. The two reference stations are the two WMO certified stations in the MET data-set: SN19710 is located in Sem, Asker and SN18700 is located at Blindern, Oslo.

4.3.1 Availability and Measurement Age

Lacking station availability is a defining characteristic of PWS networks and is caused by communication problems between the station and server, stations being removed from the network, or station owners taking the stations off-line to maintain them. When stations are accessed through an API, as was done for the Netatmo network, stations might be filtered further. When analyzing the availability in the Netatmo network, it was found that the average station was available just over 40% of the time (fig. 4.11). Further, the number of stations returned varied considerably, between 220 and 320 stations, each time precipitation data was requested. When applying a seven day mean to the number of stations returned, an apparent increase in reporting stations was observed during the collection period.

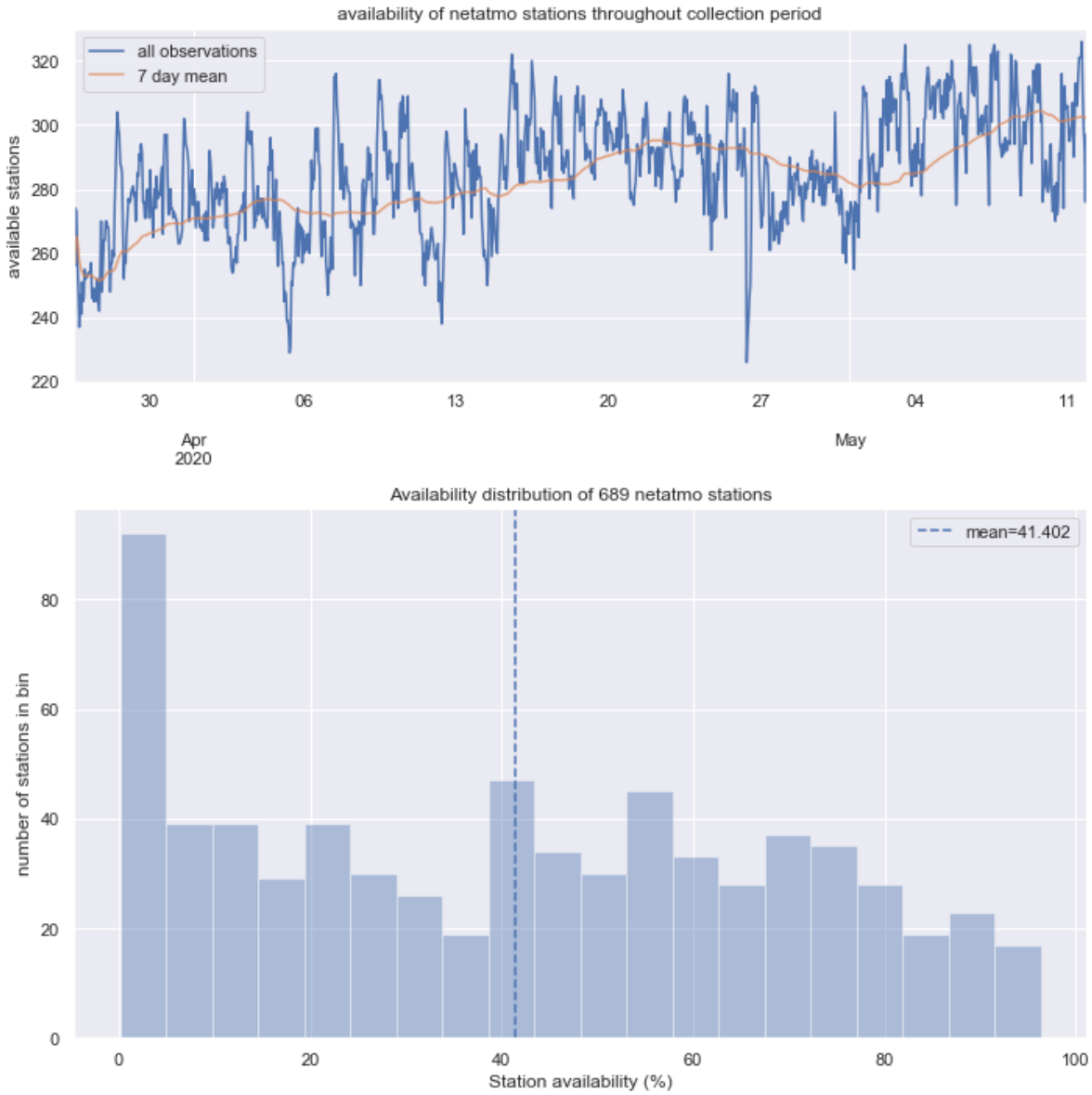

Figure 4.11: Availability of Netatmo stations during entire collection period

To determine the cause of the low availability, the stations were visualized in a matrix (fig. 4.12) for the study period. The stations were colored by whether the station returned an observation or not. Apparent in the figure is a slight diurnal variation of higher availability just left of center in the matrix. Upon closer inspection, the increase occurs simultaneously with a decrease in the left side of the matrix. This is either indicative of the API sub-sampling the stations or stations reporting under multiple identifiers. To test the possibility of the latter, it was checked if any two stations (rows in the matrix) had a correlation of -1, which would correspond to an observation always occurring in one station while it did not in the other and vice versa. No such correlations were found, which indicates that the low station availability is, in part, a result of the API.

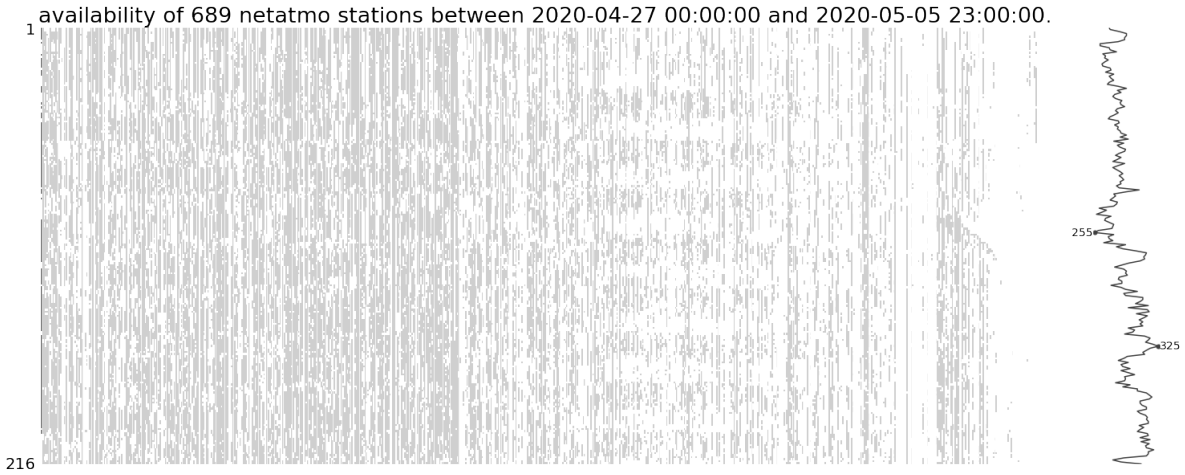

Figure 4.12: Matrix of Netatmo station availability in the study period. Each row in the matrix resembles the measurements at each hour, each column resembles a station. Each cell is colored black if a measurement exists (i.e. the station is available) or white if there is no measurement.

The measurement age analyzed for the entire collection period (fig. 4.13) was found to be between 0 and 10 minutes, with a uniform distribution. This is a consequence of data being uploaded to the API from central servers every 10 minutes, a fact that was later confirmed (Netatmo, personal communication, April 4th, 2020) through email correspondence. It was also discovered that observations are collected from stations every 5 minutes. These two facts result in a measurement age between 0 and 10 minutes when data is accessed through Netatmos API and a measurement age between 0 and 5 minutes if measurements are sent directly. The latter result assumes that stations do not report at the same time intervals, and instead report every 5 minutes at arbitrary times.

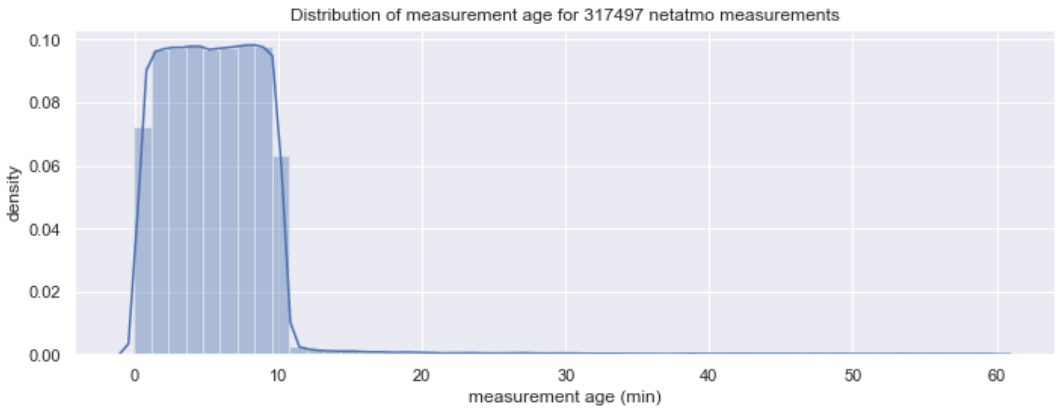

Figure 4.13: Histogram of measurement age for Netatmo hourly precipitation measurements.

4.3.2 Quality Control Results

The application of the QC algorithm on the Netatmo network during the hours selected for validation resulted in the removal of about 50 stations on average. The maximum number removed was 76, while the minimum number removed was 40. The effect of QC can be assessed by the climatological variograms in figure 4.14. The effective range (r) is almost doubled from 13.5 km to 20.1 km and the nugget (b) is reduced from 0.62 to 0.42 in the fitted models. Further, the empirical variogram (blue dots) forms a much more coherent curve after the application of QC. However, comparing the QC filtered variogram to that of the MET network (fig. 4.15 c) where range (r) and nugget (b) are 26.5 km and 0.2 respectively, indicates that the QC algorithm is not perfect as much of the nugget is likely due to inaccurate measurement. Further, a side effect of the QC algorithm not apparent in the figure is its tendency to increase network clustering. This is a consequence of applying the isolation check, which has the possibility of removing all stations in sparse areas.

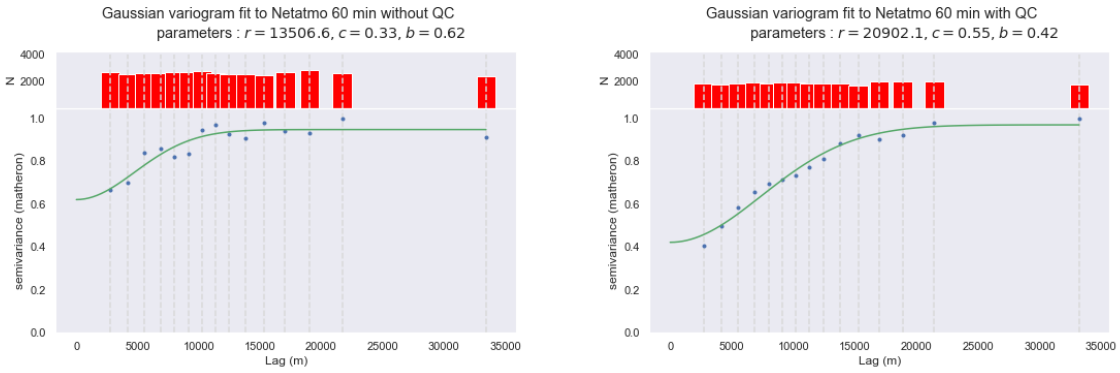

(a) Without QC **(b)** With QC

Figure 4.14: Gaussian climatological variograms computed for the study period. Precipitation instances were filtered by $R_{median} \geq 0.1$ mm resulting in 38 instances.

4.4 Spatial and Temporal Characteristics

The change in spatial characteristics of the precipitation measured by the MET network was assessed using the climatological variograms in figure 4.15, created by re-sampling the time-series to aggregation times from 1 minute to 1 day. The observed tendency of decreasing nugget and increasing range with increasing aggregation time is expected as a consequence of aggregating.

Having established that the MET network fulfills the target density corresponding to a 10 minute aggregation time, the expected nugget value should be nearly zero for both the 10 and 60-minute variograms. A possible explanation for the discrepancy could be

that the filtering condition (R_{median}) was quite low, including many instances where the median precipitation was at or near the quantization level (0.1 mm) of the rain gauges leading to very large (relative) differences between neighboring gauges. Comparing the ranges to those in table 4.4, the effective range is higher than that suggested for both 1 and 10-minute variograms. The inclusion of low-intensity precipitation instances could serve as an explanation for the range discrepancy as low-intensity, non-convective events are less localized.

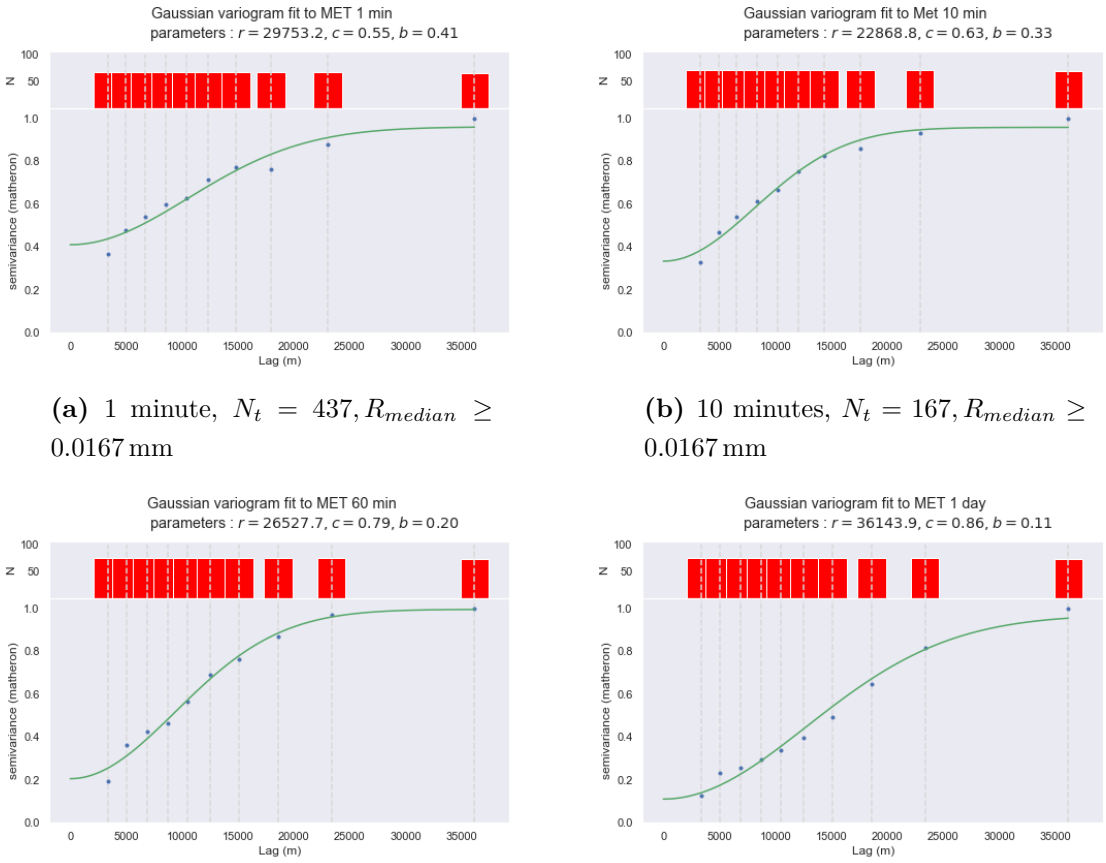

(a) 1 minute, $N_t = 437, R_{median} \geq 0.0167\,\text{mm}$

(b) 10 minutes, $N_t = 167, R_{median} \geq 0.0167\,\text{mm}$

(c) 1 hour, $N_t = 41, R_{median} \geq 0.1\,\text{mm}$

(d) 1 day, $N_t = 5, R_{median} \geq 0.6\,\text{mm}$

Figure 4.15: Gaussian climatological variograms generated from MET stations in the Oslo area for different aggregation times during the study period. Precipitation instances were filtered by a threshold value (R_{median}) resulting in N_t precipitation instances before the variograms were computed.

The uncertainty maps in figure 4.16 illustrate the location and magnitude of the error associated with precipitation maps from the three networks. The error maps are standardized where an error of 0 corresponds to an absolute error of $0mm/h$, and an error of 1 corresponds to an absolute error equal to the standard deviation of all measurements in the network. The lowest error of the networks corresponds to the nugget values identified in the variograms for the MET and Netatmo maps. In the case of the CML map,

it corresponds to the expected error at 0.1 dB quantization.

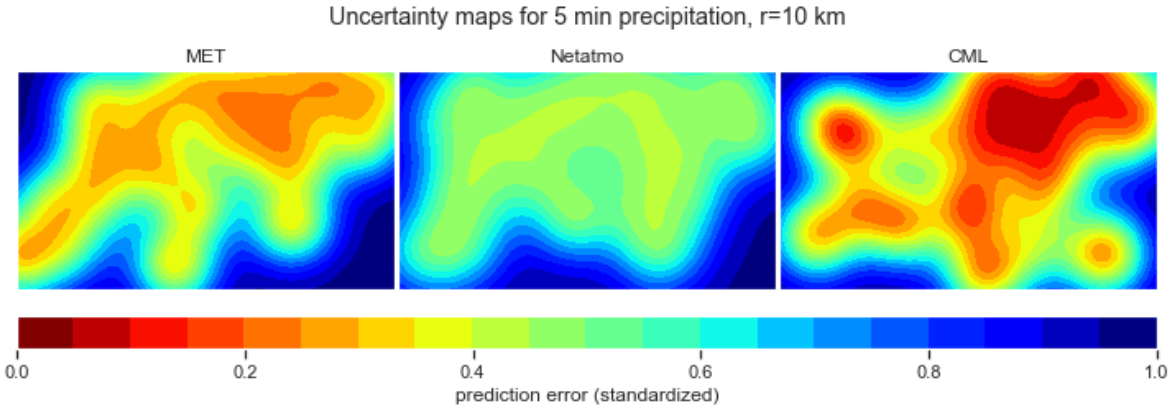

(a) 1 min

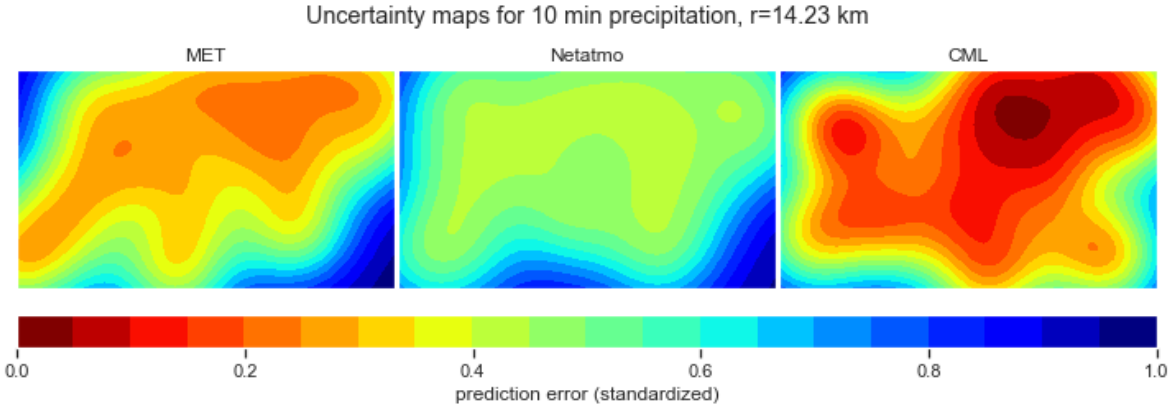

(b) 10 min

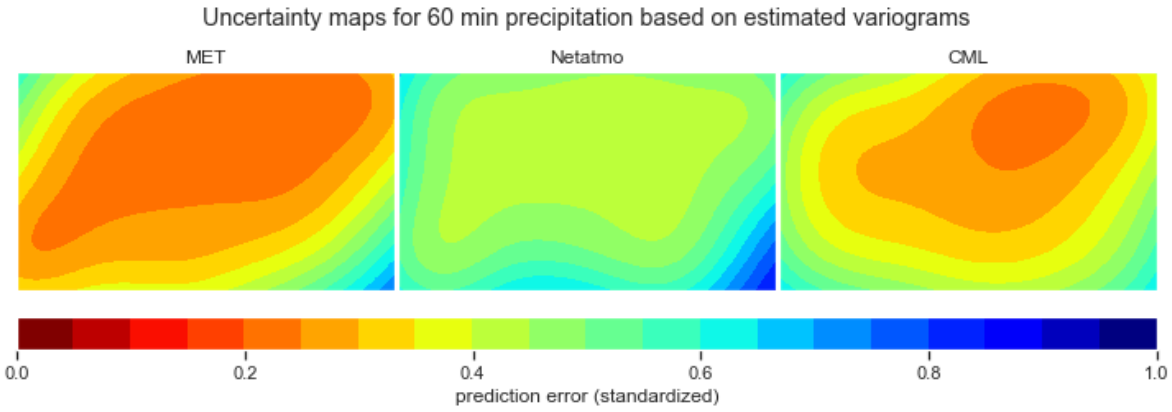

(c) 60 min

Figure 4.16: Uncertainty maps of interpolated precipitation from the networks for the Oslo study area for different aggregation times.

For the 60-minute uncertainty map, it is apparent that all networks have coverage over most of the study area. However, the error of the CML network sharply increases away from where it is the densest. For shorter aggregation times, the error becomes more

varied in space, and the locations where the error is small more closely mimics the location of stations within the network. This effect is less prominent in the Netatmo network due to higher coverage.

In figure 4.16, the Netatmo network consistently has a higher error than the MET network. This is due to the difference in nugget value, which, if the spatial precipitation characteristics agree with those in table 4.4, in turn, is due to measurement error at individual stations. To illustrate the potential of the networks if the station measurement error can be minimized through better QC and/or bias correction, the error maps have been created with an equal nugget value of 0.1 and plotted in figure 4.17. The error of the CML network is slightly higher than in (4.16 a) as the constant nugget has been added to the individual station error (α). These maps represent an ideal situation where the characteristics more closely match those identified from figure 4.5. Under these circumstances, the Netatmo network has the lowest error overall with consistent accuracy over almost the entire study area.

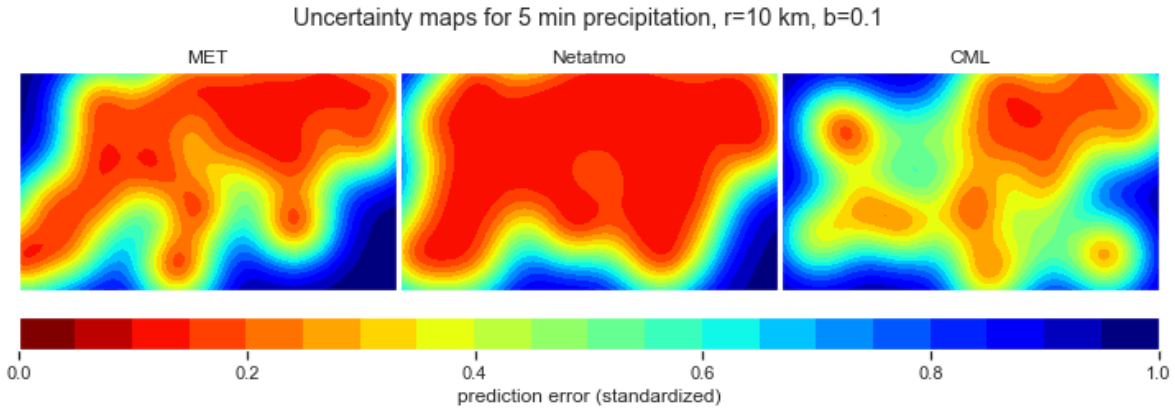

Figure 4.17: Uncertainty maps for 5 min precipitation with equal nugget for all networks. The nugget is added to the per-station error (α) for the CML network.

4.5 Predictor Selection and Validation

When selecting precipitation events to use for validation, it was decided to use all hours where the median precipitation within the Netatmo network was above 0.1 mm/h, which resulted in the 38 precipitation instances plotted in figure 4.18. The figure represents boxplots of each hour for each network before any QC was applied. The whiskers of the Netatmo boxplots extends to zero for almost every hour in the validation series, indicating the presence of faulty zeroes. The overall variation is also higher in the Netatmo network with a higher presence of data-points beyond the whiskers.

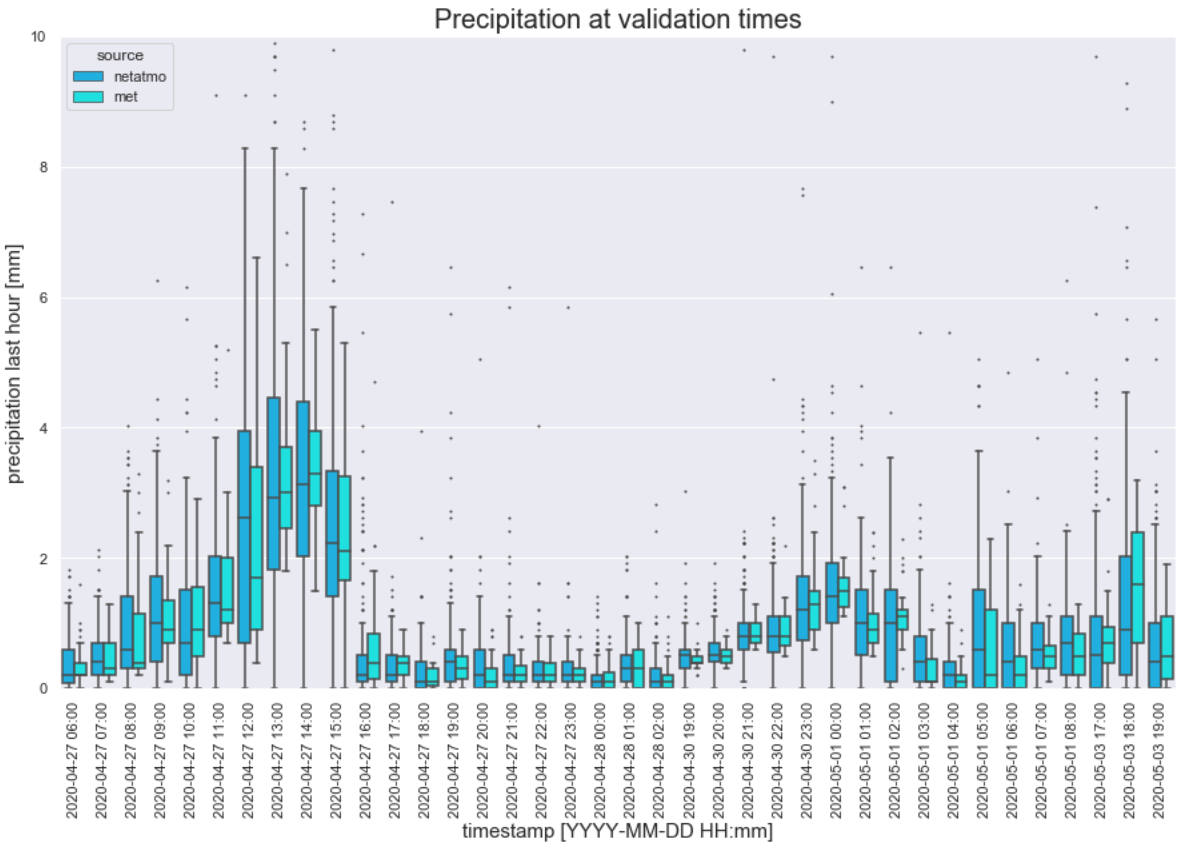

Figure 4.18: Boxplots of precipitation periods used for validation. Hours are filtered by precipitation > 0.1 mm/h. The boxes represent the IQR and the whiskers extend to data-points $\pm 1.5 * IQR$ beyond the boxes. Data beyond the whiskers are represented by black dots, some of which extend beyond 10 mm/h and are not shown.

A predicted precipitation map is presented for the different interpolation methods in figure 4.19. The parameters for the **GPR manual** model are the same as those identified in the variograms (figures 4.15 b and c for the 10-minute and daily maps, respectively, and figure 4.14 b for the 60-minute map). The maps presented clearly illustrate some key features of the interpolation methods. Firstly, the discontinuities associated with Nearest Neighbor interpolation are very apparent along the left edge of the 10-minute precipitation map, where the precipitation increases rapidly over a very short distance. Further, with the Nearest Neighbor interpolation, it is very difficult to distinguish a spatial pattern, especially if the stations aren't in agreement locally. The IDW method appears to produce spots at station location in all the maps, and interpolating conservatively (closer to the network mean) at all other locations. This is a known disadvantage of the method, but for illustration purposes can be used as a proxy for the measured values at the stations.

The 10-minute and 1-hour maps for the UK method clearly illustrate a problem that can occur with automatic, unconstrained fitting, where precipitation far outside the range

of observations is predicted, and the spatial pattern bears no resemblance to the one present in the networks. In the 1-hour map of the GPR auto method, a similar problem is evident. Here, the automatic fitting found the decorrelation distance (range) to be extremely short, possibly due to outliers or disagreement between neighboring stations and predicts the network mean over most of the study area.

By visual inspection, the **GPR manual** model appears to incorporate most of the spatial variation in the networks. It also handles disagreement between neighboring stations well, such as in the lower left quadrant of the one hour map.

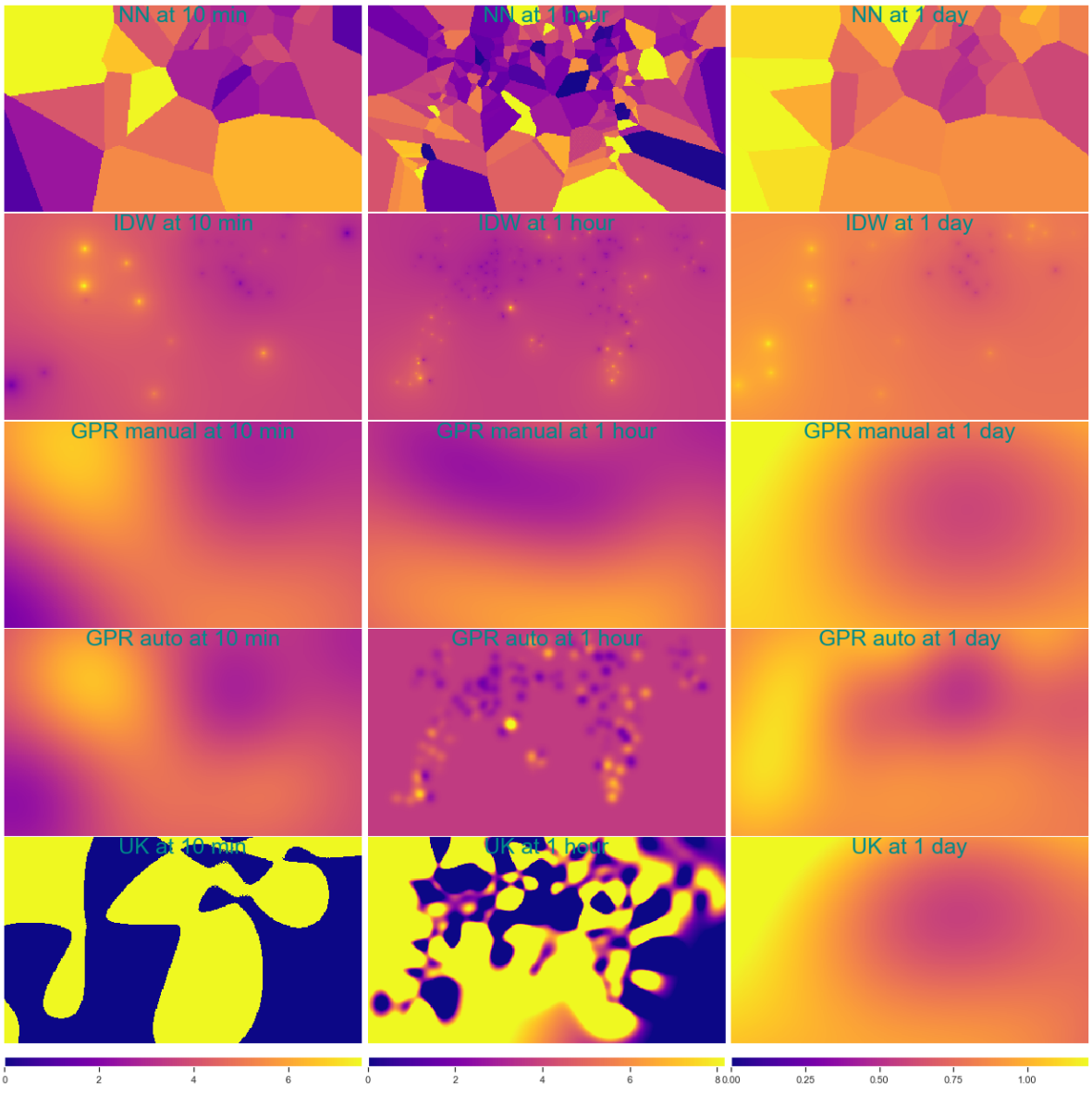

Figure 4.19: Graphic comparison of interpolation methods at different aggregation times. The 10-minute and 1-day fields are generated from MET data, while the 60-min field is generated from Netatmo data. The plots are of precipitation on the 27th of April 2020. Hourly and 10-min data are from 13:00:00. The colorbars denote precipitation intensity [mm/h] with a range from 0 to the 95th percentile of the observations in the network.

The interpolation methods were applied to the Netatmo network for all 1-hour precipitation in the validation period. The precipitation value at station locations in the MET network was predicted and compared with the observed values at those stations to assess the interpolation methods. The predicted and true (observed) value pairs are plotted for each interpolation method in figure 4.20 and serve as basis for the metrics presented in table 4.5. The NN interpolation method exhibits the highest amount of scatter, both at lower precipitation intensities, but especially at higher precipitation intensities. Both the GPR auto and UK methods exhibit scatter at larger intensities, but at a lower degree than the NN method. The IDW method shows a large scatter where the true precipitation is between 1.5 and 2.5 mm but is otherwise conservative, never predicting above 5 mm though the true precipitation extends beyond 7.5 mm. The **GPR manual** method has the least amount of scatter but also predicts conservatively at higher intensities.

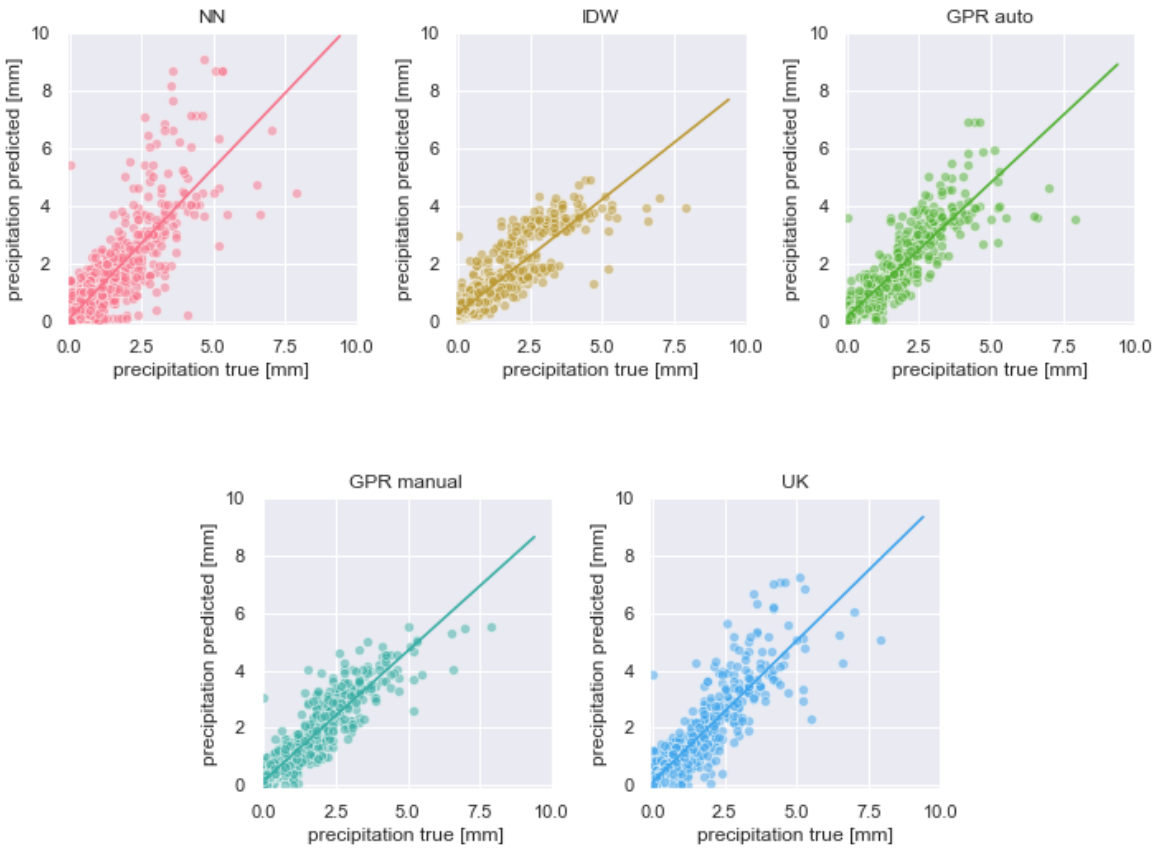

Figure 4.20: Scatterplot of predicted (based on netatmo dataset) vs true (based on full MET dataset) precipitation for all interpolation methods.

The scores in table 4.5 indicate that the best performing interpolation method was GPR manual, which scored best in both the RMSE and R^2 metrics when comparing against

both the MET network as a whole and only the WMO certified stations. Against the whole MET network, **GPR manual** was also the best performing method with respect to bias. Against the WMO stations, however, the bias was lowest for the NN method. However, the scores against WMO stations are particularly non-indicative of performance for this method as only two stations from the Netatmo network (for each hour) contribute to the predicted value.

Notably, all methods exhibit a positive bias, which is expected due to the difference in both mean and median rainfall between the two networks identified in section 4.3.

The results of the validation indicate that the NN method is the worst performing for this application and that the IDW method with $p = 1$ fails in accurately capturing the extent of variation in the field. Further, it indicates that geostatistic models perform well in general, but their performance is best when based on climatological variograms, and degrades when automatic fitting is applied, even when the parameters are (loosely) constrained such as in the GPR auto model.

		RMSE	R^2 [−]	bias	bias [%]
against wmo	**NN**	0.695_w	0.662_w	0.307_w	1.5_b
	IDW	0.569	0.774	0.293	1.8
	GPR auto	0.624	0.728	0.247	9.5
	GPR manual	0.400_b	0.888_b	0.219_b	2.7
	UK	0.605	0.751	0.296	13.6_w
against all met	**NN**	0.698_w	0.521_w	0.195	13.8_w
	IDW	0.480	0.774	0.221_w	11.6
	GPR auto	0.447	0.804	0.145_b	10.9
	GPR manual	0.393_b	0.848_b	0.160	9.6_b
	UK	0.502	0.756	0.153	12.3

Table 4.5: Validation results from 38 hourly observation sets. Scores are in mm/h unless otherwise indicated in brackets. The scores in **against wmo** are from comparison with the two WMO compliant observation stations in the MET data set totaling 76 observations. The scores in **against all met** are from comparisons with all stations in the MET data set totaling 1537 observtions. The best and worst performing predictors in each group are marked with subscripts $_{b,w}$ respectively

4.6 Source Combination

A precipitation map utilizing all three networks, Netatmo, MET, and CML, is created in figure 4.21. The map serves as an example only because the CML error is based on conservative assumptions i.e., the error is likely underestimated, and the precipitation data for the CML network is simulated. Nevertheless, it illustrates how accuracy in

precipitation maps can be gained by a combination of sources that share little commonality and are independent of each other. In the figure, one can see that the Netatmo network doesn't contribute appreciably to the combined prediction, which is due to its high error (or nugget) value. Conversely, the MET and CML networks both contribute a great deal. Incidentally, the two networks are in agreement, so it is hard to see where they each contribute. However, looking at the error maps, it shows that the error is smaller for the combined map than for either network alone.

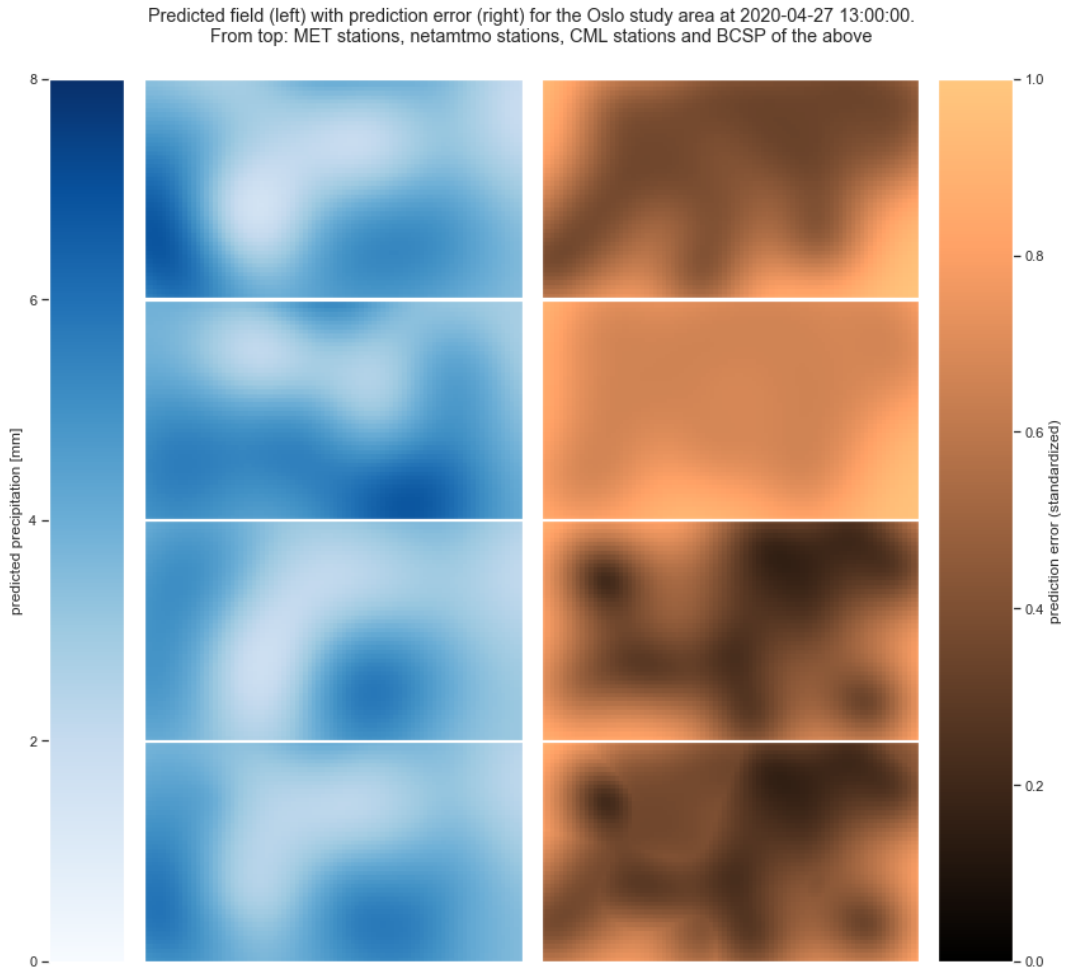

Figure 4.21: Illustration of the Best Combined Spatial Predictor from 10 minute precipitation fields of the Oslo study area. The predicted field is on the left, with its associated error map on the right. From top: MET network, Netatmo network, CML network, and a combined prediction on the bottom.

5. Discussion

The results of the network density assessment indicate that both the PWS and CML networks have higher density throughout Norway and especially in urban areas. Though this was not proved for the country at large in the case of PWS networks, the favorable conditions in the Oslo study area combined with the PWS network's tendency to mimic the population distribution indicate that good coverage of urban areas is likely in other cities also. This is further supported by the density assessment in the rural study area, in which the PWS network density was favorable.

Assessing the CML network nationally, clusters near major cities are clearly identified, though the coverage is lacking inland. The coastal prevalence of the CML network could indicate a large proportion of links across water. As these links are known to be inaccurate for precipitation mapping (Chwala and Kunstmann, 2019), they could limit the effective density of the network.

The station availability is found to be substantially limited for the PWS network studied, the effect of which restricts the avenues for QC methods markedly. However, the results of the study indicate that the limited availability is in part due to the API through which the data was collected. Consequently, accessing the data directly from the PWS network service, e.g., through a direct partnership, could increase station availability substantially and facilitate the application of more extensive QC. Additionally, direct access could decrease the measurement age of the PWS stations.

Though not studied in particular, station availability appears to be less of a concern for CML networks (de Vos et al., 2020). As CML links are part of essential communications infrastructure, they are expected to be operational most of the time and are only not when an intermittent link is blocked so the data cannot be transferred. However, links are taken offline for maintenance and taken out of- or put in commission, resulting in some unavailability, though time-series are generally assumed to be continuous for this network type.

When assessing the measured structure of rainfall with the MET network, agreement with the structure identified by Berne et al. (2004) was not found. The results indicate

that precipitation has more local variability than the literature suggests in addition to having a longer decorrelation distance. It is likely that the characteristics differ somewhat due to the difference between the Norwegian and the Mediterranean climate, where the structure in (Berne et al., 2004) was determined. However, as small scale variability and decorrelation distance are inversely correlated for precipitation, the identified structure is not likely representative of reality as there exist other explanatory factors.

Assuming the MET network to be accurate, the discrepancy could be explained by the inclusion of hours with very little (0.167 mm) precipitation while assessing the structure. Firstly, that amount of precipitation is very close to the quantization level of conventional tipping bucket rain gauges (0.1 mm), which comprise most of the MET network used in the assessment. Under such circumstances, the smallest possible difference between gauges (0.1 mm) would correspond to a relative difference upwards of 100%. Further, as light precipitation is fairly non-localized, the variation at large distances is expected to be small. The net effect on the variogram would be equal and high variation at short and long distances. As the variograms are standardized by maximum (assumed at a large distance) variation before combination, the low precipitation effectively raises the nugget. Additionally, as the structures identified by Berne et al. (2004) were calculated for extreme precipitation events, including light precipitation could invalidate the comparison. However, as the MET network in Oslo predominantly consists of partner stations without WMO certification, the accuracy of the MET network could be lower than expected and also be a contributing factor. These factors should be explored further by analyzing a longer time-series that includes more precipitation events, thereby enabling separate analysis for light and heavy precipitation.

Several interpolation techniques were performed on the PWS network. The best performing technique was found to be a geostatistical model (GPR manual) constrained by a fixed climatologic variogram. The model applied was efficient enough to be run on a laptop in a matter of seconds which indicates a potential for use at larger scales. A benefit of the model being independent in time, i.e., not needing historical data (sans the climatological variogram), is the possibility of applying it on request for a local analysis, alleviating the costs associated with constantly running the model and storing its results. A second benefit of the model is its ability to produce an accompanying error map.

As CML signal-loss data was not collected, its error structure could not be completely assessed. However, an assessment of the minimum error is made by computing the quantization levels in terms of precipitation in [mm/h] corresponding to attenuation [dB] for all links in the network. The results indicate that a low quantization level is especially important in urban areas where link lengths are shorter.

When assessing the geostatistical interpolation method for the PWS network, it was found that the prediction had high uncertainty, which in turn led it to underestimate high (possibly localized) precipitation. This is a trait that is detrimental for its application in urban hydrology where intense precipitation is of primary interest. This *smoothing* effect arises from the inclusion of the local error term (nugget effect) in the model, the use of which acts as a double-edged sword: The nugget effect makes the interpolated map non-exact at measurement locations, thereby allowing for outlying measurements, provided they are few, included in the underlying observations. However, this exact behavior is detrimental as it smooths all observations, not only clear outliers, which in turn causes the loss of *real* short scale variation.

While not being certain about the underlying structure of the precipitation, the amount of error attributed to inaccurate measurements cannot be fully determined. However, a comparison of variograms between the MET and PWS networks reveals it to be considerable.

The QC method applied to the PWS network had a significant effect on reducing the error term. However, a considerable error remained after the application. To further decrease the error, a better QC method should be applied, the development of which needs further research.

If the station availability found in this study can be increased by bypassing the API through a direct partnership with the PWS network supplier, QC methods that use continuous per-station time-series such as the one developed by de Vos et al. (2019) should be explored. If not, however, QC methods that assign a trust or error score based on past performance can be a viable option.

Regardless, efforts should be made to accurately determine the spatial characteristics of Norwegian precipitation at different intensities and local climates to better constrain both QC and subsequent models used for mapping.

With the QC applied in this study, the error maps created for the Oslo study area reveal that the PWS network does not appreciably increase the accuracy of precipitation maps compared with the traditional network. However, considering that the traditional gauge network in Oslo is about five times denser than in other urban areas, an improvement is expected elsewhere in Norway. Further, the study demonstrates that if QC and, possibly, corrections were applied to increase the per-station accuracy, the PWS map offers marked improvements over the one based on traditional networks even in the Oslo study area.

The Best Combined Spatial Predictor is found to be a viable option for combining information from the different networks. However, it requires that the error structures

for each network are properly understood and that the error is standardized to the same scale before combination.

Whether the PSW can increase the accuracy of currently operational nowcasting in Norway is uncertain as this paper limits itself to study the PWS network at a 60 minute aggregation time. However, data is available at 5 minute aggregation times from Netatmo. If the data could be accessed directly at the time it was reported from the PWS; it could aid in quantifying the forecast as the temporal resolution is higher than the update interval of the current forecast. However, it is likely that much of the rain for non-intense precipitation would be at or below the PWS quantization level (bucket size) and consequently introduce more error into the system than it mitigates.

On the other hand, the mapping methods discussed in this paper, regardless of underlying networks, are capable of producing weather maps far exceeding the spatial and temporal resolution of the current state of the art product (SeNorge2), thereby making reconstruction of single rain events a possibility.

Of the PWS networks assessed, the Netatmo network was found to be the most extensive in Norway. The recent application of the network for temperature forecasting (Nipen et al., 2020) indicates that bypassing the API and accessing the data directly through a partnership is a real possibility. To further extend coverage, several of the PWS networks identified can be integrated through similar partnerships. However, their coverage in Norway is at this time so low as to provide negligible improvement to the final product.

Another option could be to enable PWS owners to contribute directly. This could be accomplished by creating a PWS service that station owners could upload data to similar to the WOW networks or the Citizen Weather Observer Program. However, this option incurs a considerable development cost and would involve extra effort on the part of the PWS owners. The latter would likely have a detrimental effect on connectivity and, thereby, coverage. Conversely, this barrier to entry on the part of station owners has the possibility of increasing accuracy as the station owners are more cognizant of their contribution's importance and would pay closer attention to station placement and maintenance.

The result of the CML stakeholder assessment indicates a marked security concern for all the network operators. Consequently, this concern must be addressed before this network type can be used for precipitation monitoring. A likely avenue that could address this concern is through a partnership between NKOM and MET as both of these organizations likely have the appropriate security clearances. In such a design, NKOM, being in the telecommunications market, would be responsible for gathering and storing both meta- and time-series data. MET would then be responsible for facilitating

data access for research purposes, and subsequent operational use. Such a partnership could unlock a large potential as many methods for subsequent processing; QC, bias correction etc., have already been developed and will enable Norwegian CML operators and researchers to participate in an active research field internationally.

Finally, the study identifies two distinct challenges for the two opportunistic network types studied. In the case of the PWS network, more robust QC methods need to be developed to limit prediction error (smoothing) while not losing the real short-scale variability. For the CML network, the challenge lies in compelling the network operators to facilitate data access.

6. Conclusions

While the stakeholder analysis yielded limited results in the case of CML operators, it successfully identifies the relevant organizations/companies and provides new insights into the challenge of data access. In the case of PWS operators, the research identifies a single PWS network, namely Netatmo, to be the most applicable at this time.

Assessment of current precipitation maps identified a severe lack in temporal resolution for application in urban hydrology. This clearly illustrates that the proposed methodology has a market for application.

The results of the comparison between the opportunistic networks and their traditional counterparts indicate that both opportunistic networks far exceed the density and, in certain areas, the extent of the traditional gauge network. In the case of the PWS network, the main differences to the traditional network lie in accuracy and availability.

When assessing the accuracy of the precipitation maps, it was found that constrained geostatistical models yielded the highest interpolation accuracy. Further, their application provided key insights into the need for network-specific quality control and a better understanding of the underlying spatial characteristics of precipitation to constrain them. Finally, the Best Combined Spatial Predictor was identified as a viable method to combine information from dissimilar networks into a single precipitation map.

This research aimed to assess the viability of CML and PWS networks as a source for precipitation mapping in Norway. Based on a comprehensive assessment of network characteristics, precipitation mapping techniques, and the underlying spatial characteristics, it can be concluded that both networks have considerable potential for this application. The results indicate two distinct challenges going forward for the two networks, namely, more efficient quality control and facilitating data access for the PWS and CML networks, respectively.

References

Atlas, D. and Ulbrich, C. W. (Dec. 1977). Path- and Area-Integrated Rainfall Measurement by Microwave Attenuation in the 1–3 cm Band. *Journal of Applied Meteorology* 16 (12): 1322–1331. DOI: 10.1175/1520-0450(1977)016<1322:PAAIRM>2.0.CO;2.

Bao, L., Larsson, C., Mustafa, M., Selin, J., Andersson, J. C. M., Hansryd, J., Raidel, M., and Andersson, H. (2017). A brief description on measurement data from an operational microwave network in Gothenburg, Sweden. In: *15th International Conference on Environmental Science and Technology*. URL: http://cest.gnest.org/sites/default/files/presentation_file_list/cest2017_00472_oral_paper.pdf.

Berne, A. and Krajewski, W. (Jan. 2013). Radar for hydrology: Unfulfilled promise or unrecognized potential? *Advances in Water Resources* 51: 357–366. DOI: 10.1016/j.advwatres.2012.05.005.

Berne, A., Delrieu, G., Creutin, J.-D., and Obled, C. (Dec. 2004). Temporal and spatial resolution of rainfall measurements required for urban hydrology. *Journal of Hydrology* 299 (3-4): 166–179. DOI: 10.1016/j.jhydrol.2004.08.002.

Butler, M. K. (Jan. 2019). Personal weather stations and sharing weather data via the Internet. *Weather* 74 (1): 22–29. DOI: 10.1002/wea.3206.

Chen, A. B., Behl, M., and Goodall, J. L. (Nov. 2018). Trust me, my neighbors say it's raining outside. In: *Proceedings of the 5th Conference on Systems for Built Environments*. New York, NY, USA: ACM: 25–28. DOI: 10.1145/3276774.3276792.

Chwala, C., Gmeiner, A., Qiu, W., Hipp, S., Nienaber, D., Siart, U., Eibert, T., Pohl, M., Seltmann, J., Fritz, J., and Kunstmann, H. (Aug. 2012). Precipitation observation using microwave backhaul links in the alpine and pre-alpine region of Southern Germany. *Hydrology and Earth System Sciences* 16 (8): 2647–2661. DOI: 10.5194/hess-16-2647-2012.

Chwala, C., Keis, F., and Kunstmann, H. (Mar. 2016). Real-time data acquisition of commercial microwave link networks for hydrometeorological applications. *Atmospheric Measurement Techniques* 9 (3): 991–999. DOI: 10.5194/amt-9-991-2016.

Chwala, C. and Kunstmann, H. (Mar. 2019). Commercial microwave link networks for rainfall observation: Assessment of the current status and future challenges. *Wiley Interdisciplinary Reviews: Water* 6 (2): e1337. DOI: 10.1002/wat2.1337.

Cressie, N. A. C. (1991). *Statistics for Spatial Data*. John Wiley & Sons, Inc.

de Vos, L. W., Droste, A. M., Zander, M. J., Overeem, A., Leijnse, H., Heusinkveld, B. G., Steeneveld, G. J., and Uijlenhoet, R. (Feb. 2020). Hydrometeorological Monitoring Using Opportunistic Sensing Networks in the Amsterdam Metropolitan Area. *Bulletin of the American Meteorological Society* 101 (2): E167–E185. DOI: 10.1175/BAMS-D-19-0091.1.

de Vos, L., Leijnse, H., Overeem, A., and Uijlenhoet, R. (Feb. 2017). The potential of urban rainfall monitoring with crowdsourced automatic weather stations in Amsterdam. *Hydrology and Earth System Sciences* 21 (2): 765–777. DOI: 10.5194/hess-21-765-2017.

de Vos, L. W., Leijnse, H., Overeem, A., and Uijlenhoet, R. (Aug. 2019). Quality Control for Crowdsourced Personal Weather Stations to Enable Operational Rainfall Monitoring. *Geophysical Research Letters* 46 (15): 8820–8829. DOI: 10.1029/2019GL083731.

Dirks, K., Hay, J., Stow, C., and Harris, D. (July 1998). High-resolution studies of rainfall on Norfolk Island. *Journal of Hydrology* 208 (3-4): 187–193. DOI: 10.1016/S0022-1694(98)00155-3.

Elo, C. A. (2012). Correcting and quantifying radar data. *METreport* No. 2/2012. URL: https://www.met.no/publikasjoner/met-report/met-report-2012.

Ericsson (2017). *ERICSON MICROWAVE OUTLOOK Trends and needs in the microwave industry*. Tech. rep. Stockholm, Sweeden. URL: https://www.ericsson.com/en/reports-and-papers/microwave-outlook/reports.

Fleig, A. K. and Wilson, D. (2013). *Flood Estimation in small catchments*. Tech. rep. Oslo, Norway: NVE.

Fletcher, T., Andrieu, H., and Hamel, P. (Jan. 2013). Understanding, management and modelling of urban hydrology and its consequences for receiving waters: A state of the art. *Advances in Water Resources* 51: 261–279. DOI: 10.1016/j.advwatres.2012.09.001.

Fribruksforskriften (2012). *Forskrift om generelle tillatelser til bruk av frekvenser (fribruksforskriften)*. URL: https://lovdata.no/pro/SF/forskrift/2012-01-19-77.

Gillies, S. et al. (2013). *Rasterio: geospatial raster I/O for {Python} programmers*. URL: https://github.com/mapbox/rasterio.

Giuli, D., Toccafondi, A., Gentili, G. B., and Freni, A. (Sept. 1991). Tomographic Reconstruction of Rainfall Fields through Microwave Attenuation Measurements. *Journal of Applied Meteorology* 30 (9): 1323–1340. DOI: 10.1175/1520-0450(1991)030<1323:TRORFT>2.0.CO;2.

Goovaerts, P. (1997). *Geostatistics for natural resources evaluation*. Oxford, New York: Oxford University Press. URL: https://osf.io/swzm8/.

Haberlandt, U. and Sester, M. (July 2010). Areal rainfall estimation using moving cars as rain gauges – a modelling study. *Hydrology and Earth System Sciences* 14 (7): 1139–1151. DOI: 10.5194/hess-14-1139-2010.

Haberlandt, U. (Jan. 2007). Geostatistical interpolation of hourly precipitation from rain gauges and radar for a large-scale extreme rainfall event. *Journal of Hydrology* 332 (1-2): 144–157. DOI: 10.1016/j.jhydrol.2006.06.028.

Hengl, T., Heuvelink, G. B., and Stein, A. (2003). Comparison of kriging with external drift and regression kriging. *Technical note*. URL: https://www.researchgate.net/publication/228961429_Comparison_of_kriging_with_external_drift_and_regression-kriging.

Hengl, T. (2009). *A practical guide to geostatistical mapping*. URL: http://spatial-analyst.net/book/.

Hofstra, N., Haylock, M., New, M., Jones, P., and Frei, C. (Nov. 2008). Comparison of six methods for the interpolation of daily, European climate data. *Journal of Geophysical Research* 113 (D21): D21110. DOI: 10.1029/2008JD010100.

Hoås, H. (2018). Precipitation measurements from cellular microwave links : its potential in Norway. URL: http://hdl.handle.net/11250/2594299.

Islam, T., Rico-Ramirez, M. A., Han, D., and Srivastava, P. K. (Apr. 2012). A Joss-Waldvogel disdrometer derived rainfall estimation study by collocated tipping bucket and rapid response rain gauges. *Atmospheric Science Letters* 13 (2): 139–150. DOI: 10.1002/asl.376.

ITU-R (2005). *RECOMMENDATION ITU-R P.838-3 Specific attenuation model for rain for use in prediction methods*. Tech. rep. Geneva, Switserland.

Jameson, A. R. (Jan. 1991). A Comparison of Microwave Techniques for Measuring Rainfall. *Journal of Applied Meteorology* 30 (1): 32–54. DOI: 10.1175/1520-0450(1991)030<0032:ACOMTF>2.0.CO;2.

Jha, A. K., Bloch, R., and Lamond, J. (Feb. 2012). *Cities and Flooding*. The World Bank. DOI: 10.1596/978-0-8213-8866-2.

Jin, Q., Zhang, J., Shi, M., and Huang, J. (June 2016). Estimating Loess Plateau Average Annual Precipitation with Multiple Linear Regression Kriging and Geographically Weighted Regression Kriging. *Water* 8 (6): 266. DOI: 10.3390/w8060266.

Jordahl, K., Bossche, J. V. d., Wasserman, J., McBride, J., Fleischmann, M., Gerard, J., Tratner, J., Perry, M., Farmer, C., Hjelle, G. A., Gillies, S., Cochran, M., Bartos, M., Culbertson, L., Eubank, N., Bilogur, A., and maxalbert (Feb. 2020). geopandas/geopandas: v0.7.0. DOI: 10.5281/ZENODO.3669853.

Kidd, C., Becker, A., Huffman, G. J., Muller, C. L., Joe, P., Skofronick-Jackson, G., and Kirschbaum, D. B. (Jan. 2017). So, How Much of the Earth's Surface Is Covered by Rain Gauges? *Bulletin of the American Meteorological Society* 98 (1): 69–78. DOI: 10.1175/BAMS-D-14-00283.1.

Legendre, P. and Legendre, L. (1998). *Numerical Ecology*. 2nd. Amsterdam: Elsevier Science BV: 713–738.

Leijnse, H., Uijlenhoet, R., and Stricker, J. N. M. (Mar. 2007). Rainfall measurement using radio links from cellular communication networks. *Water Resources Research* 43 (3). DOI: 10.1029/2006WR005631.

Li, J. and Heap, A. D. (Mar. 2014). Spatial interpolation methods applied in the environmental sciences: A review. *Environmental Modelling & Software* 53: 173–189. DOI: 10.1016/j.envsoft.2013.12.008.

Lloyd, C. D. (2006). *Local models for spatial analysis*. 2nd. Hoboken, New Jersey: Taylor and Francis.

Lussana, C., Saloranta, T., Skaugen, T., Magnusson, J., Tveito, O. E., and Andersen, J. (Feb. 2018). seNorge2 daily precipitation, an observational gridded dataset over Norway from 1957 to the present day. *Earth System Science Data* 10 (1): 235–249. DOI: 10.5194/essd-10-235-2018.

Lussana, C., Tveito, O. E., Dobler, A., and Tunheim, K. (2019). seNorge_2018, daily precipitation and temperature datasets over Norway (Under Review). *Earth System Science Data*. DOI: 10.5194/essd-2019-43.

Ly, S., Charles, C., and Degré, A. (July 2011). Geostatistical interpolation of daily rainfall at catchment scale: the use of several variogram models in the Ourthe and Ambleve catchments, Belgium. *Hydrology and Earth System Sciences* 15 (7): 2259–2274. DOI: 10.5194/hess-15-2259-2011.

Lyra, G. B., Correia, T. P., de Oliveira-Júnior, J. F., and Zeri, M. (Nov. 2018). Evaluation of methods of spatial interpolation for monthly rainfall data over the state of Rio de Janeiro, Brazil. *Theoretical and Applied Climatology* 134 (3-4): 955–965. DOI: 10.1007/s00704-017-2322-3.

Messer, H. (May 2006). Environmental Monitoring by Wireless Communication Networks. *Science* 312 (5774): 713–713. DOI: 10.1126/science.1120034.

Messer, H. and Sendik, O. (May 2015). A New Approach to Precipitation Monitoring: A critical survey of existing technologies and challenges. *IEEE Signal Processing Magazine* 32 (3): 110–122. DOI: 10.1109/MSP.2014.2309705.

Mohr, M. (2008). *New routines for gridding of Temperature and Precipitation Observations for "seNorge.no"*. Tech. rep. URL: https://www.researchgate.net/publication/228610451_New_Routines_for_Gridding_of_Temperature_and_Precipitation_Observations_for_seNorge_no.

Mälicke, M. and Schneider, H. D. (Nov. 2019). Scikit-GStat 0.2.7: A scipy flavored geostatistical analysis toolbox written in Python. DOI: 10.5281/ZENODO.3552235.

Nebuloni, R., De Michele, C., and D'amico, M. (2017). Rainfall detection by tomographic inversion of commercial radio link data: a pilot project in italy. In: *15th International Conference on Environmental Science and Technology Rhodes*. Rhodes. URL: http://cest.gnest.org/sites/default/files/presentation_file_list/cest2017_01233_oral_paper.pdf.

Netatmo (2020). *Smart Home Weather Station's technical specifications, Accessed: 2020-05-30*. URL: https://www.netatmo.com/en-eu/weather/weatherstation/specifications.

Niemczynowicz, J. (Mar. 1999). Urban hydrology and water management – present and future challenges. *Urban Water* 1 (1): 1–14. DOI: 10.1016/S1462-0758(99)00009-6.

Nipen, T. N., Seierstad, I. A., Lussana, C., Kristiansen, J., and Hov, Ø. (Jan. 2020). Adopting Citizen Observations in Operational Weather Prediction. *Bulletin of the American Meteorological Society* 101 (1): E43–E57. DOI: 10.1175/BAMS-D-18-0237.1.

Ochoa-Rodriguez, S., Wang, L.-P., Gires, A., Pina, R. D., Reinoso-Rondinel, R., Bruni, G., Ichiba, A., Gaitan, S., Cristiano, E., van Assel, J., Kroll, S., Murlà-Tuyls, D., Tisserand, B., Schertzer, D., Tchiguirinskaia, I., Onof, C., Willems, P., and ten Veldhuis, M.-C. (Dec. 2015). Impact of spatial and temporal resolution of rainfall inputs on urban hydrodynamic modelling outputs: A multi-catchment investigation. *Journal of Hydrology* 531: 389–407. DOI: 10.1016/j.jhydrol.2015.05.035.

Overeem, A., Leijnse, H., and Uijlenhoet, R. (Oct. 2016). Two and a half years of country-wide rainfall maps using radio links from commercial cellular telecommunication networks. *Water Resources Research* 52 (10): 8039–8065. DOI: 10.1002/2016WR019412.

Pedregosa, F., Varoquaux, G., Gramfort, A., Michel, V., Thirion, B., Grisel, O., Blondel, M., Prettenhofer, P., Weiss, R., Dubourg, V., Vanderplas, J., Passos, A., Cournapeau, D., Brucher, M., Perrot, M., and Duchesnay, E. (2011). Scikit-learn: Machine Learning in {P}ython. *Journal of Machine Learning Research* 12: 2825–2830. URL: https://scikit-learn.org/stable/.

Plummer, N., Allsopp, T., and Lopez, J. A. (2003). *Guidelines on Climate Observation Networks and Systems*. Tech. rep. World Meteorological Organization. URL: www.wmo.int/pages/prog/wcp/wcdmp/documents/WCDMP-52_000.pdf.

QGIS Development Team (2019). *QGIS Geographic Information System. Open Source Geospatial Foundation Project.* URL: https://qgis.org/en/site/.

Rasmussen, C. E. and Williams, C. K. I. (2006). *Gaussian Processes for Machine Learning*. The MIT press. URL: http://www.gaussianprocess.org/gpml/.

Reback, J., McKinney, W., jbrockmendel, Bossche, J. V. d., Augspurger, T., Cloud, P., gfyoung, Sinhrks, Klein, A., Roeschke, M., Hawkins, S., Tratner, J., She, C., Ayd, W., Petersen, T., Garcia, M., Schendel, J., Hayden, A., MomIsBestFriend, Jancauskas, V., Battiston, P., Seabold, S., chris-b1, h-vetinari, Hoyer, S., Overmeire, W., alimcmaster1, Dong, K., Whelan, C., and Mehyar, M. (Mar. 2020). pandas-dev/pandas: Pandas 1.0.3. DOI: 10.5281/ZENODO.3715232.

Rios Gaona, M. F., Overeem, A., Brasjen, A. M., Meirink, J. F., Leijnse, H., and Uijlenhoet, R. (Dec. 2017). Evaluation of Rainfall Products Derived From Satellites and Microwave Links for The Netherlands. *IEEE Transactions on Geoscience and Remote Sensing* 55 (12): 6849–6859. DOI: 10.1109/TGRS.2017.2735439.

Robertson, S. and King, A. (Apr. 1946). The Effect of Rain upon the Propagation of Waves in the 1- and 3-Centimeter Regions. *Proceedings of the IRE* 34 (4): 178p–180p. DOI: 10.1109/JRPROC.1946.234239.

Roy, V., Gishkori, S., and Leus, G. (Dec. 2016). Dynamic rainfall monitoring using microwave links. *EURASIP Journal on Advances in Signal Processing* 2016 (1): 77. DOI: 10.1186/s13634-016-0367-6.

Ruf, C. S., Aydin, K., Mathur, S., and Bobak, J. P. (Apr. 1996). 35-GHz Dual-Polarization Propagation Link for Rain-Rate Estimation. *Journal of Atmospheric and Oceanic Technology* 13 (2): 419–425. DOI: 10.1175/1520-0426(1996)013<0419:GDPPLF>2.0.CO;2.

Schleiss, M. and Berne, A. (July 2010). Identification of Dry and Rainy Periods Using Telecommunication Microwave Links. *IEEE Geoscience and Remote Sensing Letters* 7 (3): 611–615. DOI: 10.1109/LGRS.2010.2043052.

Sluiter, R. (2009). Interpolation methods for climate data, a literature review. *KNMI intern rapport* (04). URL: https://www.researchgate.net/publication/242783501_Interpolation_methods_for_climate_data.

Thiessen, A. H. (1911). Precipitation averages for large areas. *Monthly Weather review* 39 (7): 1082–1089. DOI: 10.1175/1520-0493(1911)39<1082b:PAFLA>2.0.CO;2.

Tobin, C., Nicotina, L., Parlange, M. B., Berne, A., and Rinaldo, A. (Apr. 2011). Improved interpolation of meteorological forcings for hydrologic applications in a Swiss Alpine region. *Journal of Hydrology* 401 (1-2): 77–89. DOI: 10.1016/j.jhydrol.2011.02.010.

Tveito, O. E. (2008). Spatialisation of climatological and meteorological information with the support of GIS. In: *The Use of Geographic Information Systems in Climatology and Meteorology*. Luxembourg: Office for Official Publications of the European Communities. Chap. 2: 36–71. URL: https://op.europa.eu/en/publication-detail/-/publication/10328d8c-c5df-4df9-85f6-f0024f8275ef.

Tveito, O. E. (2016). The effect of homogenized input data in gridding of daily temperature and precipitation. *METreport* No. 11/201. URL: https://www.met.no/publikasjoner/met-report/met-report-2016/_/attachment/download/097dca7f-6248-4a44-a80c-a44bbef87b94:103168b99678c0919122dbc33f6d118c75906719/MET-report-11-2016.pdf.

Uijlenhoet, R., Overeem, A., and Leijnse, H. (July 2018). Opportunistic remote sensing of rainfall using microwave links from cellular communication networks. *Wiley Interdisciplinary Reviews: Water* 5 (4): e1289. DOI: 10.1002/wat2.1289.

Vejen, F., Jacobsson, C., Fredriksson, U., Moe, M., Andresen, L., Hellsten, E., Rissanen, P., Pálsdóttir, Þ., and Arason, Þ. (2002). Quality Control of Meteorological Observations - Automatic Methods Used in the Nordic Countries. *METreport* (8). URL: https://www.met.no/publikasjoner/met-report/met-report-2002/_/attachment/download/2fdbdbcf-2ae8-4bb3-86de-f7b5a6f11dae:b322c47c99e9a34086013dfa7e4a915a383d2b42/MET-report-08-2002.pdf.

Wang, S., Huang, G. H., Lin, Q. G., Li, Z., Zhang, H., and Fan, Y. R. (Nov. 2014). Comparison of interpolation methods for estimating spatial distribution of precipitation in Ontario, Canada. *International Journal of Climatology* 34 (14): 3745–3751. DOI: 10.1002/joc.3941.

WMO (2014). Measurement of meteorological variables. In: *Guide to instruments and methods of observation*. 8th. Geneva, Switzerland: WMO-World Meteorological Organization. Chap. 6: Measure: 186–208. URL: Geneva%202,%20Switzerland.

Wolff, M., Isaksen, K., Brækkan, R., Alfnes, E., Petersen-Øverleir, A., and Ruud, E. (Feb. 2013). Measurements of wind-induced loss of solid precipitation: description of a Norwegian field study. *Hydrology Research* 44 (1): 35–43. DOI: 10.2166/nh.2012.166.

Yr.no (2020). *Live precipitation forecast (only in Norway), Accessed: 2020-05-20*. URL: https://hjelp.yr.no/hc/en-us/articles/209295525-Live-precipitation-forecast-only-in-Norway-.

Chapter XI Hypsometric Curves and Longitudinal Stream Profiles (1985). In: ed. by I. Zăvoianu: 185–200. DOI: 10.1016/S0167-5648(08)70423-4.

Produktark: DTM 50

BESKRIVELSE

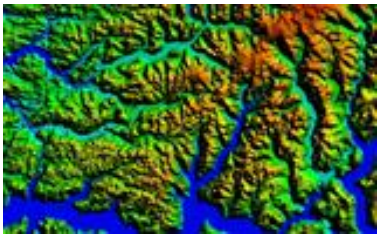

Digital terrengmodell med høyder i et rutenett på 50 x 50 meter. Laget primært på grunnlag av høydeinformasjon fra N50. Høydebærende tema er: høydekurver, høydepunkt, trigpunkt, kyst, innsjøer, veger. Lagret som ruter ("tiles") på 100 x 100 km. Navnet på rutene gjenspeiler UTM-koordinatene i nedre venstre hjørne, to siffer for nord- og to siffer for øst-koordinaten.
Standardavvik i høyde er +/- 4-6 meter.
Dataene dekker fastlands-Norge med øyer. Modellen fortsetter i øst et stykke inn på utenlandsk side med data av usikker kvalitet.
Dette er et datasett som ble produsert i 2007. Det er ikke planlagt oppdateringer av dette datasettet.

Hele landet ligger i UTM-sone 33.

FORMÅL/BRUKSOMRÅDE

Grov landsdekkende terrengmodell.

Framstilling av relieffkart med mer.
Filene kan brukes som grunnlag for enkle 3d-visualiseringer.

Ingen begrensninger på bruk er oppgitt.

EIER/KONTAKTPERSON

Kartverket
Datateknisk: Andreas Korsnes, kundesenter@kartverket.no
Fagekspert: Andreas Korsnes, kundesenter@kartverket.no

DATASETTOPPLØSNING

Målestokktall: 100000

UTSTREKNINGSINFORMASJON

KILDER OG METODE

Laget primært på grunnlag av høydeinformasjon fra N50.

AJOURFØRING OG OPPDATERING

Status
Arkivert

LEVERANSEBESKRIVELSE

Format (versjon)
USGS DEM
GeoTIFF

Projeksjoner
•EUREF89 UTM sone 33, 2d + NN54

Tilgangsrestriksjoner
Åpne data

LENKER

Link til metadata i Geonorge
Link til produktside

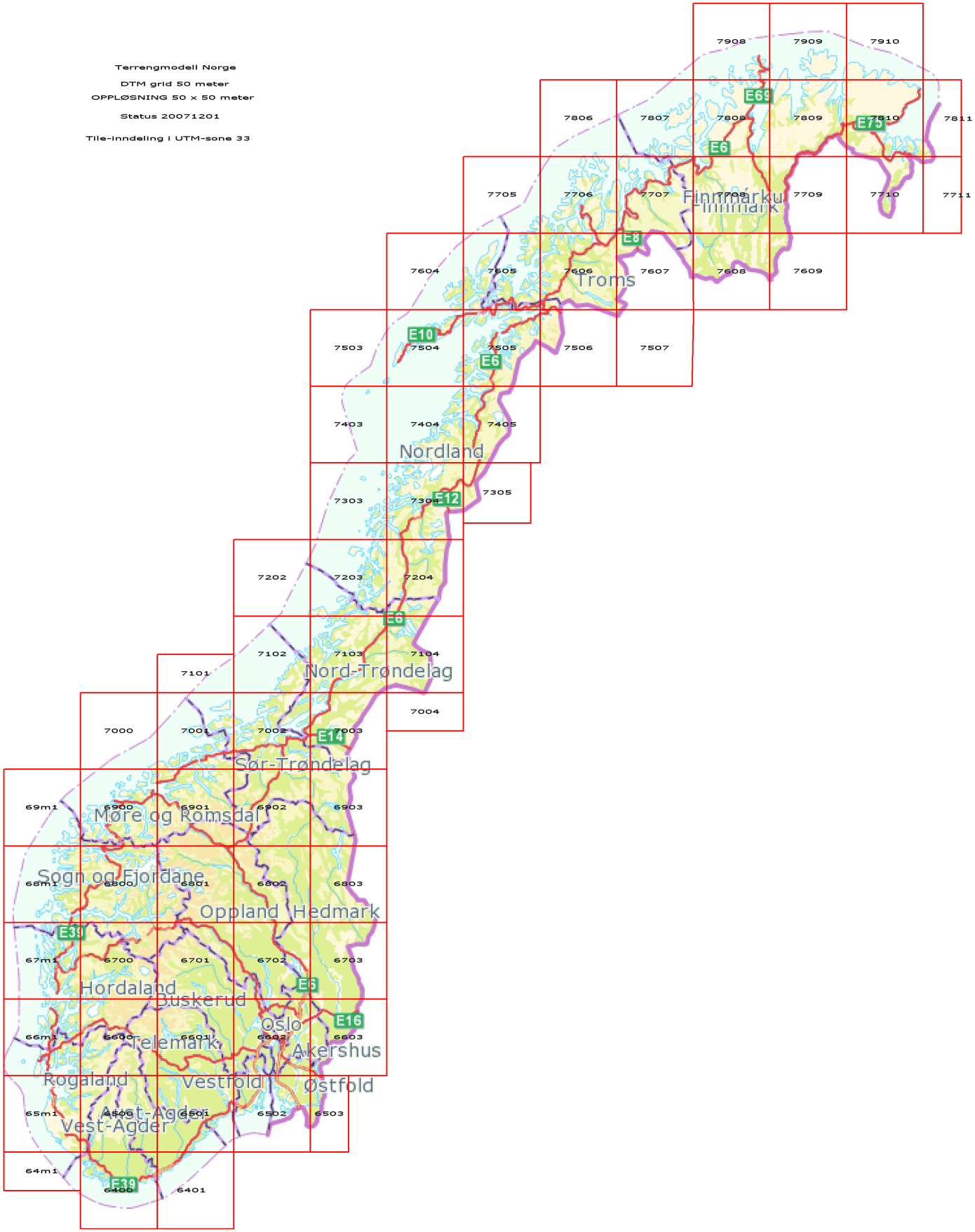
Terrengmodell Norge
DTM grid 50 meter
OPPLØSNING 50 x 50 meter
Status 20071201
Tile-inndeling i UTM-sone 33
7908
7909
7910
7806
7807
7808
7809
7810
7811
7705
7706
7707
7708
7709
7710
7711
7604
7605
7606
7607
7608
7609
7503
7504
7505
7506
7507
7403
7404
7405
7303
7304
7305
7202
7203
7204
7102
7103
7104
7101
7004
7000
7001
7002
7003
69m1
6900
6901
6902
6903
68m1
6800
6801
6802
6803
67m1
6700
6701
6702
6703
66m1
6600
6601
6602
6603
65m1
6500
6501
6502
6503
64m1
6400
6401
E69
E6
E75
E8
E10
E12
E14
E16
E39
Troms
Finnmark
Nordland
Nord-Trøndelag
Sør-Trøndelag
Møre og Romsdal
Sogn og Fjordane
Oppland
Hedmark
Hordaland
Buskerud
Oslo
Telemark
Akershus
Rogaland
Vestfold
Østfold
Aust-Agder
Vest-Agder

Appendix B. Python functions used for meta-data collection

```python
import requests
import pandas as pd
import geopandas as gpd
from pyproj import CRS
from shapely.geometry import Point
from collections import OrderedDict


def request_netatmo(
    client_ID: str,
    client_secret: str,
    pw: str,
    username: str,
    bounding_gdf: gpd.GeoDataFrame,
    areal_buffer: float,
    output_crs: str = "EPSG:32632",
    verbose=False
):

    # Authentication
    auth_params = {
        "client_id": client_ID,
        "client_secret": client_secret,
        "grant_type": "password",
        "username": username,
        "password": pw,
        "scope": "read_station",
    }
    auth_endpoint = "https://api.netatmo.com/oauth2/token"
    auth = requests.post(auth_endpoint, auth_params)
    auth_json = auth.json()
    if auth.status_code != 200:
        raise Exception(f"token request failed, response: {auth.text}")
    else:
        if verbose:
            print(f"token request succeded.")
    token = auth_json["access_token"]

    names = ("lon_sw", "lat_sw", "lon_ne", "lat_ne")
    coords = (
        bounding_gdf
        .buffer(areal_buffer)
        .to_crs("epsg:4326")
```

```
        .geometry.iloc[0]
        .bounds
    )
    bbox = dict(zip(names, coords))
    if verbose:
        print(f"after {areal_buffer}m buffer, requested bounding box was: {bbox}")

    # Get data
    endpoint = "https://api.netatmo.com/api/getpublicdata"
    parameters = {
        **bbox,
        "required_data": "rain",
    }
    r = requests.get(endpoint, parameters, headers={"Authorization": "Bearer " + token})
    json = r.json()
    if r.status_code != 200:
        raise Exception(
            f"data request returned error code {r.status_code}.\
              {json['error']['message']}"
        )
    else:
        if verbose:
            print("data resquest succeded")

    # Initial processing
    df_raw = pd.DataFrame.from_dict(json)
    df = pd.DataFrame.from_records(df_raw.body)
    df = df.drop(["measures", "modules", "module_types"], axis=1)

    df["lon"] = df.place.apply(lambda x: x["location"][0])
    df["lat"] = df.place.apply(lambda x: x["location"][1])
    df["masl"] = df.place.apply(lambda x: x["altitude"])
    df["country"] = df.place.apply(lambda x: x["country"])
    df = df.drop(["place"], axis=1)
    df = df[df.country == "NO"]  # filters by stations in norway
    df = df.rename(columns={"_id": "id"})

    # Generate GeoDataFrame
    gdf = gpd.GeoDataFrame(df)
    gdf["geometry"] = gdf.apply(lambda x: Point(x["lon"], x["lat"]), axis=1)
    gdf = gdf.drop(["lon", "lat"], axis=1)

    # Assign, then change the crs
    gdf.crs = CRS.from_epsg(4326)
    gdf = gdf.to_crs(output_crs)

    gdf["source"] = "NETATMO"
    gdf['owner'] = "PRIVATE"
    gdf["resolution"] = 60
    if bounding_gdf is not None:
        bound_polygon = bounding_gdf.geometry.iloc[0]
        clipped_gdf = gdf[gdf.geometry.within(bound_polygon)]
        removed_stations = len(gdf) - len(clipped_gdf)
        if verbose:
            print(f"{removed_stations} statinos exceeded study area and were removed.")

    return clipped_gdf

def find_primary_owner(owners:str, owner_importance: OrderedDict=None, default_owner:str="OTHER") -> str:
```

```
    """Assigns the primary owner by the first occuring defined by the dict owner_importance.
       Otherwise it assignes default value.

    Arguments:
        owners {str} -- string of all station owners

    Keyword Arguments:
        owner_importance {OrderedDict[str,str]} -- Ordered dictionary (by importance)
                                                   of owners (default: {None})
        default_owner {str} -- what to assign primary owner if none of the owners occur
                               in owner importance (default: {"private"})

    Returns:
        str -- primary owner
    """
    if owner_importance is None:
        owner_importance = OrderedDict({
            "MET.NO": "MET.NO",
            "NVE": "NVE",
            "STATENS VEGVESEN": "SVV",
            "NIBIO": "NIBIO",
            "BANE NOR": "BANE NOR",
            "KOMMUNE": "MUNICIPALITY",
            "ENERGI": "ENERGY",
            "KRAFT": "ENERGY",
            "STATNETT": "ENERGY",
            "": default_owner
        })
    for key, value in owner_importance.items():
        if key in owners:
            # TODO: info about the owners grouped to other
            return value


def request_frost(
    client_ID: str,
    client_secret: str,
    resolution: str = "all",
    bounding_gdf: gpd.GeoDataFrame = None,
    output_crs: str = "EPSG:32632",
):

    elements = OrderedDict({
        "monthly": r"sum(precipitation_amount P1M)",
        "daily": r"sum(precipitation_amount P1D)",
        "hourly": r"sum(precipitation_amount PT1H)",
        "10_min": r"sum(precipitation_amount PT10M)",
        "1_min": r"sum(precipitation_amount PT1M)"
    })
    endpoint = "https://frost.met.no/sources/v0.jsonld"
    parameters = {
        "types": "SensorSystem",
        "country": "No",
        "fields": "id,geometry,masl,stationholders,wmoid",
    }
    if resolution in elements:
        parameters["elements"] = elements[resolution]
    elif resolution == "all":
        # Wired subroutine, that should request all the resolutions and construct
```

```
        # a gdf with temporal resolution as column
        dfs = []
        for res in elements:
            gdf = request_frost(
                client_ID=client_ID,
                client_secret=client_secret,
                resolution=res,
                bounding_gdf=bounding_gdf,
                output_crs=output_crs
            )
            # Maps name to minutes
            resolution_map = {
                "monthly": int(60 * 24 * 30.5),
                "daily": int(60 * 24),
                "hourly": 60,
                "10_min": 10,
                "1_min": 1
            }
            gdf["resolution"] = resolution_map[res]
            gdf = gdf.set_index("id")
            dfs.append(gdf)
        gdf = dfs.pop(0)  # Should be the monthly resolution dataset,
                          # This should also contain all with finer resolution.
        for other in dfs:
           gdf.update(other)
        gdf = gdf.reset_index()
        return gdf
    else:
        raise ValueError(f"resolution argument must be one of {[k for k in elements]}, or \"all\"")

    # Get data
    r = requests.get(endpoint, parameters, auth=(client_ID, client_secret))
    json = r.json()
    if r.status_code != 200:
        raise Exception(
            f"request returned error code {r.status_code}.\
              {json['error']['message']}: {json['error']['reason']}"
        )
    else:
        print(f"resquest for {resolution} data succeded")

    # create df
    data = json["data"]
    df = pd.DataFrame.from_dict(data)

    # drop rows that don't include geometric information and sotre
    # coordinates
    df = df.dropna(subset=["geometry"])
    df["lon"] = df.geometry.apply(lambda x: x["coordinates"][0])
    df["lat"] = df.geometry.apply(lambda x: x["coordinates"][1])
    df = df.drop(["geometry"], axis=1)

    gdf = gpd.GeoDataFrame(df)
    gdf["geometry"] = gdf.apply(lambda x: Point(x["lon"], x["lat"]), axis=1)
    gdf = gdf.drop(["lon", "lat"], axis=1)

    # Assign, the change CRS
    gdf.crs = CRS.from_epsg(4326)
    gdf = gdf.to_crs(output_crs)
```

```
    # Gets rid of stationholders as list
    def cat_to_str(li):
        return ",".join(li)

    gdf["stationHolders"] = gdf["stationHolders"].apply(cat_to_str).apply(find_primary_owner)
    gdf = gdf.rename(columns={"stationHolders": "owner"})

    # filter by research area
    if bounding_gdf is not None:
        bound_polygon = bounding_gdf.geometry.iloc[0]
        gdf = gdf[gdf.geometry.within(bound_polygon)]

    gdf["source"] = "MET"
    return gdf


def load_CML(path: str, bounding_gdf: gpd.GeoDataFrame = None):
    gdf = gpd.GeoDataFrame.from_file(path)
    if bounding_gdf is not None:
        bound_polygon = bounding_gdf.geometry.iloc[0]
        gdf = gdf[gdf.geometry.within(bound_polygon)]
    gdf['owner'] = "TELIA"
    gdf["source"] = "CML"
    gdf["resolution"] = 0.166
    return gdf
```

Appendix C. Python functions for QC and reprocessing

```
import pandas as pd
import geopandas as gpd
import numpy as np
from math import log10, exp

def add_observations(df_meta, df_values, timestamp):
    df = df_meta.copy()
    values = df_values.loc[timestamp]
    assert len(values.shape) == 1
    df = df.set_index("id")
    df["precipitation"] = values
    return df

def faulty_zero_check(row, df, n, r):
    buffer = row.geometry.centroid.buffer(r)
    within = df[df.geometry.centroid.intersects(buffer)]
    threshold = within.precipitation.median()
    if threshold > 0:
        if row.precipitation == 0:
            return True
    return False

def buddy_check(row, df, n, r):
    buffer = row.geometry.centroid.buffer(r)
    within = df[df.geometry.centroid.intersects(buffer)]
    std = within.precipitation.std()
    mean = within.precipitation.mean()
    if abs(row.precipitation - mean) > 2*std:
        return True
    else:
        return False


def isolation_check(row, df, n, r):
    buffer = row.geometry.centroid.buffer(r)
    within = df[df.geometry.centroid.intersects(buffer)]
    if len(within) < n:
        return True
    else:
        return False


def QC(df, n, r):
```

```
    """Does QC of stations: n is the number of stations required in the
       neighbourhood and r is the circular radius of it.
    """
    df["fz_flag"] = df.apply(faulty_zero_check, args=(df, n, r), axis=1)
    df["buddy_flag"] = df.apply(buddy_check, args=(df, n, r), axis=1)
    df["isolation_flag"] = df.apply(isolation_check, args=(df, n, r), axis=1)
    return df

def add_flags_in_column(row):
    out = []
    if row.fz_flag:
        out.append("fz")
    if row.buddy_flag:
        out.append("buddy")
    if row.isolation_flag:
        out.append("isolation")
    if len(out) > 0:
        return "-".join(out)
    else:
        return "not flagged"


def pipeline(df_meta, df_values, timestamp, n_QC=5, rad_QC=3000, drop_flagged=True, drop_specific=None, apply_QC=True):
    df = add_observations(df_meta, df_values, timestamp)
    # Remove stations without observations, then apply other fuctions
    df = df.dropna(subset=["precipitation"])
    if apply_QC:
        df = QC(df, n_QC, rad_QC)
        df["flag"] = df.apply(add_flags_in_column, axis=1)  # creates single column of flags for vis
        initial = df.shape[0]
        if drop_flagged:
            df = df[~(df.buddy_flag | df.isolation_flag | df.fz_flag)]
        elif drop_specific:
            for flag in drop_specific:
                df = df[~(df[flag])]

        print("dropped: ", initial-df.shape[0], "stations")
        return df
    else:
        return df


def calculate_alpha(polarization, frequency, attenuation, length):
    # note, returns mm/hr
    specific_attenuation = attenuation / (length/1000)
    horisontal_coeff = {
        "k": {
            "a" : [-5.33980, -0.35351, -0.23789, -0.94158],
            "b" : [-0.10008, 1.26970, 0.86036, 0.64552],
            "c" : [1.13098, 0.45400, 0.15354, 0.16817],
            "m_k" : -0.18961,
            "c_k" : 0.71147,
        },
        "alpha": {
            "a": [-0.14318, 0.29591, 0.32177, -5.37610, 16.1721],
            "b": [1.82442, 0.77564, 0.63773, -0.96230, -3.29980],
            "c": [-0.55187, 0.19822, 0.13164, 1.47828, 3.43990],
            "m_alpha": 0.67849,
            "c_alpha": -1.95537
```

```
        }
    }
    vertical_coeff = {
        "k" : {
            "a": [-3.80595, -3.44965, -0.39902, 0.50167],
            "b": [0.56934, -0.22911, 0.73042, 1.07319],
            "c": [0.81061, 0.51059, 0.11899, 0.27195],
            "m_k": -0.16398,
            "c_k": 0.63297
        },
        "alpha": {
            "a": [-0.07771, 0.56727, -0.20238, -48.2991, 48.5833],
            "b": [2.33840, 0.95545, 1.14520, 0.791669, 0.791459],
            "c": [-0.76284, 0.54039, 0.26809, 0.116226, 0.116479],
            "m_alpha": -0.053739,
            "c_alpha": 0.83433
        }
    }
    if polarization == "Vertical":
        c = vertical_coeff
    elif polarization == "Horizontal":
        c = horisontal_coeff
    elif polarization == "Dual":
        return min(
            calculate_alpha("Horizontal", frequency, attenuation, length),
            calculate_alpha("Vertical", frequency, attenuation, length)
        )
    else:
        raise ValueError(f"polarisation {polarization} not recognized")
    k = c["k"]
    a = c["alpha"]

    log10k = sum([
        k["a"][i] * exp(- ((log10(frequency) - k["b"][i])/k["c"][i])**2) for i in range(4)
    ]) + k["m_k"] * log10(frequency) + k["c_k"]
    k = 10 ** log10k

    alpha = sum([
        a["a"][i] * exp(- ((log10(frequency) - a["b"][i])/a["c"][i] )**2 ) for i in range(5)
    ]) + a["m_alpha"] * log10(frequency) + a["c_alpha"]

    return (specific_attenuation / k) ** (1/alpha)

def fixed_time_series_processing(series, period='1T', limit=15):
    """Simple mode. Requires fixed period apriori i.e.
       Equal time between all observations (or nans)"""
    series = series.replace(0, np.NaN)

    # Fill with constant rainrate within 15 minutes
    series = series.cumsum(skipna=True).interpolate(
        method="linear", limit=limit, limit_area="inside"
    )
    start = series.iloc[0]

    series = series.fillna(method="pad").diff()
    series.iloc[0] == start
    return series
```

Appendix D. Python classes for prediction

```
from pykrige.uk import UniversalKriging as pk_UK
from sklearn.neighbors import KNeighborsRegressor as KNR
from sklearn.gaussian_process.kernels import ConstantKernel, Product, Sum, RBF, WhiteKernel
from sklearn.gaussian_process import GaussianProcessRegressor
import numpy as np


def idw(p):
    def f(m):
        w = (1 / m**p) / np.sum(1 / m**p)
        return w
    return f

def make_grid(bounding_gdf, resolution):
    minx, miny, maxx, maxy = bounding_gdf.total_bounds
    xx, yy = np.meshgrid(
        np.arange(minx, maxx, resolution),
        np.arange(miny, maxy, resolution)
    )
    X = np.column_stack([xx.flatten(), yy.flatten()])
    return X, xx.shape


class IDW(KNR):
    def __init__(self, p, neighbours=None):
        self.p = p
        self.neighbors = neighbours
        self.weight_fn = idw(p)

    def fit(self, X, y):
        if self.neighbors is None:
            self.neighbors = X.shape[0]
        super().__init__(
            n_neighbors=self.neighbors,
            weights=self.weight_fn,
            algorithm="brute"
        )
        _ = super().fit(X, y)
        return _

    def grid(self, bounding_gdf, resolution, flip=True):
        X, out_shape = make_grid(bounding_gdf, resolution)
        y_pred = self.predict(X)
        y_pred = y_pred.reshape(out_shape)
        if flip:
            y_pred = np.flip(y_pred, 0)
```

```
        return y_pred


class NN(KNR):

    def __init__(self, neighbors=1):
        super().__init__(
            n_neighbors=neighbors,
            weights='uniform',
            algorithm="brute",
        )

    def grid(self, bounding_gdf, resolution, flip=True):
        X, out_shape = make_grid(bounding_gdf, resolution)
        y_pred = self.predict(X)
        y_pred = y_pred.reshape(out_shape)
        if flip:
            y_pred = np.flip(y_pred, 0)
        return y_pred


class GPR(GaussianProcessRegressor):

    def __init__(
        self, kernel=None, nugget=None, total_sill=None, range_param=None, optimize=True,
        normalize_y=True, alpha=1e-10, random_state=None
    ):
        if not kernel:
            kernel = (   # Creates a gaussian covariance function with a nugget, sill and range.
                WhiteKernel(nugget,noise_level_bounds=(1e-10, 1e0))
                + ConstantKernel(total_sill - nugget, constant_value_bounds=(1e-2, 1e0))
                * RBF(0.4 * range_param, length_scale_bounds=(1e1, 1e5))
            )
        super().__init__(
            kernel=kernel,
            alpha=alpha,
            optimizer=("fmin_l_bfgs_b" if optimize else None),
            n_restarts_optimizer=50,
            normalize_y=normalize_y,
            random_state=random_state
        )

    def predict(self, X, return_std=False, return_cov=False):
        ## Wrapper to remove negative predictions
        if return_cov:
            return super().predict(X, return_std=return_std, return_cov=return_cov)
        if return_std:
            y_pred, std = super().predict(X, return_std=return_std)
            y_pred = y_pred.clip(min=0)
            return y_pred, std
        else:
            return super().predict(X).clip(min=0)

    def grid(self, bounding_gdf, resolution, flip=True, return_std=False):
        X, out_shape = make_grid(bounding_gdf, resolution)
        if return_std:
            y_pred, sigma = self.predict(X, return_std=True)
            y_pred = y_pred.reshape(out_shape)
            sigma = sigma.reshape(out_shape)
```

```
            if flip:
                y_pred = np.flip(y_pred, 0)
                sigma = np.flip(sigma, 0)
            return y_pred, sigma
        else:
            y_pred = self.predict(X)
            y_pred = y_pred.reshape(out_shape)
            if flip:
                y_pred = np.flip(y_pred, 0)
            return y_pred


class UK(pk_UK):

    def __init__(self, variogram_model="exponential", n_lags=6, drift=True, nugget=None, total_sill=None, range_param=None
        self.usr_model = variogram_model
        self.usr_lags = n_lags
        self.usr_drift = ["regional_linear"] if drift else None
        self._my_nugget = nugget
        self._my_sill = total_sill
        self._my_range = range_param

    def fit(self, X, y):
        _x = X[:,0]
        _y = X[:,1]
        _z = y
        if all((self._my_nugget, self._my_sill, self._my_range)):
            var_params = {"sill": self._my_sill, "range": self._my_range, "nugget": self._my_nugget}
            super().__init__(
                x=_x, y=_y, z=_z,
                variogram_model=self.usr_model,
                variogram_parameters=var_params
            )
        else:
            super().__init__(x=_x, y=_y, z=_z,
                             variogram_model=self.usr_model,
                             nlags=self.usr_lags,
                             drift_terms=self.usr_drift)
        return self

    def predict(self, X, return_std=False):
        y_pred, sigma = self.execute(style="points", xpoints=X[:,0], ypoints=X[:,1])

        y_pred = y_pred.clip(min=0)
        if return_std:
            return y_pred, sigma
        else:
            return y_pred

    def grid(self, bounding_gdf, resolution, flip=True, return_std=False):
        X, out_shape = make_grid(bounding_gdf, resolution)
        if return_std:
            y_pred, sigma = self.predict(X, return_std=True)
            y_pred = y_pred.reshape(out_shape)
            sigma = sigma.reshape(out_shape)
            if flip:
                y_pred = np.flip(y_pred, 0)
                sigma = np.flip(sigma, 0)
            return y_pred, sigma
```

```
        else:
            y_pred = self.predict(X)
            y_pred = y_pred.reshape(out_shape)
            if flip:
                y_pred = np.flip(y_pred, 0)
            return y_pred


class BCSP:

    def __init__(self, *trained_predictors):
        """Predictors must have a method predict(X, y, return_std)
           which returns the error of prediction at each point.
        """
        self.predictors=trained_predictors

    def predict(self, X, return_std=False):
        numerator = np.zeros_like(X[:,0], dtype=np.float64)
        denomentor =  np.zeros_like(X[:,0], dtype=np.float64)
        sigmas = []
        for predictor in self.predictors:
            y_pred, sigma = predictor.predict(X, return_std=True)
            numerator += y_pred * (1./sigma)
            denomentor += (1./sigma)
            if return_std:
                sigmas.append(sigma)
        y_pred = numerator/denomentor
        if return_std:
            sigma = np.minimum(*sigmas)
            return y_pred, sigma
        else:
            return y_pred

    def grid(self, bounding_gdf, resolution, flip=True, return_std=False):
        X, out_shape = make_grid(bounding_gdf, resolution)
        if return_std:
            y_pred, sigma = self.predict(X, return_std=True)
            y_pred = y_pred.reshape(out_shape)
            sigma = sigma.reshape(out_shape)
            if flip:
                y_pred = np.flip(y_pred, 0)
                sigma = np.flip(sigma, 0)
            return y_pred, sigma
        else:
            y_pred = self.predict(X)
            y_pred = y_pred.reshape(out_shape)
            if flip:
                y_pred = np.flip(y_pred, 0)
            return y_pred
```

Norges miljø- og biovitenskapelige universitet
Noregs miljø- og biovitskapelege universitet
Norwegian University of Life Sciences

Postboks 5003
NO-1432 Ås
Norway